Institute for System Dynamics
Prof. Dr.-Ing. O. Sawodny

University of Stuttgart
Germany

Master thesis

Model predictive approaches for building climate and seasonal energy storage control

Konzepte zur modellprädiktiven Regelung einer Gebäudekonditionierung mit saisonalem Energiespeicher

by
Simon Oskar Weber

A thesis presented to the faculty in partial fulfillment of the requirements for the degree Master of Science in
Process Engineering

Examiner
Prof. Dr.-Ing. Oliver Sawodny

Supervisor
M.Sc. Marius Oei

Examination Date
2020-05-04

Institute for System Dynamics, University of Stuttgart, Waldburgstr. 17/19, 70563 Stuttgart

Abstract

The aim of this thesis is the integration of a seasonal energy storage system into the heat supply of a building system under consideration of weather and occupancy forecasts. A thermochemical storage system based on the material system slaked lime / burnt lime is applied as seasonal energy storage. Methodically, a model of an energy system consisting of a building, a water buffer storage tank, a heat pump and a lime storage module is developed. In addition, model-predictive control concepts are developed, which optimally operate the system over a period of one year.

For an effective integration of the seasonal lime storage, weather forecasts for an entire year are required. However, public weather forecasts are only considered reliable in the time range of several days. Due to this problem the so-called base year is introduced. The base year data approximate the weather forecast beyond the public forecast period. The weather data of the base year are based on those of the typical meteorological year, which are weather data averaged over several years. On this basis, three model-predictive control concepts are developed. The hierarchy of two concepts provides for a superordinate optimal generation scheduling as well as a subordinate model-predictive control. The optimal generation scheduling uses the disturbance variable inputs of the base year and finds those system inputs through single optimisation which minimise the annual operation costs while keeping all system limits. The resulting lime storage trajectory serves as a reference for the subordinate model predictive control. These concepts now try to follow the lime storage trajectory in an optimal way on the one hand, and on the other hand to realise possible increased or decreased yields due to the public weather data of the current year. The third control concept does not require a superordinate hierarchical level. It uses the public weather forecast for the coming days and the subsequent weather data of the base year to find optimal inputs to the overall system.

This thesis demonstrates that the hybrid system consisting of heat pump and lime storage module allows the lowest operating costs for the heat supply of a building. Furthermore, all control concepts presented demonstrate that operation cost savings can be achieved by using the weather forecasts of the base year and integrating the lime storage tank. Depending on the applied configuration of the heat supply, these savings lie between 10 % and 30 % compared to the model-predictive control, which only includes forecasts over a period of several days and not months.

Kurzfassung

Das Ziel dieser Arbeit ist die Integration eines saisonalen Energiespeichers in die Wärmeversorgung eines Gebäudesystems unter Einbezug von Wetter- und Belegungsvorhersagen. Als saisonaler Energiespeicher wird ein thermochemischer Speicher auf der Basis des Stoffsystems Löschkalk / Branntkalk verwendet. Methodisch soll ein Modell eines Energiesystems aus einem Gebäude, einem Wasserpufferspeicher, einer Wärmepumpe und einem Kalkspeichermodul erarbeitet werden. Zudem sollen modellprädiktive Regelungskonzepte entwickelt werden, welche das System über ein Jahr hinweg optimal betreiben.
Für eine wirkungsvolle Integration des saisonalen Kalkspeichers werden Wettervorhersagen im Zeitraum mehrerer Monate benötigt. Amtliche Wettervorhersagen gelten jedoch nur im Zeitbereich von mehreren Tagen als zuverlässig. Aus dieser Problemstellung heraus wird das sog. Basisjahr eingeführt. Die Basisjahrdaten approximieren den Wetterverlauf über den amtlichen Vorhersagezeitraum hinaus. Für die Wetterdaten des Basisjahrs werden jene des typischen meteorologischen Jahres, das sind über mehrere Jahre gemittelte Wetterdaten angesetzt. Darauf basierend werden drei modellprädiktive Regelungskonzepte entwickelt. Die Hierarchie zweier Konzepte sieht eine übergeordnete optimale Jahresplanung sowie eine untergeordnete modellprädiktive Regelung vor. Die optimale Jahresplanung verwendet die Störgrößeneingänge des Basisjahres und findet durch einmalige Optimierung jene Systemeingänge, welche die Jahresbetriebskosten unter Einhaltung aller Systemgrenzen minimieren. Die dadurch zur Verfügung stehende Kalkspeichertrajektorie dient der untergeordneten modellprädiktiven Regelung als Referenz. Diese Konzepte versuchen nun zum einen der Kalkspeichertrajektorie optimal zu folgen und zum anderen mögliche Mehr- oder Mindererträge, mit den Wetterprognosen des aktuellen Jahres, zu realisieren. Das dritte Regelungskonzept kommt ohne übergeordnete Hierarchieebene aus. Es verwendet hierzu die aktuelle amtliche Wetterprognose der kommenden 5 Tage und anschließend Wetterdaten des Basisjahres um optimale Eingänge auf das Gesamtsystem zu finden. Diese Arbeit zeigt auf, dass das Hybridsystem aus Wärmepumpe und Kalkspeichermodul die geringsten Betriebskosten für die Wärmeversorgung eines Gebäudes ermöglichen. Außerdem weisen alle vorgestellten Regelungskonzepte nach, dass durch die Verwendung der Wettervorhersagen des Basisjahres sowie die Integration des Kalkspeichers eine Betriebskostenersparnis realisiert werden kann. Diese liegt je nach angewendeter Konfiguration der Wärmeversorgung zwischen 10 % und 30 % gegenüber jener modellprädiktiven Regelung, welche ausschließlich Vorhersagen im Zeitraum mehrerer Tage und nicht Monate miteinbezieht.

Contents

Abbreviations and Formula Signs

Abbreviations

MPC	Model Predictive Control
OGS	Optimal Generation Scheduling
TCM	Thermochemical Material
PCM	Phase Change Material
SHGC	Solar Heat Gain Coefficient
secHG	secondary Heat Gain
CSTR	Continuous Stirred Tank Reactor
BE	Building Element
AEC	Annual Energy Consumption
AOC	Annual Operation Cost

Subscripts

A	substance calcium hydroxide / slaked lime $Ca(OH)_2$
B	substance calcium oxide / quicklime CaO
C	substance water H_2O
BD	building
LS	lime storage
BS	buffer storage
Z	room zone
AMB	ambient
FL	floor
CE	ceiling
F	facade
E	east
N	north
S	south
W	west
BL	blind
CHI	chiller
RAD	radiator
HP	heat pump
IR	irradiation
R	reactor
dc	dehydration cycle
hc	hydration cycle
EHF	external heat flux
s	solid
l	liquid
g	gaseous
b	bulk
eq	equilibrium

ub	upper bound
lb	lower bound
oc	operation cost
ec	energy consumption
cy	current year
by	base year
trans	transition
tmy	typical meteorological year

Formula Signs

formula symbol	unit	description
t	s	time / prediction horizon
τ	s	time integration variable
m	kg	mass
$\dot{m}$	$^{kg}/_{s}$	mass flow
N	mol	mole mass
MW	$^{kg}/_{mol}$	molecular weight
X	$-$	molar share
T	K	temperature
ϑ	$^{\circ}C$	temperature
V	l	volume
p	bar	pressure
ρ	$^{kg}/_{m^3}$	density
H	J	enthalpy
h	$^{J}/_{mol}$	specific enthalpy
P	W	electrical power
$\dot{Q}$	W	heat power
I	$^{W}/_{m^2}$	global vertical solar irradiation flux
$u_{BL,i}$	$-$	blind level facade i
v_{OCR}	$-$	occupancy probability
s	m	wall thickness
A	m^2	area
λ	$^{W}/_{mK}$	heat conduction coefficient
α	$^{W}/_{m^2K}$	heat convection coefficient
k	$^{W}/_{m^2K}$	heat transmission coefficient
R	$^{J}/_{molK}$	gas constant
R_{th}	$^{K}/_{W}$	thermal resistance
η	$-$	electrical to thermal power conversion efficiency
ζ, κ, ξ	$-$	regression parameter
x		state vector
u		manipulated variable / control input
v, c		disturbance input for the model, objective function

Chapter 1

Introduction

Climate change is the biggest challenge of modern human history. Therefore 195 countries joined together in 2016 aiming to limit global warming to 2 °C if possible even to 1.5 °C compared with the pre-industrial age [201]. The German Federal Government has also joined the Paris Agreement. It laid down the goals and their realization in the *Klimaschutzprogramm 2030* and *Klimaschutzgesetz* [Bun20]. The main goals of the Federal Government are the reduction of greenhouse gases by 55 % by 2030 compared to 1990, a share of 65 % of renewable energies in the electricity mix by 2030 and complete climate neutrality by 2050. To this end, it introduces a minimum price for CO_2 emissions and will phase out coal-based electricity generation by 2038. More than half (53.2 %) of final energy consumption in Germany is spent on the supply of heat. Most of the energy (89.3 %) needed in private households is used as heat. This is the result of a recent study by the AG Energiebilanzen e.V., [e.V20], which was commissioned by the Federal Government to provide meaningful figures. According to this study, the supply of heat for private buildings accounts for 23 % of the total final energy consumption in Germany and therefore has an enormous savings potential.
This is the topic of the Collaborative Research Centre: CRC 1244 - Adaptive Shells and Structures for the Built Environment of the Future at the University of Stuttgart. Its goals are the reduction of the building weight and resources within the entire building life cycle. „Worldwide, construction accounts for approx. 60 % of resource consumption, approx. 50 % of mass waste and approx. 35 % of energy consumption and emissions“, [202]. Adaptive structures should enable a lighter, more resource efficient construction method that avoids over dimensioning. The Institute System Dynamics at the University of Stuttgart designs models and control concepts for the adaptive building envelope in compliance with its strict safety-critical regulations. With the low-resource construction method, a reduction of the thermal inertia is expected, resulting in an increased effort to meet comfort criteria.
In this thesis the impact of a weight reduced building envelope on the effort to meet comfort criteria shall be analysed. The main focus of this work is the design of a control system for a combined building and thermal energy storage system. This control concept is supposed to operate the system optimally over a horizon of one year and thus evaluate the possibilities of thermal energy storage as seasonal energy storage. The following questions are leading. How can an energy system of a building, water buffer storage and heat supply be optimally operated over one year under consideration of comfort criteria as well as weather and occupancy forecasts? Which is the optimal configuration of the heat supply consisting of a heat pump and or a thermochemical energy storage module? Can cost and resource efficiency of the plant be increased by integrating a thermochemical energy storage system?
The authors [MRAR18] provide a review which summaries strategies of building climate and plant control. „All controls essentially attempt to lessen the dependence on human experience

and judgement, and to achieve (or optimise) one or a number of objectives according to certain criteria ",[MRAR18]. As in the industrial sector, building control systems are differentiated according to their hierarchy level into the field level and the management level. At the field level, individual system components such as the boiler or water distribution are controlled. Therefore, field level controllers such as PID controller are still in use today. Within the management level, all functionalities in the overall system are monitored and coordinated. This control level finds inputs to all field level controllers on the basis of one or more central criteria while ensuring all restrictions are met. The supervisory control methods are classified into model-free and model-based methods. With model-free methods, such as the reinforcement learning technique, the system inputs are found on the basis of previous inputs or a learning phase. In contrast, model-based methods, such as model-predictive control, use a model to determine not only the optimum manipulated variable but also the optimum time for their change. On the basis of disturbance inputs which cannot be influenced, such as weather or occupancy forecasts, and constraints of the system states and manipulated variables, that manipulated variable trajectory is determined which minimises the performance measure.
The performance measure can include energy consumption, operating costs, emissions or comfort indices. In this thesis, operation costs *oc* and energy consumption *ec* are considered.
The models can be divided into white, grey and black box models. While white box models are based on first principle equations, black box models are obtained by adjusting for input and output data. Grey box models are in between, based on physical considerations with adjusted parameters. In this thesis, however, the influence of changes in concrete density will be investigated. Therefore, a white-box model for the entire system will be established. The building model is created by the Matlab toolbox, BRCM [Stu+14]. Compared to more detailed building models it has the disadvantage of being less accurate but provides access to gradients and thus simplifying convex optimisation [Stu14]. The BRCM model is a thermal network model based on the resistance capacitance modelling of electrical circuits. Rooms and wall layers are modelled as capacitances. The heat exchange between the spaces and layers is proportional to the temperature difference and the inversely thermal resistance. This coefficient describes heat conduction and convection simultaneously. The model of the water buffer tank is derived from an isothermal isobaric energy balance. The module of thermochemical energy storage is modelled as a cycle process of an instationary mass storage between stationary charge and discharge reactors.
Can cost and resource efficiency of the plant be raised by integrating a thermochemical energy storage system? The increasing share of renewable energies causes an growing fluctuation of energy production. Energy storage systems intervene in times of energy production peaks and release the temporarily stored energy in times of low production and high demand. They separate the generation and consumption of energy and thus create flexibility in the energy system. In the following, only thermal energy storage systems are considered. In addition to electrochemical energy storage systems, such as batteries or chemical storage systems, such as hydrogen storage, thermal energy storage systems are another way of making energy available in buildings. Since the main energy consumption in buildings is required as heat, thermal energy storage is particularly suitable. The following review [TPL13] provides a comprehensive compilation of all materials for thermal storage with building applications. Thermal energy storages are compared according to their energy density, heat transfer properties and energy losses during the storage period. For building applications high energy density is especially important due to the lack of space. Thermal energy storage is divided into sensitive, latent and thermochemical energy storage. **Sensible energy** is the energy which is contained in the temperature change of a material at a constant aggregate state. This form of energy is

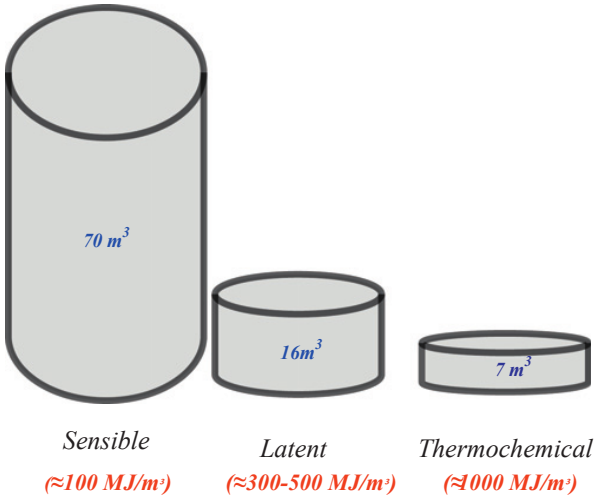

Figure 1.1: Volume needed to fully cover the annual storage need of an efficient passive house. (6480 MJ) [TPL13]

proportional to the mass, the specific heat capacity and the temperature difference. A high density, specific heat capacity or a high temperature level cause a high potential of sensitive energy storage. Water is the most common material in this context, as it has a comparatively high density and heat capacity. Sensitive energy storage is already widely used in water buffer tanks, in large aquifer reservoirs or in solar ponds. **Latent energy** is the energy that is stored within an aggregation or phase change. Changes from liquid to gas contain the highest energy, but require a large volume. Solid liquid phase change materials, such as those used in heat pads, can store energy in a small temperature range with a small volume change. They offer the possibility to absorb a lot of energy with a small change in temperature. Typical materials are wax, paraffin or salt hydrates. **Thermochemical energy** is stored within a reversible chemical reaction. Usually a gas and a solid enter into a chemical reaction. Among the thermochemical energy storages are further such combinations of materials which undergo a sorption reaction. In this case, e.g. a gas is deposited on the surface of the solid and thereby releases the entropy difference. The sorption reactions differ from the chemical reactions in that there is no change in the molecular configuration due the reaction. Thermochemical storage materials that undergo a chemical reaction include hydroxides such as calcium hydroxide $Ca(OH)_2$ and carbonates such as calcium carbonate $Ca(CO)_3$. Among the representatives of sorption reactions are zeolites, as used in the self-cooling beer barrel, or silica gels. The decisive advantage of thermochemical energy storages is their high energy density and their high temperature level during unloading. Figure 1.1 compares the required volume of the respective energy storage to cover the needs of a passive house. Compared to sensitive energy storage, thermochemical energy storage requires 10 times less volume. Further extensive advantages and disadvantages of each type of storage and their application in different scaled energy systems are shown in the current review [Ene+20]. The possibility of loss-free energy storage makes thermochemical energy storage particularly attractive for seasonal applications [TPL13]. Due to the high energy density as well as low storage costs of 0.15 €/kWh [Ang+18], calcium hydroxide is used as thermochemical energy storage in this paper.

1.1 State of Research

The model predictive control is applied comprehensively for building energy systems. Various authors focus on the simulative analysis of system properties [Fin+18; TB16; XD17; Jon+19] whereas others focus on the experimental implementation [Fio+17; Ši+11] of model predictive control. In the practical implementation [Ši+11] the MPC shows a reduction of energy consumption between 15 % and 29 % as well as a lower comfort violation compared to an operation mode per heating curve. Finck et al. [Fin+18] applied MPC to a system of building, heat pump and thermal energy storage and found out that the sensitive hot water storage tank captures 3 times more energy than the thermochemical energy storage tank and thus offers a higher potential to provide short-term energy flexibility in the system. Previously, the same research group [FLZ15] carried out a single cost optimisation and considered the operating costs of different heat supply configurations over an entire year. In combination with a heat pump, a solar-powered phase change storage tank or thermochemical storage tank reduces the operating costs by 13 % and 8 % respectively compared to a storage-less configuration. The thermochemical energy storage is particularly suitable for seasonal energy storage. This work expands the state of research by providing a complete system consisting of a building and a water buffer storage for short-term heat storage as well as a seasonal thermochemical heat storage. In contrast to the publication [Fin+18], partial differential equations for the description of the reaction modelling of the seasonal thermochemical storage are omitted, since a different reactor system with faster dynamics is used. More about this is described in Subsection 2.1.3. There're also a couple of works dealing with model predictive control approaches for seasonal thermal energy storage [XD17; Jon+19]. Xu et al. [XD17] focuses on the detailed dynamics description of solar heated borehole storage with a prediction horizon of 5 days whereas Jonin et al. [Jon+19] focuses on the inertial behaviour of different layers within a seasonal solar heated water tank over a whole year. This work shall introduce an MPC which operates the thermochemical storage optimally over a prediction horizon of one year. There are many publications in the literature dealing with hierarchical approaches to model-predictive control of microgrids [Pet+16] or building energy systems [Fio+17; TB16; Lef+13]. Throughout, a hierarchy of higher-level planning and dynamic control is introduced. The superordinate planning optimizes the operating costs [Lef+13; Pet+16; TB16] or the energy consumption [Fio+17] over the prediction horizon. This horizon is not greater than three days in any publication. The objective of the subordinate dynamic control was formulated as an explicit reference tracking [Lef+13; TB16; Fio+17], a mixture of grid stabilisation and reference tracking of storage states [Pet+16] or as pure operating costs [TB16]. The present work uses the hierarchy of a superordinate planning level and a subordinate dynamic control and develops two approaches based on this. The superordinate scheduling level minimises either the operating costs *oc* or the energy consumption *ec*. The target value of the dynamic control reflects a mixture of a minimisation of operating costs or energy consumption and a reference tracking of the lime storage state. In addition, a further MPC approach is being developed, which does not require a superordinate hierarchy as reference.
Chapter 2 presents the models used in detail and introduces the control concepts. Chapter 3 presents the results of the different overall concepts which are discussed in Chapter 4. The thesis summary is provided and open questions as well as further research topics are discussed in Chapter 5.

Chapter 2

Fundamentals

2.1 System Model

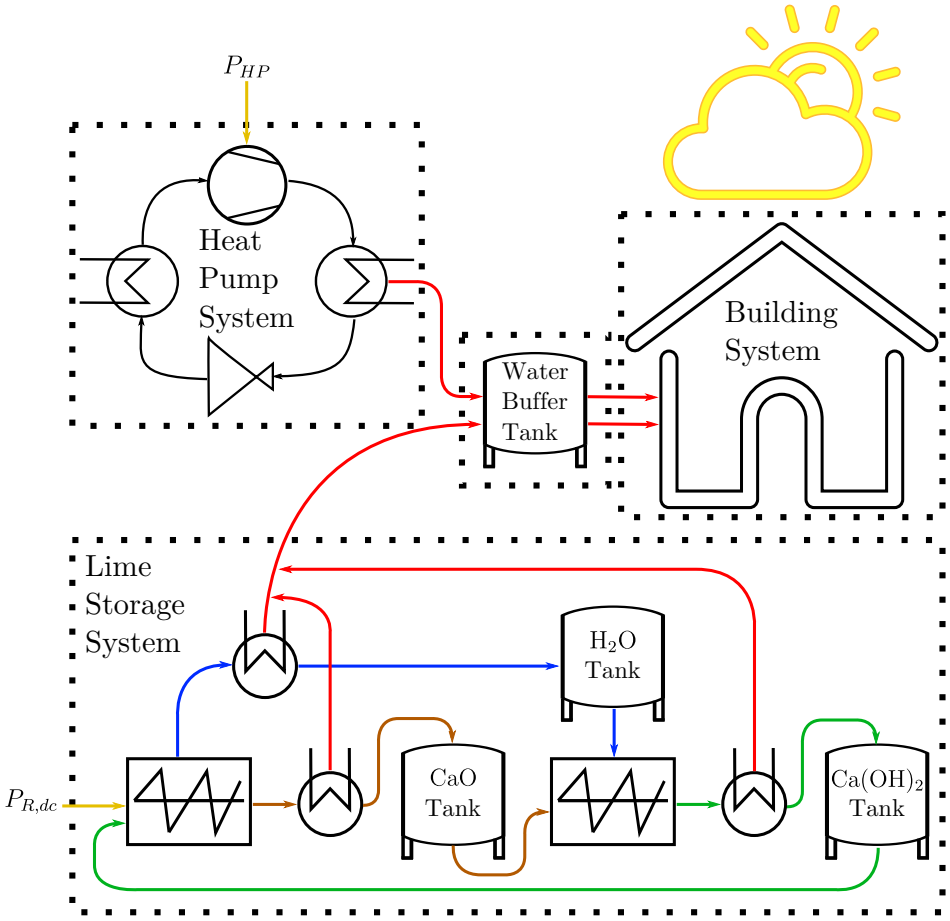

Figure 2.1: Process flow diagram total energy system

In this thesis an energy system is considered, which contains a building, a water buffer storage and a heat supply. In order to compare the different heat supply modules different system configurations are introduced. The system configuration *HP* receives its heat from a heat pump whereas the lime storage module ensures the required heat within the configuration *LS*. In the system configuration *LSHP*, the heat pump and the lime storage module provide the heat. All configurations contain the building states and the water buffer state, which reflects

the current state of the hot water tank V_{BS}. The building states are the room temperature T_Z as well as temperatures of the building walls, ceiling and floor, $T_{F,i}\,, T_{FL}\,, T_{CE}$ respectively. The configurations with lime storage additionally contain the state $m_{B,LS}$. The inputs for the building are the blind positions in each window of each facade $u_{BL,i}$ as well as the heating and cooling power $\dot{Q}_{RAD}\,, \dot{Q}_{CHI}$. As the heat is provided by the lime storage module, the inputs of the reactor input power for the dehydration of lime $P_{R,dc}$ and the mass flow of charged lime $\dot{m}_{B,hc}$ leaving the lime storage must be considered. The lime storage mass $m_{B,LS}$ as well as the lime storage inputs $P_{R,dc}$, $\dot{m}_{B,hc}$ are set to zero within simulations for the configuration case *HP*. Consequently, the heat pump is set to zero when simulations are carried out to the *LS* configuration.

The disturbance input v consists of the current occupancy probability v_{OCR}, the ambient temperature T_{AMB} and the vertically incident radiation intensities $I_{F,i}$ on each facade. The disturbance input c is the hourly electricity cost. The occupancy probability v_{OCR}, cmp. Figure 2.2 was taken from the publication [FLZ16] and applied for each weekday of the year without holidays. The weather data was taken from the European Union database [HMG12] based on the location of the Institut System Dynamics student room (N 48.7246° E 9.1084°). The electricity costs are accessible via the online platform of the federal network agency [Bun]. If the electricity prices were negative at some hours, they were set to a fixed positive value of 0.1 €/MWh. All monetary costs are based on prices on the electricity exchange and therefore do not include levies and taxes. When talking about the disturbance inputs of the base year, this disturbance inputs were formed from averaged weather data (2005-2016) and electricity prices (2015-2018). The occupancy probability data weren't averaged. If the current year is mentioned, data from 2016 were used. The occupancy data are the same for the so called base and current year.

The predominantly linear system dynamic is shown by Equation 2.1. It's matrices are assembled from the subsystems matrices via transformation matrices. In the following subchapters the subsystems dynamics are introduced.

$$\dot{x} = Ax + B_u u + B_v v + \sum_{i=1}^{n_u} B_{vu,i} v u_i + K \tag{2.1}$$

$$x = (x_{BD}, x_{BS}, x_{LS})^T \tag{2.2}$$

$$x_{BD} = (T_Z, T_{FL}, T_{CE}, T_{F,E}, T_{F,N}, T_{F,S}, T_{F,W})^T \tag{2.3}$$

$$x_{BS} = V_{BS} \tag{2.4}$$

$$x_{LS} = m_{B,LS} \tag{2.5}$$

$$u = (u_{BL,E}, u_{BL,N}, u_{BL,S}, u_{BL,W}, \dot{Q}_{CHI}, \dot{Q}_{RAD}, \dot{Q}_{HP}, P_{R,dc}, \dot{m}_{B,hc})^T \tag{2.6}$$

$$v = (v_{OCR}, T_{AMB}, I_{F,E}, I_{F,N}, I_{F,S}, I_{F,W})^T \tag{2.7}$$

$$A = \begin{pmatrix} A_{BD}T_{x,BD} \\ A_{BS}T_{x,BS} \\ 0 \end{pmatrix} \quad B_u = \begin{pmatrix} B_{u,BD}T_{u,BD} \\ B_{u,BS}T_{u,BS} \\ B_{u,LS}T_{u,LS} \end{pmatrix} \quad B_v = \begin{pmatrix} B_{v,BD}T_{v,BD} \\ B_{v,BS}T_{v,BS} \\ 0 \end{pmatrix} \tag{2.8}$$

$$B_{vu,i} = \begin{pmatrix} B_{vu,BD,i}T_{vu,BD,i} \\ 0 \\ 0 \end{pmatrix} \quad K = \begin{pmatrix} 0 \\ K_{BS} \\ 0 \end{pmatrix} \tag{2.9}$$

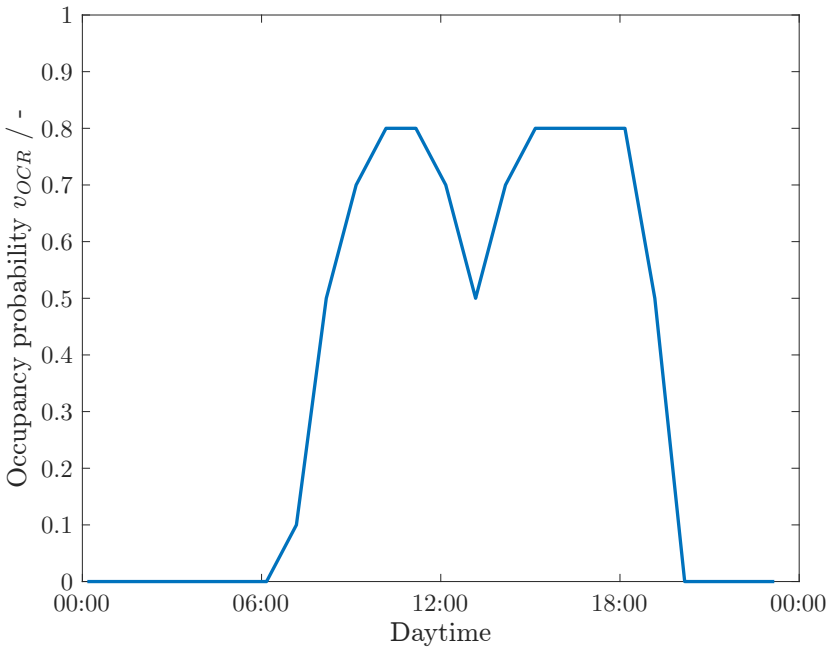

Figure 2.2: Occupancy probability from the literature [FLZ16]

Constraints

The variables of the system are subject to constraints. Equation 2.10 and 2.11 provide the time dependent state and manipulate input constraint set, respectively.

$$\mathbb{X}(t) := \left\{ x \in \mathbb{R}^9 : \begin{array}{ll} \vartheta_Z & \in \begin{cases} [21;24] & v_{OCR}(t) > 0 \\ [11;34] & \text{otherwise} \end{cases} \\ V_{BS} & \in [0; V_{BS,ub}] \\ m_{B,LS} & \in [0;\infty) \end{array} \right\} \tag{2.10}$$

$$\mathbb{U} := \left\{ u \in \mathbb{R}^8 : \begin{array}{ll} u_{BL,E} & \in [0;1] \\ u_{BL,N} & \in [0;1] \\ u_{BL,S} & \in [0;1] \\ u_{BL,W} & \in [0;1] \\ \dot{Q}_{CHI} & \in [0; \dot{Q}_{CHI,ub}] \\ \dot{Q}_{RAD} & \in [0; \dot{Q}_{RAD,ub}] \\ \dot{Q}_{HP} & \in [0; \dot{Q}_{HP,ub}] \\ P_{R,dc} & \in [0; P_{R,dc,ub}] \\ \dot{m}_{B,hc} & \in [0;\infty) \end{array} \right\} \tag{2.11}$$

The room temperature ϑ_Z must be within the limits specified by the norm [V.c]. As long as there is no person in the room, these limits have been relaxed. The volume of the hot water tank V_{BS} must not exceed an upper limit $V_{BS,ub}$ of 1000 l. The position of the blinds stay within the values zero and one. This corresponds to a completely lowered or raised position. The upper bounds are set to $\dot{Q}_{CHI,ub} = \dot{Q}_{RAD,ub} = 5.6\,\text{kW}$ and $\dot{Q}_{HP,ub} = 5.6\,\text{kW}$ according to the specification data sheet of the Bosch Climate 5000 RAC. The electrical reactor power

input has a upper bound of $P_{R,dc,ub} = 10\,\text{kW}$, according to the experimental study [Sch+14]. The upper limits $V_{BS,ub}$, $\dot{Q}_{CHI,ub}$, $\dot{Q}_{RAD,ub}$, $\dot{Q}_{HP,ub}$ and $P_{R,dc,ub}$ are part of the investigation and were also varied.

Discretisation

Under zero-order hold assumption for the manipulated variable inputs and disturbance inputs the systems discretisation is as follows with a discretisation step dT.

$$x_{k+1} = A_d x_k + B_{u,d} u_k + B_{v,d} v_k + \sum_{i=E,N,S,WB} B_{vu,d,i} v_k u_{BL,i,k} + K_d \tag{2.12}$$

$$A_d = e^{AdT}, \quad B_{u,d} = \int_0^{dT} e^{A\tau} d\tau B_u, \quad B_{v,d} = \int_0^{dT} e^{A\tau} d\tau B_v, \tag{2.13}$$

$$B_{vu,d,i} = \int_0^{dT} e^{A\tau} d\tau B_{vu,i}, \quad K_d = \int_0^{dT} e^{A\tau} d\tau K \tag{2.14}$$

2.1.1 Building

The building model was developed with the Building Resistance Capacitance Modelling (BRCM) Matlab toolbox [Stu+14]. The resulting model is mainly linear, but bilinear in the interaction between the blinds position and the solar radiation. The model is divided into a thermal model, cmp. Equation 2.15 and a model of external heat fluxes (EHF) $\dot{Q}_{EHF}$, cmp. Equation 2.16.

$$\dot{x}_{BD} = A_{t,BD} x_{BD} + B_{t,BD} \dot{Q}_{EHF}(x, u, v) \tag{2.15}$$

$$\dot{Q}_{EHF}(x, u, v) = A_{q,BD} x_{BD} + B_{q,u,BD} u_{BD} + B_{q,v,BD} v_{BD} + \sum_{i=1}^{n_{u_{BD}}} B_{q,vu,BD,i} v_{BD} u_{BD,i} \tag{2.16}$$

$$\dot{x}_{BD} = A_{BD} x_{BD} + B_{u,BD} u_{BD} + B_{v,BD} v_{BD} + \sum_{i=1}^{n_{u_{BD}}} B_{vu,BD,i} v_{BD} u_{BD,i} \tag{2.17}$$

The thermal model consists of energy balances of the building rooms, so-called zones, and layers of all building walls. The thermal model describes the heat exchange between all building elements and the external heat flows. The heat exchange is always convective except for the conductive heat exchange between individual wall layers. A spatial homogeneous temperature distribution is assumed for the individual energy balances. Within the toolbox different boundary conditions for the building elements can be considered. The building in this thesis was designed as one floor of an office building, with a floor area of $100\,\text{m}^2$ and a ceiling height of $3\,\text{m}$, cmp. Figure 2.3. The heat exchange of the floor downwards and the ceiling upwards is considered adiabatic and thus the heat transfer coefficient is zero. The facades have the ambient temperature as outside boundary condition. The convective heat transfer coefficients inside the room towards the wall and from the outside towards the facade

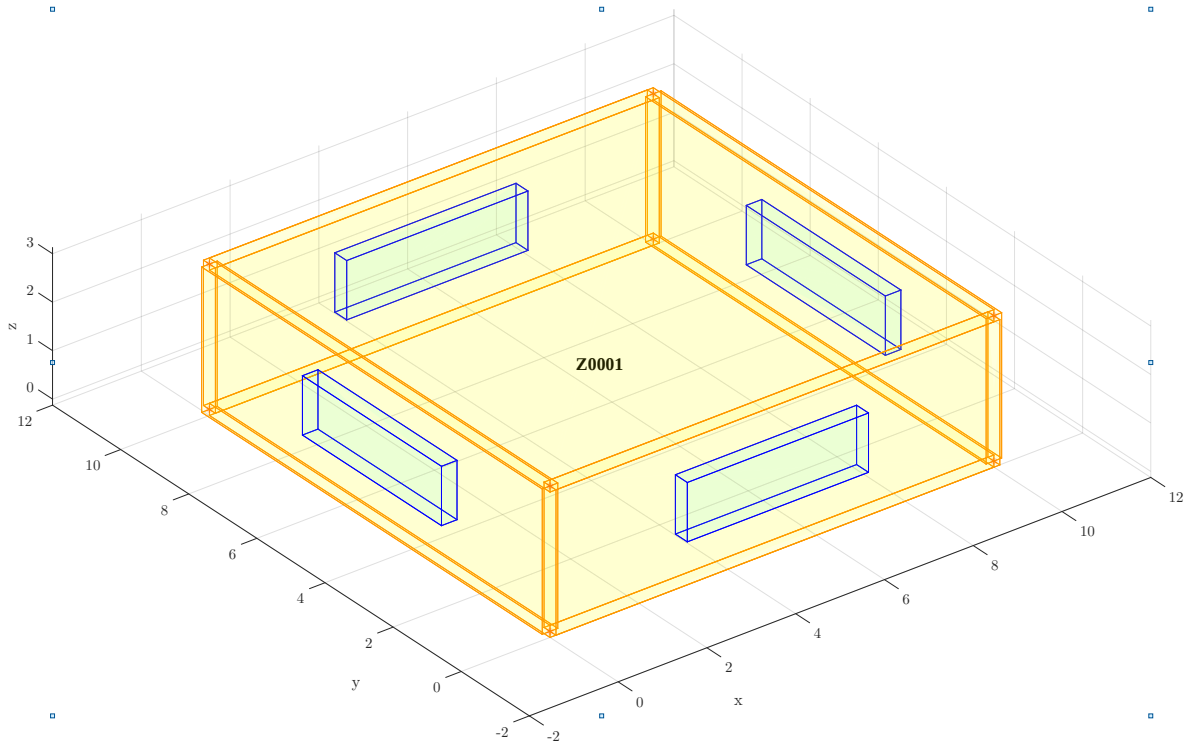

Figure 2.3: Buildings construction with four windows, a floor area of 100 m^2 and a ceiling height of 3 m

were taken from the calculation methods of the EN ISO 6946 standard, cmp. Table 7 [V.a] with $\alpha_{s,i} = 7.7\,\mathrm{W\,m^{-2}\,K^{-1}}$ and $\alpha_{s,e} = 25\,\mathrm{W\,m^{-2}\,K^{-1}}$, respectively.

The employed construction and material information of the walls, floor and ceiling are given in Table 2.1. The parameters were obtained from the publication [FLZ16]. The outer wall consists of two layers. The outer layer is mineral insulation and then the structural concrete layer. To save computation time, both layers were merged into one. The merging rules, cmp. Equation 2.18 were applied. The ceiling and the floor consist of one layer of concrete. Since the goal of the Collaborative Research Centre is the reduction of weight and resources, a hypothetical lightweight concrete was designed to compare the original concrete properties and to analyse this influence. The *light* concrete is four times less dense than the real concrete. This also changes the other properties of the walls.

$$\frac{1}{\lambda_{ges}} = \frac{1}{s_{ges}} \sum_i \frac{s_i}{\lambda_i} \tag{2.18}$$

$$\rho_{ges} = \frac{1}{s_{ges}} \sum_i s_i \rho_i \tag{2.19}$$

$$c_{p,ges} = \frac{1}{\rho_{ges} s_{ges}} \sum_i c_{p,i} s_i \rho_i \tag{2.20}$$

$$\tag{2.21}$$

The window and frame area was selected such that it corresponds to one sixth of the facade

Table 2.1: Construction and material properties of the exemplary walls.

Wall type / Building element	$s[m]$	c_p[J/kgK]	λ[W/mK]	ρ[kg/m³]
Mineral insulation	0.05	830	0.04	90
Concrete	0.30	921	0.73	1920
Concrete light	0.30	921	0.73	480
Ceiling / floor wall	0.25	921	0.73	1920
Facade wall	0.35	920.3	0.21	1658.57
Ceiling / floor wall light	0.25	921	0.73	480
Facade wall light	0.35	918.2	0.21	424.29

Table 2.2: Specification parameter of the exemplary windows.

A_{glas}	A_{frame}	U [W/m²K]	f_{SHGC} [−]
3.1	1.9	1.3	0.6

area. This area in turn consists of 62 % glazing area. This corresponds to the glazing area fraction of the author's home windows. The combined heat transfer coefficient of frame and glass U and the Solar Heat Gain Coefficient (SHGC) were taken from the German Energy Saving Regulation. The SHGC is the proportion of incident solar radiation that passes through the window and is converted into thermal energy. The parameters used are listed in Table 2.2.

The heat flows due to external inputs, such as solar radiation or occupancy density, are implemented under the term external heat flux model. Heat flows caused by internal gains have a direct impact on the zone temperature. These are caused by lost heat from people, lighting and computers. According to the standard [V.c] Table 5, auxiliaries (computers, lighting) produce a heat energy $Q = 60\,\mathrm{W\,h\,m^{-2}\,d^{-1}}$ and 8 persons in the office produce a daily heat energy $Q = 42\,\mathrm{W\,h\,m^{-2}\,d^{-1}}$. The daily total heat production Q_{IG} by internal gains is given in Equation 2.22. Based on this, the current heat power is modelled proportional to the occupancy probability.

$$Q_{IG} = (60 + 42) A_Z = 2830\,\mathrm{W\,h} \tag{2.22}$$

$$= \int_0^{24} a\, v_{OCR}\, dt = a\, 8.5\,\mathrm{h} \tag{2.23}$$

$$\dot{Q}_{IG} = a\, v_{OCR} = 1200\, v_{OCR}\,\mathrm{W} \tag{2.24}$$

The ambient temperature influences the building in three ways. It changes the temperature of each external wall as well as the room temperature on the one hand directly through the window and on the other hand via the air exchange. The resulting heat flows are always proportional to the temperature difference with the ambient temperature. The heat flow on the outer walls $\dot{Q}_{AMB,BE\,i}$, cmp. Equation 2.26 is influenced by the facade surface and the inverse thermal resistance. This thermal resistance $R_{th,BE\,i}$ describes the convective and conductive heat exchange. The heat flow through the window to the room volume

$\dot{Q}_{AMB,windowi,Z}$ is dependent on the window area and the heat transfer coefficient U, cmp. Equation 2.27. The heat flow through the mandatory air exchange $\dot{Q}_{AC,Z}$ is dependent on the energy density of air and the air change rate acr in addition to the temperature difference. For the air change rate, a value of $acr = 0.6\,\mathrm{h}^{-1}$ averaged over the entire time of day was assumed according to the standard [V.c]. The solar radiation on each facade $I_{F,i}$ heats the outer walls and the room. The radiant heat flow on the outer walls $\dot{Q}_{IR,BE\,i}$ is reduced by the absorption factor $\gamma = 0.5$, cmp. Equation 2.29. The proportion of solar radiation that passes through the window glass surfaces and is converted into heat is described by the solar heat gain coefficient f_{SHGC}. A fraction of the transmitted radiation heat affects the room temperature, cmp. Equation 2.30. The other part influences all walls, the ceiling and the floor from the inside, cmp. Equation 2.31. The so-called secondary heat gain coefficient f_{secHG} splits the transmitted radiant heat. It amounts to $f_{secHG} = 0.1$ and is, like the absorption coefficient γ, a default setting of the BRCM Toolbox.

$$R_{th,BE\,i} = \frac{1}{\alpha_{s,e}} + \frac{s_{BE\,i}}{2\lambda_{BE\,i}} \tag{2.25}$$

$$\dot{Q}_{AMB,BE\,i} = \frac{A}{R_{th,BE\,i}}(T_{AMB} - T_{BE\,i}) \tag{2.26}$$

$$\dot{Q}_{AMB,windowi,Z} = U(A_{glas} + A_{frame})(T_{AMB} - T_Z) \tag{2.27}$$

$$\dot{Q}_{AC,Z} = \rho_{air} c_{p,air} \frac{acr}{3600}(T_{AMB} - T_Z) \tag{2.28}$$

$$\dot{Q}_{IR,BE\,i} = A\gamma I_{F,i} \tag{2.29}$$

$$\dot{Q}_{IR,windowi,Z} = f_{secHG} A_{glass} f_{SHGC} I_{F,i} u_{BL,i} \tag{2.30}$$

$$\dot{Q}_{IR,windowi,BE\,i} = \frac{A_{BE\,i}}{\sum_j A_{BE\,j}}(1 - f_{secHG}) A_{glass} f_{SHGC} I_{F,i} u_{BL,i} \tag{2.31}$$

The heat power provided by a radiator $\dot{Q}_{RAD}$ has an exclusive and direct effect on the room temperature. This also holds for the cooling power $\dot{Q}_{CHI}$. The total external heat flux $\dot{Q}_{EHF}$ is the sum of all external heat flux models which have been presented above. After defining the input files, the BRCM Toolbox provides the matrices A_{BD}, $B_{u,BD}$, $B_{v,BD}$, $B_{vu,BD}$. These are included in the overall system by the transformation matrices $T_{x,BD}$, $T_{u,BD}$, $T_{v,BD}$.

$$A_{BD} \in \mathbb{R}^{7\times 7} \quad B_{u,BD} \in \mathbb{R}^{7\times 6} \quad B_{v,BD} \in \mathbb{R}^{7\times 6} \quad B_{vu,BD,i} \in \mathbb{R}^{7\times 6} \tag{2.32}$$

$$T_{x,BD} = \begin{pmatrix} 1\cdots 0 & 0\cdots 0 \\ \vdots\ddots\vdots & \vdots \\ 0\cdots 1 & 0\cdots 0 \end{pmatrix} \in \mathbb{R}^{7\times 9} \quad T_{u,BD} = \begin{pmatrix} 1\cdots 0 & 0\cdots 0 \\ \vdots\ddots\vdots & \vdots \\ 0\cdots 1 & 0\cdots 0 \end{pmatrix} \in \mathbb{R}^{6\times 9} \tag{2.33}$$

$$T_{v,BD} = \begin{pmatrix} 1\cdots 0 \\ \vdots\ddots\vdots \\ 0\cdots 1 \end{pmatrix} \in \mathbb{R}^{6\times 6} \quad T_{vu,BD,i} = \begin{pmatrix} 1\cdots 0 \\ \vdots\ddots\vdots \\ 0\cdots 1 \end{pmatrix} \in \mathbb{R}^{6\times 6} \tag{2.34}$$

2.1.2 Buffer Storage

The buffer tank contains hot water, which is a short-term energy storage between the heat supply and the building. The hot water is supplied by the heat pump $\dot{Q}_{HP}$ and or both heat flow components of the lime storage module $\dot{Q}_{LS,dc}$ and $\dot{Q}_{LS,hc}$. The required heat $\dot{Q}_{RAD}$ and domestic hot water supply $\dot{Q}_{DHW}$ reduces the energy in the storage tank. Due to the current hot water volume and the permanent hot water supply in the house pipes, heat losses $\dot{Q}_{BS,loss}$ occur. These losses were calculated using the standards [V.c; V.b].

$$\frac{\partial H_{BS}}{\partial t} = -\dot{Q}_{RAD} + \dot{Q}_{HP} + \dot{Q}_{LS,dc} + \dot{Q}_{LS,hc} - \dot{Q}_{DHW} - \dot{Q}_{loss,BS} \tag{2.35}$$

The dynamics of the water storage tank is developed from the energy balance, cmp. Equation 2.35. It is assumed that the temperature is spatial homogeneous at a constant storage temperature of $\vartheta_{BS} = 55\,°\mathrm{C}$. All material properties were taken from the NIST Chemistry WebBook database [LM].

$$V_{DHW} = \frac{Q_{DHW}}{\rho_C(h_C(\vartheta_{BS}) - h_C(\vartheta_K))} = 79\mathrm{l} \tag{2.36}$$

$$= \int_0^{24} \dot{V}_{DHW} dt = \int_0^{24} a v_{OCR} dt = a \int_0^{24} v_{OCR} dt = a \cdot 8.5h \tag{2.37}$$

$$a = 9.3\mathrm{l/h} \tag{2.38}$$

$$\dot{Q}_{DHW} = \rho_C(h_C(\vartheta_{BS}) - h_C(\vartheta_K))\dot{V}_{DHW} = 506\mathrm{W} \cdot v_{OCR} \tag{2.39}$$

The heat flow due to domestic hot water $\dot{Q}_{DHW}$ is derived from the daily demand of utility energy per person, cmp. Table 7 in the norm [V.c]. For the daily utility energy of all 8 persons Q_{DHW} of 4.3 kW h it is assumed that one of them takes a daily shower. This results in a daily hot water volume of 79 l with the sensible energy density between the storage temperature and the cold water inlet temperature $\vartheta_K = 10\,°\mathrm{C}$ taken from the standard, cmp. Equation 2.36. It is supposed that the volume flow $\dot{V}_{DHW}$ is proportional to the occupancy probability v_{OCR}. This can then be used to determine the DHW heat power $\dot{Q}_{DHW}$, cmp. Equation 2.39.

$$\dot{Q}_{loss,BS} = \dot{Q}_{loss,BS,pip} + \dot{Q}_{loss,BS,stor} \tag{2.40}$$

$$\dot{Q}_{loss,BS,pip} = U_{pip} L_{pip} (\vartheta_{DHW} - \vartheta_S) = 533\,\mathrm{W} \tag{2.41}$$

The heat losses in the buffer storage tank $\dot{Q}_{loss,BS}$ occur on the one hand within the piping $\dot{Q}_{loss,BS,piping}$ and on the other hand at the buffer storage itself $\dot{Q}_{loss,BS,stor}$, cmp. Equation 2.40. The losses within the piping occur, since the water must be permanently provided there at tapping temperature $\vartheta_{DHW} = 57.5\,°\mathrm{C}$. The heat transmission coefficient U_{pip} of 0.26 W/mK , the pipe length L_{pip} of 56 m and the storage ambient temperature $\vartheta_S = 20\,°\mathrm{C}$, which is constant over the year, were taken from the standard [V.b]. The pipings heat loss is therefore constant at 533 W, cmp. Equation 2.41.

$$A_{BS,min} = 3\pi^{\frac{1}{3}} V_{BS}^{\frac{2}{3}} = \arg\min_{H_{cyl}} \quad 2\pi r_{cyl} H_{cyl} + \pi r_{cyl}^2 \quad \text{subject to} \quad V_{BS} = \pi r_{cyl}^2 H_{cyl} \tag{2.42}$$

On the other hand, heat losses occur at the buffer tank. Therefore a heat loss model is created depending on the current storage volumes exchange surface A_{BS}. The minimum surface of a cylindric tank is derived from the optimal problem, cmp. Equation 2.42. In order to apply a linear model for the surface the optimal linearisation within its given maximum storage volume $V_{BS,ub}$ is derived from the optimal problem, cpm. Equation 2.43.

$$A_{BS} = \frac{27}{8}\pi^{\frac{1}{3}} V_{BS,ub}^{-\frac{1}{3}} V_{BS} = a^* V_{BS} \quad a^* = \arg\min_{a} \quad \int_0^{V_{BS,ub}} (A_{BS,min} - aV_{BS})^2 dV_{BS} \tag{2.43}$$

The optimal linearised model for the tank surface is then used for the modelling of heat loss at the water buffer tank. For the heat transfer coefficient of the water buffer tank k_{BS} a wall thickness of metal $s_{met} = 5\,\text{mm}$ ($\lambda_{met} = 45\,\text{W/mK}$) and of insulation $s_{ins} = 8\,\text{cm}$ ($\lambda_{ins} = 0.04\,\text{W/mK}$) is assumed. The material properties are taken from the VDI Heat Atlas [e.V13]. Finally, Equation 2.46 describes the model used for the heat loss at the water buffer tank.

$$\dot{Q}_{loss,BS,stor} = k_{BS}(\vartheta_{BS} - \vartheta_S) A_{BS} \tag{2.44}$$

$$\frac{1}{k_{BS}} = \frac{s_{met}}{\lambda_{met}} + \frac{s_{ins}}{\lambda_{ins}} + \frac{1}{\alpha_{s,i}} = 2.13\,\text{m}^2\,\text{K}\,\text{W}^{-1} \tag{2.45}$$

$$\dot{Q}_{loss,BS,stor} = 0.81 V_{BS,ub}^{-\frac{1}{3}} V_{BS} \tag{2.46}$$

The linearisation of the two heat outputs of the lime storage module $\dot{Q}_{LS,dc}$, $\dot{Q}_{LS,hc}$ is preceded by the following subchapter, cmp. Equations 2.47 and 2.48.

$$\dot{Q}_{LS,dc} = \zeta\, P_{R,dc} \tag{2.47}$$

$$\dot{Q}_{LS,hc} = \xi\, \dot{m}_{B,hc} \tag{2.48}$$

With the volumetric energy content of water at the storage temperature $\rho_C h_C(\vartheta_{BS}) = 2.3 \times 10^5\,\text{J}\,\text{l}^{-1}$ the buffer storage model can be summarised in the following dynamic and transformation matrices.

$$\frac{\partial V_{BS}}{\partial t} = A_{BS}x_{BS} + B_{u,BS}u_{BS} + B_{v,BS}v_{BS} \tag{2.49}$$

$$A_{BS} = \frac{1}{\rho_C h_C(\vartheta_{BS})}\left(0.81 V_{BS,ub}^{-\frac{1}{3}}\right) \tag{2.50}$$

$$B_{u,BS} = \frac{1}{\rho_C h_C(\vartheta_{BS})}\begin{pmatrix}-1 & 1 & \zeta & \xi\end{pmatrix} \tag{2.51}$$

$$B_{v,BS} = \frac{1}{\rho_C h_C(\vartheta_{BS})}\begin{pmatrix}-506\end{pmatrix} \tag{2.52}$$

$$K_{BS} = \frac{1}{\rho_C h_C(\vartheta_{BS})}\begin{pmatrix}-533\end{pmatrix} \tag{2.53}$$

$$T_{x,BS} = \begin{pmatrix}0 & \cdots & 0 & 1 & 0\end{pmatrix} \in \mathbb{R}^{1\times 9} \tag{2.54}$$

$$T_{u,BS} = \begin{pmatrix}0 & \cdots & \cdots & 0 & 1 & 0 & \cdots & 0\\ \vdots & \ddots & & \vdots & 0 & \ddots & \ddots & \vdots\\ \vdots & & \ddots & \vdots & \vdots & \ddots & \ddots & 0\\ 0 & \cdots & \cdots & 0 & 0 & \cdots & 0 & 1\end{pmatrix} \in \mathbb{R}^{4\times 9} \tag{2.55}$$

$$T_{v,BS} = \begin{pmatrix}1 & 0 & \cdots & 0\end{pmatrix} \in \mathbb{R}^{1\times 6} \tag{2.56}$$

2.1.3 Lime Storage

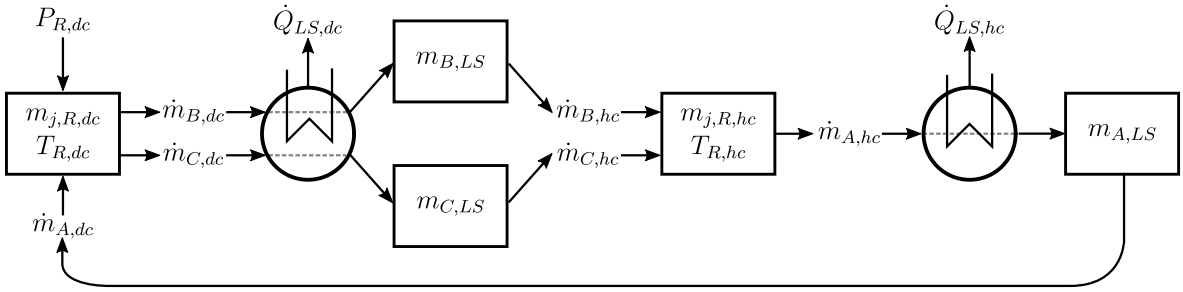

Figure 2.4: Flow diagram of the total lime storage module

The lime storage module, cmp. Figure 2.4, consists of a dehydration cycle (dc), a hydration cycle (hc) and the storage balances of all substances in between. These substances are calcium hydroxide $Ca(OH)_2$, also called slaked lime, calcium oxide CaO, also called burnt lime and water H_2O in liquid and gaseous states. The underlying chemical equation is given in Equation 2.57 and 2.58. Dehydration produces water vapour, whereas liquid water is used for hydration. Thus the reaction enthalpies differ in the evaporation enthalpy of water.

$$\mathrm{Ca(OH)_{2(s)}} + 104.4\,\mathrm{kJ/mol} \xrightarrow{\mathrm{dc}} \mathrm{CaO_{(s)}} + \mathrm{H_2O_{(g)}} \tag{2.57}$$

$$\mathrm{Ca(OH)_{2(s)}} + 63.8\,\mathrm{kJ/mol} \xleftarrow{\mathrm{hc}} \mathrm{CaO_{(s)}} + \mathrm{H_2O_{(l)}} \tag{2.58}$$

The charging reaction (dc) takes place in the dehydration cycle. Here calcium hydroxide reacts under the influence of thermal energy, at about $\vartheta_{R,dc} = 450\,°\mathrm{C}$, to calcium oxide and

water vapour according the literature [Ang+18]. Then the sensible and latent heat of both products is extracted in the heat exchanger up to the storage temperature $\vartheta_S = 20\,°C$. The discharge reaction takes place in the hydration cycle. During this process, the temporarily stored substances calcium oxide and liquid water react to form slaked lime, releasing the reaction enthalpy reduced by the evaporation enthalpy of water. This leads to the formation of the second part of the previously used reactor power $\dot{Q}_{LS,hc}$. The balances always assume a 100 % conversion rate of the educts. Therefore, there is no more educt in the product stream. All substance data used have been taken from the NIST Chemistry Webbook [LM] and the literature [Sch+12]. The reaction model and parameter have been taken from the literature [Ang+18].

The model of a reaction depends on the respective reactor concept and the specific reaction modelling. Therefore a short review of different reactor concepts is given. Different reactor concepts are summarised in the following review [PZ17]. In fixed bed reactors the reaction masses are, as the name suggests, distributed locally fixed in the reactor volume in the form of a powder bulk. The temperature level to start the dehydration reaction is provided by a either direct or indirect heat transfer. The indirect heat transfer occurs through the contact of the reaction mass with heating tubes or heating plates. The heat transfer medium flows in the areas thus separated and provides the necessary temperature level. The disadvantages of the concept are its limitations due to the low permeability and heat conduction of the fixed powder phase. The advantage of the separation of heat supply and reaction volume is that the equilibrium pressure of the reaction in the reactor volume is independent of that in the heat supply circuit [Sch+14]. A direct heat transfer is considered in the publication [Sch+13]. For this purpose, nitrogen is used as an inert gas for mass and heat transfer. The heated inert gas flows through the powder and thus provides the temperature level. Higher performances can be expected by a direct heat transfer. The modelling is based on a two-dimensional continuum model for gas and solid phase with partial differential equations to depict the thermal inertia of the powder bulk. A further decisive disadvantage of this discontinuous reactor concept is the coupling of the reactor power to the storage capacity [Ang+18]. In contrast, the reaction mass in the fluidised bed reactor flows continuously through the reactor. Due to an inflowing gas stream, the powder material is fluidised. This gas stream should consist of pure water vapour, since this allows the efficient removal of its condensation enthalpy after the reactor, which accounts for 40 % of the energy used [Ang+18]. For this reason the reactions take place in a pure steam atmosphere. The heat input can be realised indirectly via tube bundle heat exchangers or electric heating rods. This concept therefore not only offers the possibility of decoupling storage capacity and reactor power, but also shows a higher heat and mass transfer. Due to the prevailing homogeneity of the air and solid phase, this reactor concept can be modelled as a stationary continuous stirred tank reactor (CSTR) [Ang+18]. In this thesis a CSTR model was applied under the same assumptions. Further reactor concepts are presented in the review [PZ17].

The response time is the time in which the reactor temperature jumps to a steady state. In experimental studies [Cri+17] of fluidised-bed reactors, the response time is in the range of minutes for the dehydration and within seconds for the hydration reaction. The reactor dynamics are regarded as stationary throughout. The same assumption was applied in the literature [Ang+18].

The following subchapters apply the same systematic approach to the modelling of the reactors. First, all general balance equations, mass, component and energy balance of the model

are presented, then simplifying assumptions are made and the system of equations is reduced. Subsequently, the stationary reactor outlets, heat flows and mass flows are adjusted to an straight of origin.

Modelling of the Dehydration Reactor

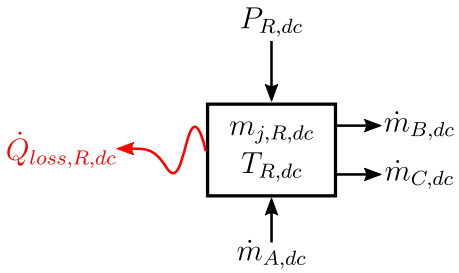

Figure 2.5: Balance element of the reactor for calcium hydroxide dehydration.

The reactor for dehydration of the calcium hydroxide is modelled as a continuous stirred tank reactor. Accordingly, the pressure $p_{R,dc}$, the temperature $T_{R,dc}$ and all concentrations of the educts and products are spatial homogeneous in the reactor. Equations 2.59 to 2.63 describe the total mass balance, the mole component balances of all substances and the energy balance of the system. The index A stands for calcium hydroxide ($Ca(OH)_2$), the index B stands for calcium oxide (CaO) and the index C stands for water. Since the reactor is assumed to be isobaric and warming effects due to friction are neglected, the impulse balance is not used. The enthalpy flux of calcium hydroxide flows into the reactor at storage temperature. However, the enthalpy flows of the products leave the reactor at reactor temperature. To differentiate this in the energy balance, the enthalpy flux of calcium hydroxide is identified with dependence on the storage temperature ϑ_S. The reactor factor η describes the transition of the electrical reactor input power $P_{R,dc}$ to the thermal energy available for the reaction. The influence of the factor η is discussed in the results section. The temperature inside the reactor causes a heat loss $\dot{Q}_{loss,R,dc}$ through the reactor shell.

$$\frac{\partial m_{R,dc}}{\partial t} = \dot{m}_{A,dc} - \dot{m}_{B,dc} - \dot{m}_{C,dc} = \sum_j \frac{\partial N_{j,R,dc}}{\partial t} MW_j \tag{2.59}$$

$$\frac{\partial N_{A,R,dc}}{\partial t} = \dot{N}_{A,dc} - V_R r_{R,dc} \tag{2.60}$$

$$\frac{\partial N_{B,R,dc}}{\partial t} = -\dot{N}_{B,dc} + V_R r_{R,dc} \tag{2.61}$$

$$\frac{\partial N_{C,R,dc}}{\partial t} = -\dot{N}_{C,dc} + V_R r_{R,dc} \tag{2.62}$$

$$\frac{\partial H_{R,dc}}{\partial t} = \dot{H}_{A,dc}(\vartheta_S) - \dot{H}_{B,dc} - \dot{H}_{C,dc} + \eta P_{R,dc} - \dot{Q}_{loss,R,dc} \tag{2.63}$$

In the following the assumptions for the above system of equations are introduced. The assumption A1 is valid, since both products of the dehydration reaction are formed in equal proportions in the reactor and are thus present in equal molar quantities. The assumption

A2 assumes a constant mass in the reactor $m_{R,dc}$. The same mass leaves the reactor as flows into it. There is no accumulation and reduction of the reactor mass.

$$A1 : N_{B,R,dc} = N_{C,R,dc} \quad \Rightarrow \frac{\partial N_{B,R,dc}}{\partial t} = \frac{\partial N_{C,R,dc}}{\partial t} \tag{2.64}$$

$$\Rightarrow \dot{N}_{B,dc} = \dot{N}_{C,dc} \tag{2.65}$$

$$A2 : \frac{\partial m_{R,dc}}{\partial t} = 0 \quad \Rightarrow \frac{\partial N_{B,R,dc}}{\partial t} = -\frac{\partial N_{A,R,dc}}{\partial t} = \frac{\partial N_{C,R,dc}}{\partial t} \tag{2.66}$$

$$\Rightarrow \dot{N}_{A,dc} = \dot{N}_{B,dc} = \dot{N}_{C,dc} \tag{2.67}$$

With A2 the mole mass of solid material $N_{s,dc}$ is constant. The mass of solid material m_R is prepared in the same way in the reactor for dehydration and hydration. It is the mass of calcium hydroxide with the bulk density $\rho_b = 470\,\mathrm{kg\,m^{-3}}$ in the reactor volume $V_R = 20\,\mathrm{l}$ and has the value $m_R = 9.4\,\mathrm{kg}$. For the molar mass of solid in the dehydration reactor $N_{s,dc}$ it is assumed that pure calcium hydroxide is present within the reactor. The approach for the reaction rate $r_{R,dc}$ was taken from the literature [Ang+18], because the author used a CSTR model and provided experimentally validated data in a pure water vapour atmosphere. This approach is dependent on the dimensionless reaction rate $\frac{\partial X_{dc}}{\partial t}$, the reactor temperature $T_{R,dc}$, the reactor pressure p_R, the equilibrium pressure of the reaction $p_{eq,dc}$ and the actual molar solid concentration of calcium hydroxide $X_{A,R,dc}$, cmp. Equations 2.69 to 2.71. The description of the dimensionless reaction rate, cmp. Equation 2.70 is divided according to a uniform scheme in its dependence on the reactor temperature $T_{R,dc}$, the reactor pressure p_R and the reactant concentration $X_{A,R,dc}$. Within the study [Ang+18], first standardised approaches were compared and then all theoretical parameters such as the collision factor and the activation energy were adjusted to the experimental data. The equilibrium pressure $p_{eq,dc}$ is the pressure that occurs when the reaction is left at chemical equilibrium at a selected temperature. Equation 2.71 was adjusted to the experimental data. The reactor pressure is the same for dehydration and hydration at $p_R = 1.5\,\mathrm{bar}$.

$$N_{s,dc} = N_{A,R,dc} + N_{B,R,dc} = \frac{m_R}{MW_A} \tag{2.68}$$

$$r_{R,dc} = \frac{N_{s,dc}}{V_R}\frac{\partial X_{dc}}{\partial t} \tag{2.69}$$

$$\frac{\partial X_{dc}}{\partial t} = 449974 \exp\left(-\frac{91282}{R\,T_{R,dc}}\right)\left(1 - \min\left\{1, \frac{p_R}{p_{eq,dc}}\right\}\right)^{3.47} X_{A,R,dc} \tag{2.70}$$

$$p_{eq,dc} = \exp\left(-\frac{13090}{T_{R,dc}} + 16.443\right) \tag{2.71}$$

$$X_{A,R,dc} = \frac{N_{A,R,dc}}{N_{s,dc}} \tag{2.72}$$

The enthalpy change in the reactor is isobaric and thus only depends on the reactor temperature and component change. Equation 2.73 show the total differential of the enthalpy according to temperature and the components mole mass. The enthalpy change after temperature is generally proportional to the specific heat capacity $c_{p,j}$ of a component j as well

as its mole mass $N_{j,R,dc}$ in the balance volume, cmp. Equation 2.74. The mean specific heat capacity $\bar{c}_{p,dc}$ is averaged over the molar solid concentrations, cmp. Equation 2.75. The enthalpy change after the component mole mass is generally the specific molar enthalpy $h_{j,R,dc}$, cmp. Equation 2.76. This work does not include mixing enthalpies, which why the specific molar enthalpies are equal to the pure substance enthalpies. This applies to dehydration as well as hydration. The component balances, Equations 2.60 to 2.62, are now inserted into the second part of the total differential. The reaction enthalpy $\Delta h_{r,dc}$ is formed from the specific enthalpies scaled with the stoichiometric coefficient $\nu_{j,dc}$.

$$\frac{dH_{R,dc}}{dt} = \left.\frac{\partial H_{R,dc}}{\partial T_{R,dc}}\right|_{N_{j,R,dc}\forall j} \frac{dT_{R,dc}}{dt} + \sum_{j}^{A,B,C} \left.\frac{\partial H_{R,dc}}{\partial N_{j,R,dc}}\right|_{T_{R,dc}} \frac{dN_{j,R,dc}}{dt} \tag{2.73}$$

$$\left.\frac{\partial H_{R,dc}}{\partial T_{R,dc}}\right|_{N_{j,R,dc}\forall j} = \sum_{j}^{A,B,C} N_{j,R,dc} c_{p,j} = N_{s,dc}\bar{c}_{p,dc} \tag{2.74}$$

$$\bar{c}_{p,dc} = (X_{A,R,dc}c_{p,A} + (1 - X_{A,R,dc})(c_{p,B} + c_{p,C})) \tag{2.75}$$

$$\left.\frac{\partial H_{R,dc}}{\partial N_{j,R,dc}}\right|_{T_{R,dc}} = h_{j,R,dc} \tag{2.76}$$

$$\sum_{j} h_{j,R,dc}\nu_{j,dc} = \Delta h_{r,dc} \tag{2.77}$$

All simplified Equations 2.74 to 2.77 are now summarised in Equation 2.78. This equation is then applied to the initial energy balance of Equation 2.63.

$$\frac{dH_{R,dc}}{dt} = N_{s,dc}\bar{c}_{p,dc}\frac{dT_{R,dc}}{dt} + h_{A,R,dc}\dot{N}_{A,dc} - \dot{H}_{B,dc} - \dot{H}_{C,dc} + \Delta h_{r,dc}V_R r_{R,dc} \tag{2.78}$$

$$N_{s,dc}\bar{c}_{p,dc}\frac{dT_{R,dc}}{dt} = \dot{N}_{A,dc}(h_{A,R,dc}(\vartheta_S) - h_{A,R,dc}) - \Delta h_{r,dc}V_R r_{R,dc} + \eta P_{R,dc} - \dot{Q}_{loss,R,dc} \tag{2.79}$$

The enthalpy difference, cmp. Equation 2.80 corresponds to the energy required to heat the calcium hydroxide. For the heat losses $\dot{Q}_{loss,R,dc}$ a reactor is assumed with the wall and insulation specifications of the water buffer tank. Therefore, the same heat transmission coefficient k_{BS} is applied. Additionally, the reactor surface A_R is that of a cube with the reactor volume V_R.

$$h_{A,R,dc}(\vartheta_S) - h_{A,R,dc} = -\int_{T_S}^{T_{R,dc}} c_{p,A}dT \tag{2.80}$$

$$\dot{Q}_{loss,R,dc} = \frac{1}{R_{th,R}}(T_{R,dc} - T_S) \tag{2.81}$$

$$R_{th,R} = \frac{1}{k_{BS}A_R} \tag{2.82}$$

$$A_R = 6V_R^{\frac{2}{3}} = 0.442\,\mathrm{m}^2 \tag{2.83}$$

The dynamics of the dehydration reactor can be summarised by the following differential equations. Due to the endothermic, self-cooling reaction the reaction enthalpy is greater than zero. It's value is $\Delta h_{r,dc} = 104.4\,\mathrm{kJ\,mol^{-1}}$ and was obtained from the publication [Ang+18].

$$\frac{\partial X_{A,R,dc}}{\partial t} = \frac{\dot{N}_{A,dc}}{N_{s,dc}} - \frac{\partial X_{dc}}{\partial t} \tag{2.84}$$

$$\frac{\partial T_{R,dc}}{\partial t} = \frac{1}{\bar{c}_{p,dc}} \left(-\frac{\dot{N}_{A,dc}}{N_{s,dc}} \int_{T_S}^{T_{R,dc}} c_{p,A} dT - \frac{\partial X_{dc}}{\partial t} \Delta h_{r,dc} + \frac{\eta P_{R,dc} - \frac{1}{R_{th,R}} (T_{R,dc} - T_S)}{N_{s,dc}} \right) \tag{2.85}$$

As indicated in the introduction, the unsteady effects of heating and cooling the reactor volume are neglected due to the short response time. In addition, a constant solid concentration of $X_{A,R,dc} = 1$, pure calcium hydroxide in the reactor is defined. According to this, there is always as much educt flowing into the reactor as products flow out. The relation of the steady state reactor temperature to the incoming reactor power $T_{R,dc} = f(P_{R,dc})$ is determined by the following zero point problem.

$$0 = -\frac{\partial X(T_{R,dc})}{\partial t} \left(\int_{T_S}^{T_{R,dc}} c_{p,A} dT + \Delta h_r(T_{R,dc}) \right) + \frac{\eta P_{R,dc} - \frac{1}{R_{th,R}} (T_{R,dc} - T_S)}{N_{s,dc}} \tag{2.86}$$

The energy balance of the subsequent heat exchanger provides the heat flow $\dot{Q}_{LS,dc}$ during dehydration, cmp. Equation 2.88. Therefore the water vapour is completely condensed and cooled down to storage temperature as the calcium oxide. The mass flow of the calcium oxide product is only a temperature dependent function, cmp. Equation 2.89.

$$\dot{Q}_{LS,dc} = \dot{N}_{B,dc}(h_B(T_{R,dc}) - h_B(T_S)) + \dot{N}_{C,dc}(h_C(T_{R,dc}) - h_C(T_S)) \tag{2.87}$$

$$= N_{s,dc} \frac{\partial X(T_{R,dc})}{\partial t} \int_{T_S}^{T_{R,dc}} c_{p,B} + c_{p,C} dT \tag{2.88}$$

$$\dot{m}_{B,dc} = \frac{1}{MW_B} \dot{N}_{B,dc} = \frac{1}{MW_B} N_{s,dc} \frac{\partial X(T_{R,dc})}{\partial t} \tag{2.89}$$

For the dynamics of the overall system the dependencies, $\dot{Q}_{LS,dc} = f(P_{R,dc})$ and $\dot{m}_{B,dc} = f(P_{R,dc})$ are decisive. These are linear, determined by the steady-state reactor temperature and adjusted to an origin line. The following adjustment lines were used for the further investigations.

$$\dot{Q}_{LS,dc} = \zeta\, P_{R,dc} = 0.4636\, P_{R,dc} \tag{2.90}$$

$$\dot{m}_{B,dc} = \kappa\, P_{R,dc} = 4.3520 \cdot 10^{-7}\, P_{R,dc} \tag{2.91}$$

According to this, about 46 % of the input power turns directly into heat whereas 54 % is stored in the form of chemical energy.

Modelling of the Hydration Reactor

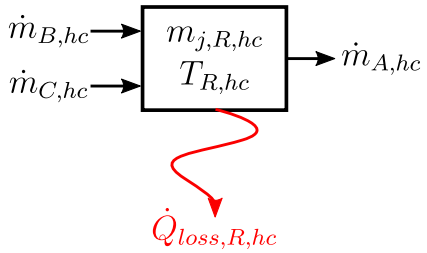

Figure 2.6: Balance element of the reactor for calcium oxide hydration.

The reactor for hydration of the calcium oxide is also modelled as a continuous stirred tank reactor. Equations 2.92 to 2.96 describe the total mass balance, the mole component balances of all components and the energy balance of the system. The enthalpy flux of calcium oxide and liquid water flow into the reactor at storage temperature. However, the enthalpy flow of calcium hydroxide leave the reactor at reactor temperature. The reactor temperature causes the heat loss $\dot{Q}_{loss,R,hc}$ through the reactor shell.

$$\frac{\partial m_{R,hc}}{\partial t} = -\dot{m}_{A,hc} + \dot{m}_{B,hc} + \dot{m}_{C,hc} = \sum_j \frac{\partial N_{j,R,hc}}{\partial t} MW_j \tag{2.92}$$

$$\frac{\partial N_{A,R,hc}}{\partial t} = -\dot{N}_{A,hc} + V_R r_{R,hc} \tag{2.93}$$

$$\frac{\partial N_{B,R,hc}}{\partial t} = \dot{N}_{B,hc} - V_R r_{R,hc} \tag{2.94}$$

$$\frac{\partial N_{C,R,hc}}{\partial t} = \dot{N}_{C,hc} - V_R r_{R,hc} \tag{2.95}$$

$$\frac{\partial H_{R,hc}}{\partial t} = -\dot{H}_{A,hc} + \dot{H}_{B,hc}(\vartheta_S) + \dot{H}_{C,hc}(\vartheta_S) - \dot{Q}_{loss,R,hc} \tag{2.96}$$

The assumptions A1 and A2 are similar to those in the dehydration reactor. The mass of solid m_R is prepared in the same way in the reactor for dehydration and hydration. The powder mass m_R is 9.4 kg. Though pure calcium oxide is used for the molar mass of solids $N_{s,hc}$, cmp. Equation 2.101.

$$A1 : N_{B,R,hc} = N_{C,R,hc} \qquad \Rightarrow \frac{\partial N_{B,R,hc}}{\partial t} = \frac{\partial N_{C,R,hc}}{\partial t} \tag{2.97}$$

$$\Rightarrow \dot{N}_{B,hc} = \dot{N}_{C,hc} \tag{2.98}$$

$$A2 : \frac{\partial m_{R,hc}}{\partial t} = 0 \qquad \Rightarrow \frac{\partial N_{B,R,hc}}{\partial t} = -\frac{\partial N_{A,R,hc}}{\partial t} = \frac{\partial N_{C,R,hc}}{\partial t} \tag{2.99}$$

$$\Rightarrow \dot{N}_{A,hc} = \dot{N}_{B,hc} = \dot{N}_{C,hc} \tag{2.100}$$

The approach for the hydration reaction rate $r_{R,hc}$, cmp. Equations 2.102 to 2.104 was also taken from the literature [Ang+18]. The description is similar to those of the dehydration,

cmp. Equations 2.69 to 2.71. The reactor pressure is equal for dehydration and hydration at $p_R = 1.5\,\mathrm{bar}$.

$$N_{s,hc} = N_{A,R,hc} + N_{B,R,hc} = \frac{m_R}{MW_B} \tag{2.101}$$

$$r_{R,hc} = \frac{N_{s,hc}}{V_R}\frac{\partial X_{hc}}{\partial t} \tag{2.102}$$

$$\frac{\partial X_{hc}}{\partial t} = 390827 \exp\left(-\frac{87460}{R\,T_{R,hc}}\right)\left(\max\left\{1, \frac{p_R}{p_{eq,hc}}\right\} - 1\right)^{3.43} X_{B,R,hc} \tag{2.103}$$

$$p_{eq,hc} = \exp\left(-\frac{9713.3}{T_{R,hc}} + 12.725\right) \tag{2.104}$$

$$X_{B,R,hc} = \frac{N_{B,R,hc}}{N_{s,hc}} \tag{2.105}$$

The total differential is established under the same assumptions as for dehydration. From this results the simplified description of the enthalpy change, cmp. Equation 2.106. Equation 2.107 repeats the energy balance of hydration for the understanding of further simplifications.

$$\frac{dH_{R,hc}}{dt} = N_{s,hc}\bar{c}_{p,hc}\frac{dT_{R,hc}}{dt} - \dot{H}_{A,hc} + \dot{N}_{B,hc}h_{B,R,hc} + \dot{N}_{C,hc}h_{C,R,hc} + \Delta h_{r,hc}V_R r_{R,hc} \tag{2.106}$$

$$= -\dot{H}_{A,hc} + \dot{N}_{B,hc}h_{B,R,hc}(\vartheta_S) + \dot{N}_{C,hc}h_{C,R,hc}(\vartheta_S) - \dot{Q}_{loss,R,hc} \tag{2.107}$$

The enthalpy difference, cmp. Equation 2.108 corresponds to the energy required to condition the calcium oxide and water. For the heat losses in the reactor $\dot{Q}_{loss,R,hc}$ the same approach is assumed as for the dehydration reactor.

$$h_{B,R,hc}(\vartheta_S) - h_{B,R,hc} + h_{C,R,hc}(\vartheta_S) - h_{C,R,hc} = -\int_{T_S}^{T_{R,hc}} c_{p,B} + c_{p,C}dT \tag{2.108}$$

$$Q_{loss,R,hc} = \frac{1}{R_{th,R}}(T_{R,hc} - T_S) \tag{2.109}$$

The dynamics of the hydration reactor can be summarised by the following differential equations. Due to the exothermic, self-heating reaction the reaction enthalpy is less than zero. Its value is $\Delta h_{r,hc} = -65\,\mathrm{kJ\,mol^{-1}}$. This reaction enthalpy is lower than that of the dehydration reaction due to the evaporation enthalpy of water.

$$\frac{\partial X_{B,R,hc}}{\partial t} = -\frac{\dot{N}_{B,hc}}{N_{s,hc}} + \frac{\partial X_{hc}}{\partial t} \tag{2.110}$$

$$\frac{\partial T_{R,hc}}{\partial t} = \frac{1}{\bar{c}_{p,hc}}\left(-\frac{\dot{N}_{B,hc}}{N_{s,hc}}\int_{T_S}^{T_{R,hc}} c_{p,B} + c_{p,C}dT - \frac{\partial X_{hc}}{\partial t}\Delta h_{r,hc}(T_{R,hc})\right) - \frac{1}{\bar{c}_{p,hc}}\left(\frac{1}{R_{th,R}N_{s,hc}}(T_{R,hc} - T_S)\right) \tag{2.111}$$

The hydration reaction is also regarded as steady state. In addition, a constant solid concentration of $X_{B,R,hc} = 1$, pure calcium oxide is used in the reactor. Thus, only as much educts are fed into the reactor as react and product flows out. The dependence of the steady state reactor temperature on the incoming amount of reactant $T_{R,hc} = f(\dot{m}_{B,hc})$ is determined by the following zero point problem.

$$0 = -\frac{\dot{N}_{B,hc}}{N_{s,hc}} \left(\int_{T_S}^{T_{R,hc}} c_{p,B} + c_{p,C} dT + \Delta h_{r,hc}(T_{R,hc}) \right) - \frac{1}{R_{th,R} N_{s,hc}} (T_{R,hc} - T_S) \tag{2.112}$$

The energy balance surrounding the subsequent heat exchanger provides the heat flow $\dot{Q}_{LS,hc}$ resulting from hydration.

$$\dot{Q}_{LS,hc} = \frac{\dot{m}_{B,hc}}{MW_B} (h_B(T_{R,hc}) - h_B(T_S)) \tag{2.113}$$

The dependency, $\dot{Q}_{LS,hc} = f(\dot{m}_{B,hc})$, which is important for the dynamics of the overall system, is linear, determined by the steady-state reactor temperature and adjusted to an straight of origin. The following adjustment lines were used for the investigations.

$$\dot{Q}_{LS,hc} = \xi \, \dot{m}_{B,hc} = 1175950.97 \, \dot{m}_{B,hc} \tag{2.114}$$

Modelling of the Lime Storage

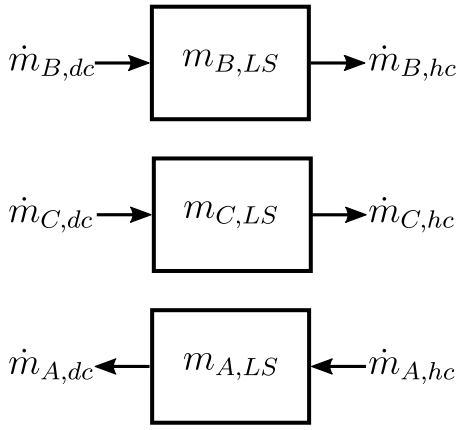

Figure 2.7: Balance elements of the lime storage for each components.

The dynamics, Equations Equation 2.115 to 2.117 represent the three component balances of the storage elements. No energy balance is necessary, since the substances are stored isothermal. Valid assumptions of hydration and dehydration, cmp. Equation 2.67 and 2.100 reduce the equations.

$$\frac{\partial N_{B,LS}}{\partial t} = \dot{N}_{B,dc} - \dot{N}_{B,hc} \tag{2.115}$$
$$\frac{\partial N_{C,LS}}{\partial t} = \dot{N}_{C,dc} - \dot{N}_{C,hc} \tag{2.116}$$
$$\frac{\partial N_{A,LS}}{\partial t} = -\dot{N}_{A,dc} + \dot{N}_{A,hc} \tag{2.117}$$

The entire dynamics of the lime storage module can therefore be summarised in Equation 2.118. The parameter κ is set according to Equation 2.91.

$$\frac{\partial m_{B,LS}}{\partial t} = \kappa P_{R,dc} - \dot{m}_{B,hc} = B_{u,LS} u_{LS} \tag{2.118}$$
$$B_{u,LS} = \begin{pmatrix} \kappa & -1 \end{pmatrix} \tag{2.119}$$
$$T_{u,LS} = \begin{pmatrix} 0 & \cdots & 0 & 1 & 0 \\ 0 & \cdots & 0 & 0 & 1 \end{pmatrix} \in \mathbb{R}^{2\times 9} \tag{2.120}$$

2.2 Model Predictive Control

2.2.1 General MPC Setting

„Model Predictive Control (MPC) is a method of designing and implementing feedback control systems that, in many situations, perform better than those created by other methods “,[RL19, p. 3]. MPC belongs to the class of optimal controllers. It differs from the simplest optimal controller, the linear quadratic regulator (LQR), by offering the possibilities to control nonlinear multi-input-multi-output systems (MIMO), to consider actuator saturations and to realise a large class of performance measures. Furthermore, the infinite horizon closed loop optimal control problem is divided into a repeated solution of open loop finite horizon problems. In contrast to the LQR, there is no explicit optimal feedback law but an optimal input sequence. This leads to a quickly increasing calculation complexity with the prediction horizon. MPC is becoming more and more attractive compared to classical controllers and is increasingly spreading in applications due to the growing computing power. Equation 2.121 provides the basic mathematical formulation of the MPC setting. The cost function J is often formulated as an integral about the stage cost L by time. Some MPC setting use a terminal cost F to consider the terminal state. The optimal problem is extended by various constraints that have to be satisfied. The system model makes the prediction possible under consideration of the optimal input sequence and the initial state x(t). The state and input constraints as well as the terminal region consider plant design specifications, cmp. $\mathbb{X}$, $\mathbb{U}$ and $\mathbb{X}^f$. Predicted variables are marked by a bar.

$$
\begin{aligned}
u(\cdot,t)^* = \underset{\bar{u}(\cdot,t)}{\arg\min} \quad & J(x(t),\bar{u}(\cdot,t)) = \int_t^{t+T} L(\bar{x}(\tau,t),\bar{u}(\tau,t))d\tau + F(\bar{x}(t+T,t)) \\
\text{subject to} \quad & \bar{x}(t,t) = x(t), \\
& \dot{\bar{x}}(\tau,t) = f(\bar{x}(\tau,t),\bar{u}(\tau,t)) \quad \forall \tau \in [t,t+T], \\
& \bar{u}(\tau,t) \in \mathbb{U} \quad \forall \tau \in [t,t+T], \\
& \bar{x}(\tau,t) \in \mathbb{X} \quad \forall \tau \in [t,t+T], \\
& \bar{x}(t+T,t) \in \mathbb{X}^f \subseteq \mathbb{X}
\end{aligned}
\tag{2.121}
$$

The MPC algorithm is structured as follows: **first** the open loop finite horizon optimal problem is solved based on the initial value x(t). For this purpose the system model is used to predict all system states. Now the performance measure evaluates each individual possibility of the input sequence and selects the optimal sequence based on the criterion. As a **second** step, the first value of the optimal input sequence is applied to the system. As a **third** step, the system response or the now existing system state is measured. The algorithm then starts from the beginning.

Among the most important properties of MPC are closed-loop stability, recursive feasibility and optimality. The book [RL19] offers more detailed information and proofs. Several MPC problems differ according to the performance measure, the more or less extensive use of constraints and the handling of disturbances or references. Robust MPC or stochastic MPC algorithms use informations about bounded or distributed disturbances on system states and inputs to narrow their origin constraint set and ensure feasibility. The following authors developed a robust [Tan+17] and a stochastic MPC approach [Old+10] for building climate control. While stabilising MPC algorithms usually include quadratic costs, this limitation on the stage cost is not present in economic MPC. With economic MPC, the focus is on maximising profits or minimising operation costs. The stage cost is therefore often an economic measure. In this work an economic MPC approach is followed. The stage costs reflect the consumption of electrical energy or the financial operation costs.

2.2.2 Fundamentals of the MPC Approaches

„In hierarchical multilayer systems, the control action is performed by a number of regulators working at different time scales“, [Sca09]. Hierarchical control algorithms are used if the system is characterised by very different dynamics or if the control task is to be divided into an optimisation and a stabilisation or reference tracking of the manipulated variables set points. This structure is given, among others, in the petrochemical industry. The top level represents the slowest system dynamics, which must be optimised over a long period of time. This corresponds to the level of Real Time Optimisation (RTO) in the process engineering industry and is accompanied by a detailed non-linear system model and a mostly economic performance measure. These inputs have to be met by the lower hierarchical layers, which have fast dynamics. The sampling rate of the control decreases with the hierarchy level. „In order to guarantee that references computed at the higher layer are feasible for the lower layer dynamics and constraints, as well as to consider the presence of disturbances acting at the lower layer, some additional information has often to be transmitted bottom-up“, [Sca09].

In order to guarantee the stability of the system dynamics, the controllers of the lowest level of the hierarchy must eliminate possible errors of the manipulated variables within their sampling rate. This procedure is generally referred to as cascade control. „In the design phase, the inner loops are often closed with standard PI or PID regulators, while MPC is used to design the control algorithm for the slowest system“, [Sca09].

Figure 2.8 shows the two different types of hierarchy in the approaches for seasonal energy storage developed in this work.

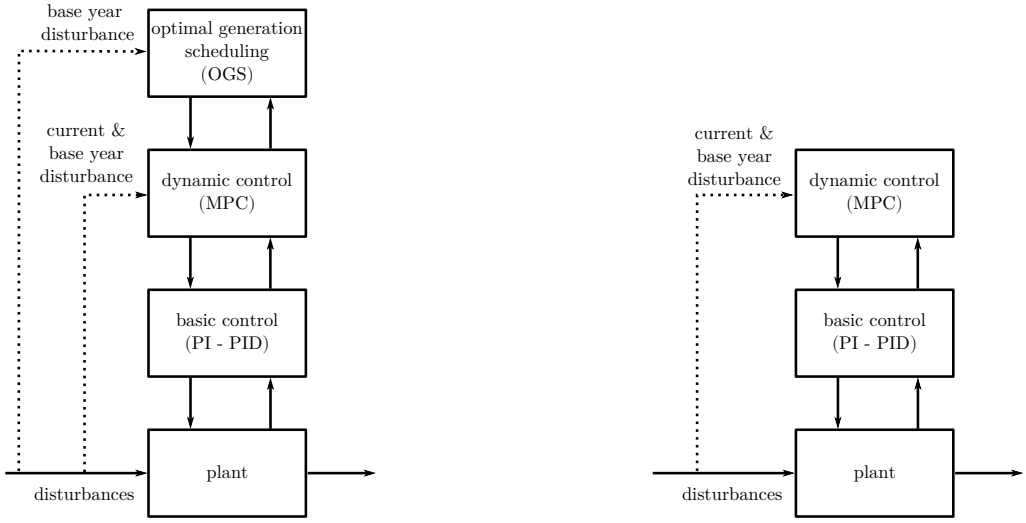

Figure 2.8: Hierarchy approaches for system control. Left: Flexible reference tracking, Right: mixed approach

The hierarchical approaches of this work covers two levels of superior hierarchy. The field level is not treated. All approaches use the weather and occupancy data of the upcoming 5 days of the current year to determine the optimal system inputs. As the lime storage module doesn't offer advantages within this short time, a possibility to estimate the forthcoming weather and occupancy data must be found. Therefore, the weather and occupancy data of the base year are used for this purpose. They provide the information to access the lime mass to be stored in the future. All approaches differ only in the supply of this base year information. As mentioned in the introduction, the base year consists of averaged weather data. The occupancy data are the same for the current and base year. In this paper we also examine the approximation by the base year information. For this purpose weather data from 2015 or 2016 are used as base year data besides averaged data. More about this in the results section. As described in Figure 2.8 the **flexible reference tracking** , abbr. flex, approaches consists of a longterm energy management or optimal generation scheduling (OGS) and short term dynamic MPC. The OGS supplies state set points of the lime storage mass $m_{B,LS}$, to the dynamic MPC. The current work discusses two different approaches to dynamic MPC within the flexible reference tracking hierarchy. Both approaches consist of a short term energy management within the current year prediction horizon t_{cy} for the next 5 days and a reference tracking part of the lime storage state. The first approach flex1 does not use disturbance data of the base year. It includes the value of the lime storage level at the end of the current year prediction horizon in the objective function. The second approach flex2 should be fixed at the lime storage level of the higher-level schedule OGS_{by} after the end of a transition period t_{trans}. During the transition period it also includes the base year's

disturbance data. It is necessary to find a trade-off in order to follow the OGS trajectory from the best and on the other hand to use possible increased or decreased yields in the current year. In contrast, the **mixed approach**, abbr. mixed, has no superior OGS. It contains the 5 days current year disturbance prediction and the base year disturbance prediction within the horizon t_{by}. Figure 2.9 summaries all approaches.

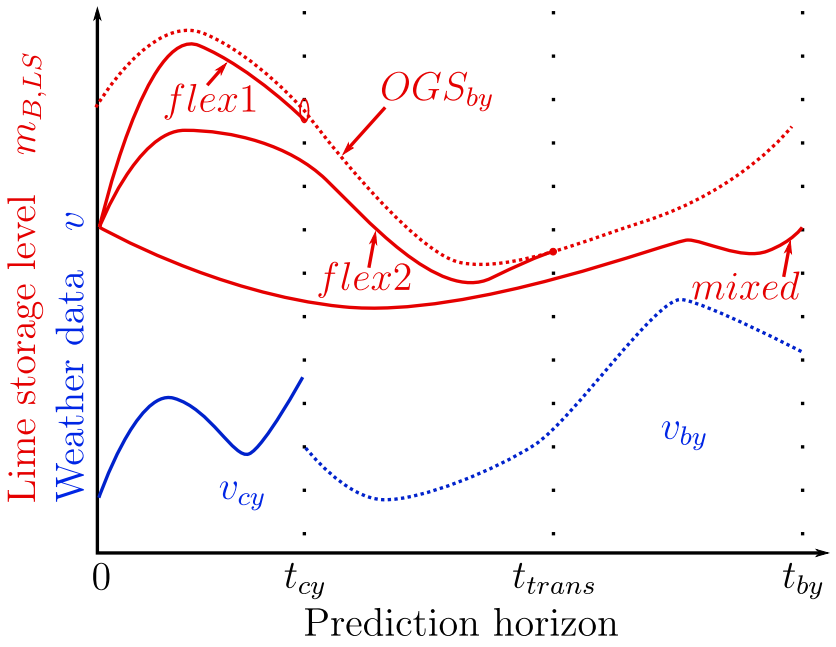

Figure 2.9: Summary of proposed control approaches and disturbance approximation.

Both approaches will be compared with the OGS trajectory of the current year 2016. It reflects the best possible lime storage trajectory, since the entire disturbance data of 2016 are considered in one optimal problem. The calculations of OGS or MPC simulations were carried out with the algorithmic differentiation Matlab toolbox CasADi [And+19].

2.2.3 Flexible Reference Tracking

Optimal Generation Scheduling

The OGS algorithm uses the disturbance inputs of the base year to determine the most optimal trajectory of system states and inputs in terms of energy costs or energy consumption. The optimisation setting for OGS, Equation 2.122 is discretised with a with a time step of 3600 seconds or one hour. The stage cost is the annual energy consumption *ec*, cmp. Equation 2.123. The coefficients of performance of the chiller and heat pump were extracted from the literature [Fin+18] and have the values $COP_{CHI} = 4.4$ and $COP_{CHI} = 3.5$. Simulations called *oc* have the same settings but the annual operation cost as target, cmp. Equation 2.124. The time variant state and manipulated input constraint sets are those of Equation 2.10 and 2.11, respectively. The initial condition of the optimisation setting reflects the periodicity of the disturbance input. All results of the system analysis from section 3.1 are created and compared using this optimisation setting.

$$
\begin{aligned}
\underset{u}{\text{minimize}} \quad & \sum_{k=0}^{n-1} L_{oc,by}(k)dT \\
\text{subject to} \quad & n = 8760, \\
& x(0) = x(n), \\
& x(k+1) = f(x(k), u(k), v_{by}(k)) \quad \forall k \in [0, n-1], \\
& u(k) \in \mathbb{U} \quad \forall k \in [0, n-1], \\
& x(k) \in \mathbb{X}(k) \quad \forall k \in [0, n]
\end{aligned} \tag{2.122}
$$

$$L_{ec,by}(k) = \frac{\dot{Q}_{CHI,by}(k)}{COP_{CHI}} + \frac{\dot{Q}_{HP,by}(k)}{COP_{HP}} + P_{R,dc,by}(k) \tag{2.123}$$

$$L_{oc,by}(k) = c_{by}(k) L_{ec,by}(k) \tag{2.124}$$

Dynamic MPC: Approach 1

The dynamic control of the flexible reference tracking approach is based on the idea to design a performance measure, which on the one hand uses the current weather forecast of the next 5 days and on the other hand follows a previously calculated optimal trajectory (OGS) of the lime storage level. Therefore, this approach is called flexible reference tracking. The performance measure is derived for system configurations with lime storage *LS*, cmp. Equation 2.124 without the heat pump input, and then adopted for the configuration lime storage plus heat pump *LSHP*. It is derived from the idea that the weather / occupancy forecast consists of the current year forecast of the next 5 days and then the forecasts within a transition time t_{trans} based on the base disturbance inputs at this time of the year. Therefore, the performance measure is divided into the current year prediction horizon, cmp. Equation 2.127 and the transition time, cmp. Equation 2.128. Both integrals differ only in the disturbance input data. At the end of the transition period, possible deviations of the lime storage level from that of the scheduling hierarchy should be eliminated.

$$J = \int_{t_0}^{t_{cy}+t_{trans}} L_{oc}(\tau)d\tau \tag{2.125}$$

$$= \int_{t_0}^{t_{cy}} L_{oc}(\tau)d\tau + \int_{t_{cy}}^{t_{trans}} L_{oc}(\tau)d\tau \tag{2.126}$$

$$\int_{t_0}^{t_{cy}} L_{oc}(\tau)d\tau = \int_{t_0}^{t_{cy}} c(\tau) \left(\frac{\dot{Q}_{CHI}(\tau)}{COP_{CHI}} + P_{R,dc}(\tau) \right) d\tau \tag{2.127}$$

$$\int_{t_{cy}}^{t_{trans}} L_{oc}(\tau)d\tau = \int_{t_{cy}}^{t_{trans}} c_{by}(\tau) \left(\frac{\dot{Q}_{CHI}(\tau)}{COP_{CHI}} + P_{R,dc}(\tau) \right) d\tau \tag{2.128}$$

For the second range, $\tau \in [t_{cy}, t_{trans}]$, cmp. Equation 2.128 the error dynamic, cmp. Equation 2.132 is applied to derive a prediction of the inputs within the transition period. This is based on the idea that the building states and inputs correspond to those of the base year

with the same disturbance inputs. Accordingly the error variables of the system are reduced to the states and inputs of the storage parts, cmp. Equation 2.133.

$$\Delta x = x - x_{by} \tag{2.129}$$
$$\Delta u = u - u_{by} \tag{2.130}$$
$$\Delta v = v - v_{by} \tag{2.131}$$
$$\Delta \dot{x} = A\Delta x + B_u \Delta u + B_v \Delta v + \sum_{i=1}^{dim_u} B_{vu,i} v u_i - B_{vu,i} v_{by} u_{by,i} \tag{2.132}$$
$$\Delta x = \begin{pmatrix} 0 \\ \vdots \\ 0 \\ \Delta V_{BS} \\ \Delta m_{B,LS} \end{pmatrix} \quad \Delta u = \begin{pmatrix} 0 \\ \vdots \\ 0 \\ \Delta P_{R,dc} \\ \Delta \dot{m}_{B,hc} \end{pmatrix} \quad \Delta v = \begin{pmatrix} 0 \\ \vdots \\ 0 \end{pmatrix} \tag{2.133}$$

These assumptions, cmp. Equation 2.133 are now inserted into the error dynamic, cmp. Equation 2.132. Further simplifications have been applied through the zeros included in the matrix $B_{v,u,i}$. Thus a reduced error dynamic, cmp. Equation 2.134 can be isolated, which describes the deviation of the storage states. Equation 2.135 describes the inverse of the dynamics equation.

$$\begin{pmatrix} \Delta \dot{V}_{BS} \\ \Delta \dot{m}_{B,LS} \end{pmatrix} = \begin{pmatrix} e & 0 \\ 0 & 0 \end{pmatrix} \begin{pmatrix} \Delta V_{BS} \\ \Delta m_{B,LS} \end{pmatrix} + \begin{pmatrix} a & c \\ d & b \end{pmatrix} \begin{pmatrix} P_{R,dc} \\ \Delta \dot{m}_{B,hc} \end{pmatrix} \tag{2.134}$$
$$\begin{pmatrix} \Delta P_{R,dc} \\ \Delta \dot{m}_{B,hc} \end{pmatrix} = \frac{1}{ab - cd} \begin{pmatrix} b & -c \\ -d & a \end{pmatrix} \begin{pmatrix} \Delta \dot{V}_{BS} - e\Delta V_{BS} \\ \Delta \dot{m}_{B,LS} \end{pmatrix} \tag{2.135}$$

The previously mentioned linear decrease of the error within the interval, $\tau \in [t_{cy}, t_{trans}]$, reflect Equations 2.136 and 2.137. The error dynamics of the storage states can be derived from this, cmp. Equation 2.138 and 2.139. Equations Equation 2.140 and 2.141 describe two parameters that precede the following derivation.

$$\Delta V_{BS}(\tau) = (t_{trans} - \tau) \frac{\Delta V_{BS}(t_{cy})}{t_{trans} - t_{cy}} \tag{2.136}$$
$$\Delta m_{B,LS}(\tau) = (t_{trans} - \tau) \frac{\Delta m_{B,LS}(t_{cy})}{t_{trans} - t_{cy}} \tag{2.137}$$
$$\Delta \dot{V}_{BS}(\tau) = \frac{-\Delta V_{BS}(t_{cy})}{t_{trans} - t_{cy}} \tag{2.138}$$
$$\Delta \dot{m}_{B,LS}(\tau) = \frac{-\Delta m_{B,LS}(t_{cy})}{t_{trans} - t_{cy}} \tag{2.139}$$
$$p_1 = \frac{b(1 + e(t_{trans} - t_{cy}))}{(ab - cd)} \tag{2.140}$$
$$p_2 = -\frac{c}{ab - cd} \tag{2.141}$$

These assumptions are then used in the prediction of the reactor input power, cmp. Equation 2.142.

$$\Delta P_{R,dc} = \frac{b}{ab-cd}\left(\Delta\dot{V}_{BS} - e\Delta V_{BS}\right) - \frac{c}{ab-cd}\Delta\dot{m}_{B,LS} \tag{2.142}$$

$$= \frac{b}{ab-cd}\frac{-\Delta V_{BS}(t_{cy})}{t_{trans}-t_{cy}}(1+e(t_{trans}-\tau)) + \frac{c}{ab-cd}\frac{\Delta m_{B,LS}(t_{cy})}{t_{trans}-t_{cy}} \tag{2.143}$$

$$= -p_1\frac{\Delta V_{BS}(t_{cy})(1+e(t_{trans}-\tau))}{(t_{trans}-t_{cy})(1+e(t_{trans}-t_{cy}))} - p_2\frac{\Delta m_{B,LS}(t_{cy})}{t_{trans}-t_{cy}} \tag{2.144}$$

This allows the analytical evaluation of the objective function in the range $\tau \in [t_{cy}, t_{trans}]$, cmp. Equation 2.146. The first part of this equation is only dependent on the inputs of the base year, thus doesn't affect the performance measure and is summarised as $J_{t_{cy}-t_{trans},by}$. It is therefore neglected in the flex1 optimisation setting, cmp. Equation 2.150. The description of the reactor input power, cmp. Equation 2.142, is used for the second part of Equation 2.146. It is therefore assumed that the electricity price is at its mean value $\bar{c}_{by}$ within the interval $\tau \in [t_{cy}, t_{trans}]$.

$$\int_{t_{cy}}^{t_{trans}} L_{oc}(\tau)d\tau = \int_{t_{cy}}^{t_{trans}} c_{by}(\tau)\left(\frac{\dot{Q}_{CHI}(\tau)}{COP_{CHI}} + P_{R,dc}(\tau)\right)d\tau \tag{2.145}$$

$$= \int_{t_{cy}}^{t_{trans}} c_{by}(\tau)\left(\frac{\dot{Q}_{CHI,by}(\tau)}{COP_{CHI}} + P_{R,dc,by}(\tau)\right)d\tau + \int_{t_{cy}}^{t_{trans}} c_{by}(\tau)\Delta P_{R,dc}(\tau)d\tau \tag{2.146}$$

$$= J_{t_{cy}-t_{trans},by} - \int_{t_{cy}}^{t_{trans}} c_{by}(\tau)p_1\frac{\Delta V_{BS}(t_{cy})(1+e(t_{trans}-\tau))}{(t_{trans}-t_{cy})(1+e(t_{trans}-t_{cy}))}d\tau \tag{2.147}$$

$$- \int_{t_{cy}}^{t_{trans}} c_{by}(\tau)p_2\frac{\Delta m_{B,LS}(t_{cy})}{t_{trans}-t_{cy}}d\tau \tag{2.148}$$

$$= J_{t_{cy}-t_{trans},by} + p_1\bar{c}_{by}(V_{BS,by}(t_{cy}) - V_{BS}(t_{cy})) + p_2\bar{c}_{by}(m_{B,LS,by}(t_{cy}) - m_{B,LS}(t_{cy})) \tag{2.149}$$

For the first approach of the dynamic control within the flexible reference tracking hierarchy, the following discrete optimisation problem appears with a discretisation step size of one hour $dT = 3600\,\mathrm{s}$ and a prediction horizon of the current year t_{cy} of 5 days, this corresponds to the time steps $n = 120$, cmp. Equation 2.150. During the elaboration of the flex reference tracking approach it turned out that a change of the power m and the introduction of the pre-factor p_v within the objective has a positive effect on the annual performance. The coefficient p_2 has been set to zero due to infeasibility problems. Accordingly, only a reference tracking of the lime storage level is applied.

$$\begin{aligned}
\underset{u}{\text{minimize}} \quad & \sum_{k=0}^{n-1} c(k) \left(\frac{\dot{Q}_{CHI}(k)}{COP_{CHI}} + \frac{\dot{Q}_{HP}(k)}{COP_{HP}} + P_{R,dc}(k) \right) dT \\
& + p_v \bar{c}_{by} (p_1 (V_{BS,by}(n) - V_{BS}(n))^m + p_2 (m_{B,LS,by}(n) - m_{B,LS}(n))^m) dT \\
\text{subject to} \quad & n = \frac{t_{cy}}{dT}, \\
& x(0) = x(t_0), \\
& x(k+1) = f(x(k), u(k), v(k)) \qquad \forall k \in [0, n-1], \\
& u(k) \in \mathbb{U} \qquad \forall k \in [0, n-1], \\
& x(k) \in \mathbb{X}(k) \qquad \forall k \in [0, n]
\end{aligned} \tag{2.150}$$

Dynamic MPC: Approach 2

The second approach for dynamic MPC within the flexible reference method is now introduced. As the first approach it also has the objective costs within the current year prediction horizon t_{cy} of 5 days. The second part describes the operation costs within the transition period t_{trans} within which possible deviations of the states from those of the base year should disappear. The disturbance inputs within the transition period are those of the base year. The decisive differences to the first approach are on the one hand that all inputs within the transition period are also part of the optimisation. On the other hand this approach receives its information of the superordinate scheduling by the final state constraint of the lime storage mass. The discretisation step is also one hour $dT = 3600\,\text{s}$. The states $\tilde{x}$ and inputs $\tilde{u}$ are those within the transition period.

$$\begin{aligned}
\underset{u}{\text{minimize}} \quad & \sum_{k=0}^{n_{cy}-1} c(k) \left(\frac{\dot{Q}_{CHI}(k)}{COP_{CHI}} + \frac{\dot{Q}_{HP}(k)}{COP_{HP}} + P_{R,dc}(k) \right) dT \\
& + \sum_{l=0}^{n_{by}-1} \tilde{c}_{by}(l) \left(\frac{\tilde{\dot{Q}}_{CHI}(l)}{COP_{CHI}} + \frac{\tilde{\dot{Q}}_{HP}(l)}{COP_{HP}} + \tilde{P}_{R,dc}(l) \right) dT \\
\text{subject to} \quad & n_{cy} = \frac{t_{cy}}{dT}, \\
& n_{by} = \frac{t_{trans}}{dT}, \\
& x(0) = x(t_0), \\
& x(k+1) = f(x(k), u(k), v(k)) \qquad \forall k \in [0, n_{cy}-1], \\
& u(k) \in \mathbb{U} \qquad \forall k \in [0, n_{cy}-1], \\
& x(k) \in \mathbb{X}(k) \qquad \forall k \in [0, n_{cy}-1], \\
& \tilde{x}(0) = x(n_{cy}), \\
& \tilde{x}(l+1) = f(\tilde{x}(l), \tilde{u}(l), \tilde{v}_{by}(l)) \qquad \forall l \in [0, n_{by}-1], \\
& \tilde{u}(l) \in \mathbb{U} \qquad \forall l \in [0, n_{by}-1], \\
& \tilde{x}(l) \in \mathbb{X}(l) \qquad \forall l \in [0, n_{by}], \\
& \tilde{m}_{B,LS}(n_{by}) = m_{B,LS,by}(n_{by})
\end{aligned} \tag{2.151}$$

2.2.4 Mixed Approach

The mixed approach does not include any hierarchical higher-level scheduling. Instead, the performance measure is divided into two intervals with different discretisation step and disturbance inputs. In the first interval there is a discretisation step dT_{cy} of one hour with the weather forecasts of the current year within the 5 days prediction horizon t_{cy}. In the second interval there is a variable discretisation dT_{by} and with the weather data of the base year within the prediction horizon t_{by}. Both parameters dT_{by}, t_{by} are part of the investigation. The base year prediction horizon is comparable to the transition time in the flexible reference tracking approaches. As with the second reference tracking approach the states and inputs within the base year prediction horizon are indicated by a tilde in Equation 2.152. The values are averaged over an the discretisation interval. The main difference to the second reference tracking approach is that there is no final lime storage constraint, no higher scheduling hierarchy. The following problem setting only includes the operation cost as the control algorithms are only minimised with respect to the operation costs.

$$
\begin{aligned}
\underset{u}{\text{minimize}} \quad & \sum_{k=0}^{n_{cy}-1} c(k) \left(\frac{\dot{Q}_{CHI}(k)}{COP_{CHI}} + \frac{\dot{Q}_{HP}(k)}{COP_{HP}} + P_{R,dc}(k) \right) dT_{cy} \\
& + \sum_{l=0}^{n_{by}-1} \bar{c}_{by}(l) \left(\frac{\bar{\dot{Q}}_{CHI}(l)}{COP_{CHI}} + \frac{\bar{\dot{Q}}_{HP}(l)}{COP_{HP}} + \bar{P}_{R,dc}(l) \right) dT_{by} \\
\text{subject to} \quad & n_{cy} = \frac{t_{cy}}{dT_{cy}}, \\
& n_{by} = \frac{t_{by}}{dT_{by}}, \\
& x(0) = x(t_0), \\
& x(k+1) = f(x(k), u(k), v(k)) && \forall k \in [0, n_{cy}-1], \\
& u(k) \in \mathbb{U} && \forall k \in [0, n_{cy}-1], \\
& x(k) \in \mathbb{X} && \forall k \in [0, n_{cy}-1], \\
& \bar{x}(0) = x(n_{cy}), \\
& \bar{x}(l+1) = \bar{f}(\bar{x}(l), \bar{u}(l), \bar{v}_{by}(l)) && \forall l \in [0, n_{by}-1], \\
& \bar{u}(l) \in \mathbb{U} && \forall l \in [0, n_{by}-1], \\
& \bar{x}(l) \in \mathbb{X} && \forall l \in [0, n_{by}]
\end{aligned}
\tag{2.152}
$$

Chapter 3

Results

3.1 Comparison of the Energy System Settings

Table 3.1: Annual energy consumption (AEC) and annual operation cost (AOC) of different optimisation targets, building properties and system configurations. The upper bounds $\dot{Q}_{CHI,ub}$, $\dot{Q}_{RAD,ub}$, $\dot{Q}_{HP,ub}$, $P_{R,dc,ub}$, $V_{BS,ub}$ are infinite. Minimum values were printed in bold.

Config No.	1	2	3	4	5	6	7	8	9	10	11	12	13	14	15	16	17	18	19	20
oc	•	•	•	•	•	•	•	•	•	•										
ec											•	•	•	•	•	•	•	•	•	•
light	•	•	•	•	•						•	•	•	•	•					
heavy						•	•	•	•	•						•	•	•	•	•
HP	•					•					•					•				
LS $\eta = 1$		•					•					•					•			
LS $\eta = 0.7$			•					•					•					•		
LSHP $\eta = 1$				•					•					•					•	
LSHP $\eta = 0.7$					•					•					•					•
AEC [kWh]	5267	10096	13829	5267	5267	5387	10297	14081	5387	5387	**3499**	9267	12692	**3499**	**3499**	3559	9425	12909	3559	3559
AOC [₰]	**44**	45	45	**44**	**44**	45	46	46	45	45	127	339	465	127	127	131	348	477	131	131

Table 3.1 shows the comparison of the annual energy consumption (AEC) and the annual operation costs (AOC) compared to different system characteristics as well as optimisation targets. The target of optimisation can either be the energy consumption or operation costs, what corresponds to the abbreviation *ec* and *oc*, respectively, cmp. Equation 2.124 and 2.123. The previous mentioned aim of the collaborative research centre is to minimise the material usage for buildings. This aspect is realised with the entry *light* as well as *heavy*. Therefore, a *light* buildings concrete has the artificial density of $480\,\mathrm{kg\,m^{-3}}$. The *heavy* buildings concrete has a common density of $1920\,\mathrm{kg\,m^{-3}}$. The system configuration consists of the heat supply,

the buffer storage tank and the building. In order to compare the efficiency of the seasonal lime storage module as heat supply, it was once only represented by the heat pump *HP*, the lime storage system *LS* and the combination of heat pump and lime storage system *LSHP*, respectively. The configurations with the lime storage system were additionally varied by the conversion efficiency η. It is the efficiency of electrical to thermal energy conversion and thus influences the temperature level for dehydration reaction, cmp. Equation 2.63. With $\eta = 0.7$ a higher electrical power is needed to provide the temperature level. The results in Table 3.1 provide several insights based on simulations with varying optimisation target, building properties and heat supply configuration. Referring to the constraints set introduced in the fundamental part, in these simulations the upper limits of the chiller power $\dot{Q}_{CHI,ub}$, the heater power $\dot{Q}_{RAD,ub}$, ther heat pump power $\dot{Q}_{HP,ub}$, the reactor input power $P_{R,dc,ub}$ and the volume of buffer tank $V_{BS,ub}$ are at infinity.

The annual energy consumption of a building with light concrete is on average 2 % lower than that of a building with heavy concrete with the same other system options. For the annual operation cost, the identical trend can be observed with 2 % relative deviation.
The optimisation target has a large influence on the two performance criteria (AEC, AOC), if the concrete and configuration options are equal. Comparing systems with heat pump, *HP* or *LSHP*, for example configuration 1 and 11 from Table 3.1 the annual energy consumption is about 36 % lower with the optimisation target *ec*, but the AOC is approximately 190 % higher. Comparing the system configurations only with the lime storage module *LS* the AEC is about 8 % lower with the optimisation target *ec* but the AOC is between 660 % and 940 % higher than the comparable simulations with the optimisation target *oc*. The lime storage module therefore shows a moderately increased energy consumption but strongly reduced operating costs insofar as the objective function is *oc*.
An interesting equality is recognisable. There is no difference in the AEC and AOC within configurations *HP* and *LSHP* at the same optimisation target and building property but between configurations *HP* or *LSHP* and *LS*. The configuration with heat pump has a 92 % lower AEC and a 1 % lower AOC if the optimisation target is the operation cost *oc*. There is an even higher difference between the configurations *HP* and *LS* if the optimisation target is the energy consumption *ec*.
There is no influence of the conversion efficiency η on the AOC and AEC within configurations *LSHP* but within configurations only with the lime storage module *LS*. The AEC of system configurations with *LS* and $\eta = 0.7$ is 37 % higher than their equivalent with $eta = 1$. A change in AOC with η can only be observed if the target value is the energy consumption *ec*.

Table 3.2: Additional results of the different configurations with light concrete in Table 3.1. The values in each cell are the mean electricity price at heat pump operation $\bar{c}_{HP}$ [€/MWh], mean prize at $P_{R,dc}$-Operation $\bar{c}_{LS}$ [€/MWh], maximum buffer storage level $V_{BS,max}$ [m^3], maximum lime storage level $m_{S,B,max}$ [kg]

Config No.	1	2	4	11	12	14
		oc			ec	
$\bar{c}_{HP}$ / €*MWh	0.1	-	0.1	34.9	-	34.9
$\bar{c}_{LS}$ / €*MWh	-	0.1	0.0	-	34.9	0.0
$V_{BS,max}$ / l	106	34	106	0	0	0
$m_{S,B,max}$ / kg	-	10934	0	-	568	0

Table 3.2 provides a deeper analysis of the investigation. As discussed in the introduction the electricity price was taken from the electricity price exchange for the corresponding years. This price was negative at some hours of the year. Therefore, these electricity prices were corrected to a minimum price of 0.1 €/MWh. The configurations with optimisation target *oc* only operate at the minimum possible electricity price 0.1 €/MWh. Additionally for the configuration *LSHP* there is no lime stored. Therefore, the lime storage module within the configuration *LSHP* doesn't operate at any optimisation target. If the optimisation target is *ec* the buffer storage tank is additional continuously zero. The mean prize during lime storage module or heat pump operation is 34.9 €/MWh. This corresponds to the average electricity price used for the simulations.

Table 3.3: Annual energy consumption (AEC) and annual operation cost (AOC) of system configurations from Table 3.1 with light concrete and reactor parameter $\eta = 1$. The variable upper bounds are set to $\dot{Q}_{CHI,ub} = 5.3\,\text{kW}$, $\dot{Q}_{RAD,ub} = \dot{Q}_{HP,ub} = 5.6\,\text{kW}$, $P_{R,dc,ub} = 10\,\text{kW}$ and $V_{BS,ub} = 1000\,\text{l}$.

Config No.	1	2	3	4	5	6
oc	•	•	•			
ec				•	•	•
HP	•			•		
LS		•			•	
LSHP			•			•
AEC / kWh	3673	9583	4311	3533	9351	3533
AOC / €	98	190	93	127	339	127
$\bar{c}_{HP}$ / €*MWh	23.6	-	23.3	34.9	-	34.9
$\bar{c}_{LS}$ / €*MWh	-	17.9	1.3	-	34.9	0.0
$V_{BS,max}$ /l	1000	1000	1000	62	0	62
$m_{S,B,max}$ / kg	-	6159	1050	-	795	0

In reality it is not possible to develop plants without specifying their design parameters, as the simulation experiments in Table 3.1 suggest. In order increase the model fidelity, constraints for the inputs have now been introduced. As mentioned in the introduction we apply upper bounds $\dot{Q}_{CHI,ub} = 5.3\,\text{kW}$, $\dot{Q}_{HP,ub} = \dot{Q}_{RAD,ub} = 5.6\,\text{kW}$ according to the specification data sheet of the Bosch Climate 5000 RAC. The electrical reactor input power $P_{R,dc}$ has a upper limit of 10 kW, according to an experimental study [Sch+14]. The volume of the buffer storage tank V_{BS} is limited to 1000 l. The reactor parameter shall be kept at $\eta = 1$.

Table 3.3 shows the results of the AOC and AEC of a light building with the above mentioned design specification. Those simulations which have *ec* as a target do neither change their AEC nor AOC by introducing the upper bounds. Additionally the mean electricity price during heat pump or lime storage module operation isn't changing either. The influence of constraints is clear with the optimisation target *oc*. The configuration *HP* has an AEC decrease of 30 % but AOC increase of 120 %. The configuration *LS* energy reduction is mild at 5 % but the AOC increase is strong at 325 %. The hybrid system consisting of heat pump and lime storage module *LSHP* reduces its AEC by 18 % and increases its cost by 110 %. This configuration has now a higher AEC but lower AOC, albeit very small with 5 %, as the configuration *HP* by the introduction of constraints. This observation suggests that the lime reservoir now offers an advantage. This is only valid with the optimisation target *oc*. The mean electricity price

during the operation of the heat pump or lime storage module increases from 0.1 €/MWh to approx. 20 €/MWh. In particular, a low operation price for the systems *LSHP* lime storage module is now apparent. At 1.6 €/MWh its significantly lower than the price during heat pump operation at 23.3 €/MWh. Additionally, the maximum lime mass stored is not zero. Simulations with *oc* as target value use the entire available volume of the buffer tank. Therefore, the lime storage module within the configuration *LSHP* is operating with the optimisation target *oc* but still not if the energy consumption should be minimised.

According to a publication of the Federal Environment Agency [Umw], cmp. Table 2-6, the annual specific energy consumption for space heating and hot water of new residential buildings (2009-2012) in Germany is 84 kWh/m^2. In comparison, the specific annual energy consumptions by configurations within this work are as follows: 37 kWh/m^2 for the *HP* configuration, 96 kWh/m^2 for the configuration *LS* and 43 kWh/m^2 for the configuration *LSHP*. It is important to note that one is taxed consumer prices and the other is wholesale prices excluding taxes and levies.

Diagrams in the Appendix A provide more detailed information about the daily and annual behaviour of the system states and inputs varying the optimisation setting and the heat supply configuration.

Based on this results the configurations for the further MPC control approaches have a system with light concrete, the optimisation target is *oc* and the configurations are *LS* and *LSHP* with $\eta = 1$. In the following results, only the configurations with the lime storage module were considered further, since in this thesis only control strategies for building energy systems with a seasonal horizon are developed. The variable upper bounds are set to $\dot{Q}_{CHI,ub} = 5.3\,\text{kW}$, $\dot{Q}_{RAD,ub} = \dot{Q}_{HP,ub} = 5.6\,\text{kW}$, $P_{R,dc,ub} = 10\,\text{kW}$ and $V_{BS,ub} = 1000\,\text{l}$.

3.2 Comparison of the MPC Settings for the Flexible Reference Tracking Approach 1

As introduced in the fundamental part, the flexible reference tracking approach 1 is analysed by varying the parameters p_v and m as well as the system configurations *LS*,*LSHP*. The pre-factor p_v offers the possibility to attach specific weights to the several part of the optimal criterion, cmp. Equation 2.150. Thus it allows statements, whether the controller should rather look at the states and inputs of the first 5 days of the current year more intensively or should rather ideally track the optimal lime storage level of the base year. The power factor m was introduced, because it offers the possibility to disadvantage over- and underrun of the target trajectory to the same extent. The trajectory resulting from the MPC control is compared with the trajectories by the OGS algorithm, which once use the complete disturbance variables of the base year or the year 2016. The trajectory created by the OGS algorithm for the current year OGS_{16} represents the best possible trajectory to be achieved by the controller. The trajectory through the control has the same starting value as the optimal trajectory but not the same final value. Therefore, the annual operation costs resulting from the controllers trajectory can only be compared to a limited extent with those of the optimum trajectory in 2016. The central criterion for comparison is the relative deviation *rdev* of the annual operation costs of the MPC controller compared to those of the optimal schedule in the current year. A correction of the relative deviation by the final state difference is not

made, since no comprehensible unambiguous criterion for the conditions of the state change could be established.

$$rdev = \frac{AOC_{MPC,16} - AOC_{OGS,16}}{AOC_{OGS,16}} \tag{3.1}$$

Table 3.4: Results of the relative deviation rdev varying optimal setting parameter m and p_v at $t_{trans} = 2\,weeks$ with system configuration *LS* and *LSHP*.

Simulation No.	1	2	3	4	5	6	7	8
m	1				2			
p_v	0	1e-4	1e-2	1	0	1e-4	1e-2	1
$rdev_{LS}$ / %	33	33	31	202	33	14	19	20
$rdev_{LSHP}$ / %	9	9	6	212	9	5	7	8

Table 3.4 shows the influence of the optimisation parameters m, p_v and the system configuration *LS* or *LSHP* on the relative deviation of the AOC from the best possible result. With the same parameter p_v the relative deviations with $m = 2$ are always less than those with $m = 1$ for comparable other parameters. Within the potency parameter m, a minimum of the relative deviation can be seen with varying scaling parameter p_v. This minimum is about $p_v = 1 \times 10^{-1}$ for simulations with power parameter $m = 1$ and $p_v = 2 \times 10^{-4}$ for power parameter $m = 2$. For configurations with lime storage tank *LS* the deviations from its optimal AOC are always higher compared to configurations *LSHP* with heat pump. Subsequently, the optimal parameter tuple $\{m^*,p_v^*\}$, which minimises the relative deviation, was searched within a system configuration. The system *LS* has an optimal parameter tuple $\{m^* = 2, p_v^* = 2 \times 10^{-4}\}$, which significantly reduces the relative deviation to $rdev^* = 9.7\,\%$. The same behaviour is seen in the system configurations *LSHP*. Those simulations show at $\{m^* = 2, p_v^* = 3.5 \times 10^{-4}\}$ their optimum of $rdev^* = 2.8\,\%$. The following diagrams for those configurations *LS* and *LSHP* compare the graphs of the annual costs and the lime storage level with the pre-factor p_v.

Figure 3.1 and 3.2 compare the graphs of the operation costs as well as the lime storage level with variation of the pre-factor p_v for the configuration *LS* and a power factor $m = 2$. The graph of the lime storage level by the MPC control MPC, p_v depends strongly on the pre-factor p_v. With a pre-factor of $p_v = 0$ the lime storage level breaks down and fluctuates slightly around the zero point. On the other hand, a pre-factor of $p_v = 1$ leads to an apparently strict tracking of the graph created by the optimal generation scheduling on the basis of disturbance inputs of the base year OGS_{by}. The curve with an optimal pre-factor of $p_v = 2 \times 10^{-4}$ differs clearly from the optimal lime storage graph of the base year as well as the current year 2016, OGS_{by} or OGS_{16}. In Figure 3.2 the graph of the operation costs is shown. It is important to note that the end costs are only comparable to a limited extent, since the lime storage curves using the MPC control MPC, p_v and the scheduling algorithm OGS_{16} have the same starting point but not the same end point. Additional costs would be generated to overcome this end state difference. The graph with optimal pre-factor $p_v^* = 2 \times 10^{-4}$, in yellow, is most of the time around or below the optimal graph OGS_{16}, in purple. Towards the end of the year, approximately from the time when the MPC, p_v curve approaches zero, the costs increase rapidly to a level higher than OGS_{16}. The graph of the operation costs by the scheduling

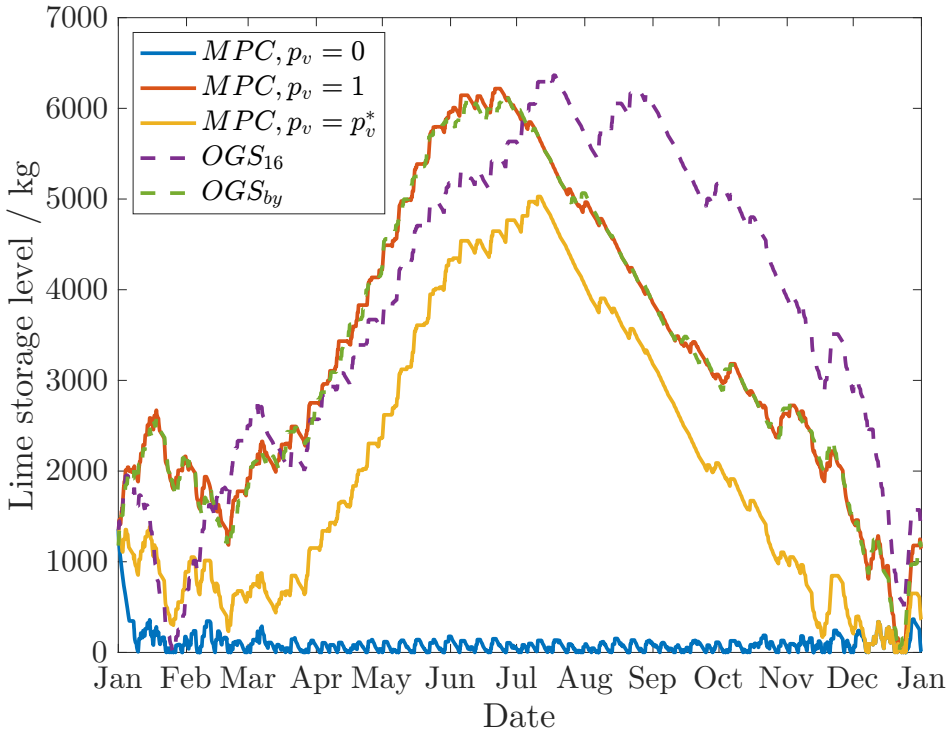

Figure 3.1: Lime storage trajectory of the flexible reference tracking control approach 1 with system configuration LS varying parameter p_v at $m = 2$.

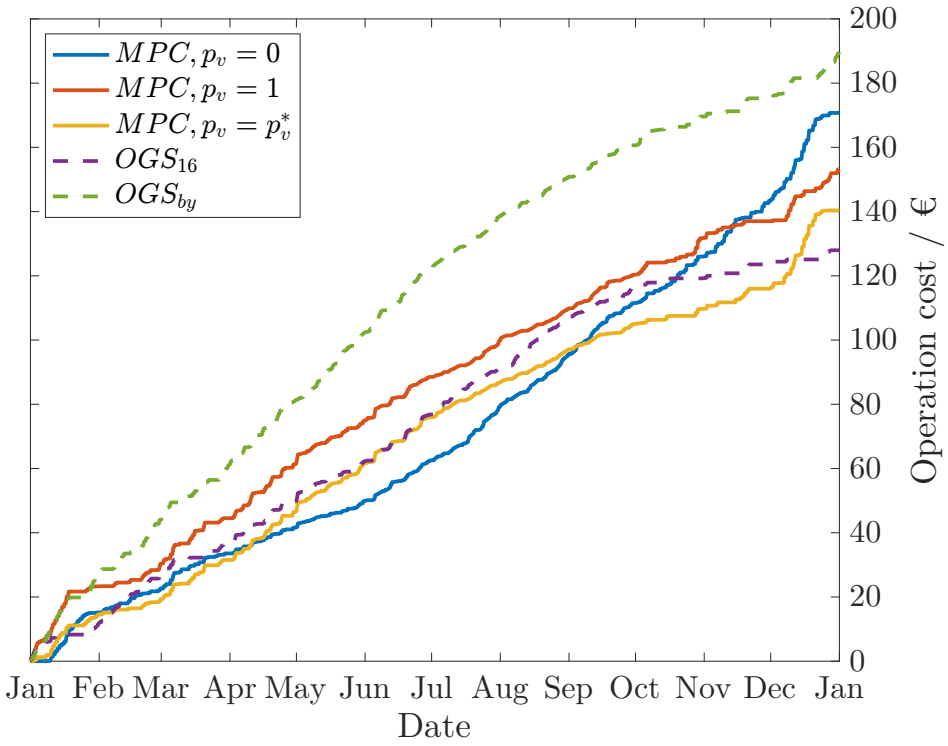

Figure 3.2: Operation cost of the flexible reference tracking control approach 1 with system configuration LS varying parameter p_v at $m = 2$.

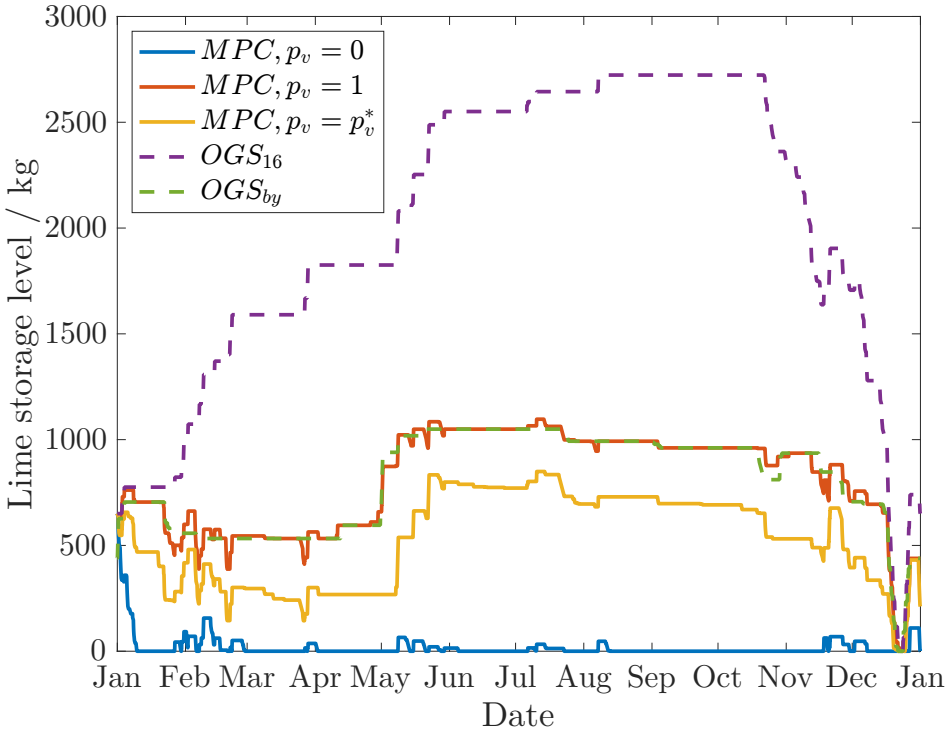

Figure 3.3: Lime storage trajectory of the flexible reference tracking control approach 1 with system configuration *LSHP* varying parameter p_v at $m = 2$.

algorithm for disturbance inputs of the base year OGS_{by}, in green, is throughout the year above that of MPC, p_v.

Figure 3.3 and 3.4 show the graphs of the lime storage level and the operation costs of the system configuration *LSHP*, by the MPC control, with optimal parameter tuple $\{m, p_v\}$, or the OGS algorithm. The lime storage levels by MPC control are all well below OGS_{16}. Varying the pre-factor p_v shows the same behaviour as with the configuration *LS*. At $p_v = 0$ the lime storage trajectory is about zero, at $p_v = 1$ it tracks the OGS_{by}-trajectory and with the optimal value $p_v = 3.5 \times 10^{-4}$ it is in between those two curves. Comparing the curves between the configuration it is clear that the curve of the lime storage level with the configuration *LSHP* is more step-like, discontinuous than the respective course with the configuration *LS*. According to this, lime is stored at lesser time points in the year. In addition, it is shown that within the configuration *LSHP* smaller amounts of lime are stored than in the configuration *LS* without heat pump. The operating cost curves are more similar to the OGS_{by} line than the comparable curves for the *LS* configuration. In addition, they deviate significantly less from the optimum cost curve than they do from the optimum lime storage curve. The last two control parameters that were studied are t_{trans} and t_{skip}. As described in the fundamental part, the parameter t_{trans} is the transition period in which possible differences of the storage states from their respective values in the base year disappear. After a successful optimisation of all inputs for the next 5 days, the controller jumps theoretically one time step, one hour further and calculates from here again the coming optimal trajectory. Due to reasons of computing time the flexible reference tracking approach not only jumps one hour further but 60 hours, corresponding two and a half days. This was the case in all previously presented results. The parameter t_{skip} was therefore $t_{skip} = 60\,\mathrm{h}$. This parameter as well as t_{trans} should now be

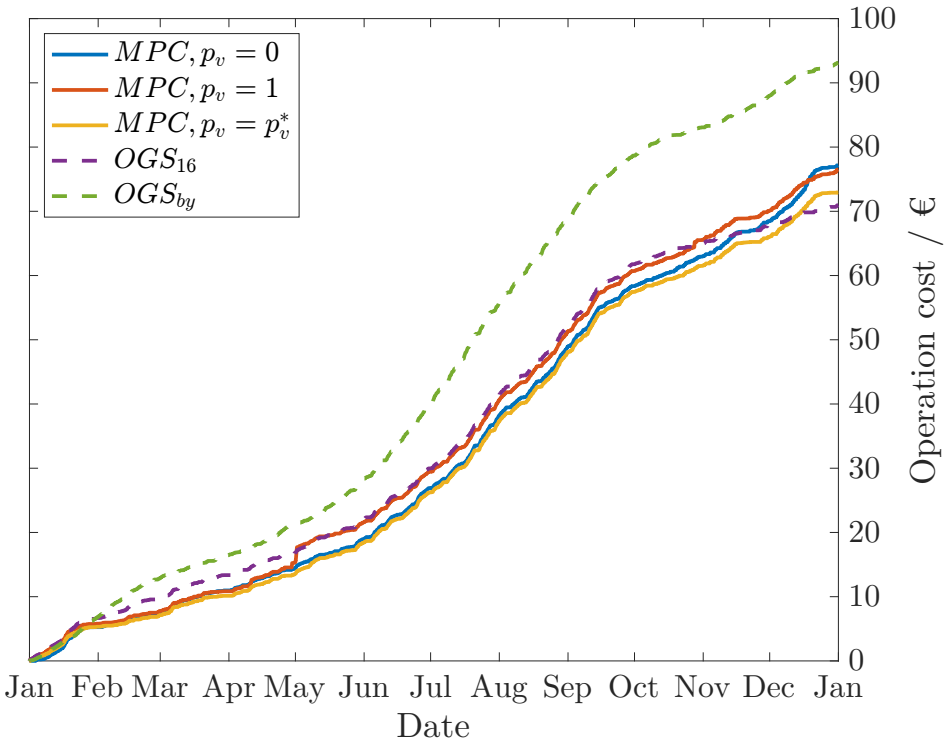

Figure 3.4: Operation cost of the flexible reference tracking control approach 1 with system configuration *LSHP* varying parameter p_v at $m = 2$.

released to show its influence on the relative deviation and the computing time t_{comp}. The results are based on the system *LS* with optimal parameter tuple $\{m^*,p_v^*\}$.

Table 3.5: Results of the relative deviation rdev and computation time t_{comp} varying optimal setting parameter t_{trans} and t_{skip} at optimal parameter tuple $\{m^*,p_v^*\}$ with system configuration *LS*.

Simulation No.	1	2	3	4	5	6	7	8
	t_{trans}				t_{skip}/h			
	1 h	1 d	2 w	8 w	1	12	24	60
$rdev$ / %	13.38	10.82	9.71	10.09	8.83	8.81	8.89	9.71
t_{comp} / min	-	-	-	-	94	9	4	2

Table 3.5 shows the influence of the parameters t_{trans} and t_{skip} on the relative deviation. For simulation 1 to 4 a $t_{skip} = 60\,\text{h}$ was used. For simulations 5-8 a $t_{trans} = 2\,\text{weeks}$ was used. With the transition period t_{trans} of two weeks there is the smallest relative deviation. Surprisingly the relative deviation when changing the parameter t_{skip} is not optimal at $t_{skip} = 1\,\text{h}$ but at $t_{skip} = 12\,\text{h}$. It is in turn only 0.9 % less than a simulation with $t_{skip} = 60\,\text{h}$. The computation time is however more than 4 times as much.

3.3 Comparison of the MPC Settings for the Flexible Reference Tracking Approach 2

The investigation of the second reference tracking approach is carried out with the variation of the transition time t_{trans}, cmp. Equation 2.151. Compared to the first approach, besides the inputs of the first 5 days, all additional inputs during the transition period are optimised. For this purpose, the objective function is calculated directly from the inputs. In addition, the lime storage mass at the end of the transition period is set as a hard constraint to the lime storage mass of the base year. With the first approach, however, only the deviation of the lime storage mass at the beginning of the transition period is minimised. For reasons of time, the investigation of the parameter t_{skip} is omitted here. In the following, results are presented for the system configurations *LS* and *LSHP* with varying transition time t_{trans}.

Table 3.6: Results of the relative deviation rdev and computing time t_{cmp} varying optimal setting parameter t_{trans} system configuration *LS* and *LSHP*.

t_{trans} / days	2	14	42	84	168	224	360	402
$rdev_{LS}$ / %	18	10	7	12	27	39	55	57
$rdev_{LSHP}$ / %	6.65	2.46	1.14	0.35	0.25	0.22	0.53	1.00
$t_{cmp,LS}$ / min	3	4	24	25	65	89	190	403
$t_{cmp,LSHP}$ / min	3	4	28	30	77	103	479	568

Table 3.6 shows an optimum of the relative deviation at transition time about 6 weeks in the simulations of the configuration *LS*. More detailed investigations revealed an optimum transition time of $t^*_{trans} = 42\,\text{days}$ with a relative deviation $rdev^*_{LS} = 7\,\%$. This deviation is less than the minimum achieved by the first approach. For the simulations of the configurations *LSHP* the optimum transition time is at a transition period of $t^*_{trans} = 224\,\text{days}$ with $rdev^*_{LSHP} = 0.2\,\%$ and is also below the best deviation achieved by the first approach.

Figure 3.5 to 3.6 compare the lime storage level and operation costs of the configuration *LS* by the reference tracking approach 2. With a parameter t_{trans} of 2 days a strict tracking of the OGS_{by} trajectory can be seen. With a transition period of one year and six weeks, $t_{trans} = 402\,\text{days}$, the amount of lime storage increases significantly above all other trajectories and remains there until the end of the year. The optimal transition period, $t_{trans} = 42\,\text{days}$ leads to an lime storage curve which is almost throughout above the other lime storage levels. In the middle of the year, when the OGS_{by} algorithm reduces the lime reservoir, it moves below the level of OGS_{16}. The operating costs also depend on the transition period. With a total prediction horizon of one year, with $t_{trans} = 402\,\text{days}$ the operating cost are the highest cost among all possible. The course of operating costs with a transition period of 2 days and 42 days differ slightly.

Figure 3.7 to 3.8 compare the lime storage level and operation costs of the configuration *LSHP* by the reference tracking approach 2. With a parameter t_{trans} of 2 days a strict tracking of the OGS_{by} trajectory can be seen. In contrast, with a transition period of 402 days the lime storage course is almost throughout the year as the the optimal course OGS_{16}. Both courses distinguish only in December. During this period, the optimal curve shows a stronger fluctuation and decrease than in the months before. The optimal course with a transition time of 224 days deviates over the year more than $MPC, \{402\}$ from the optimal curve OGS_{16}.

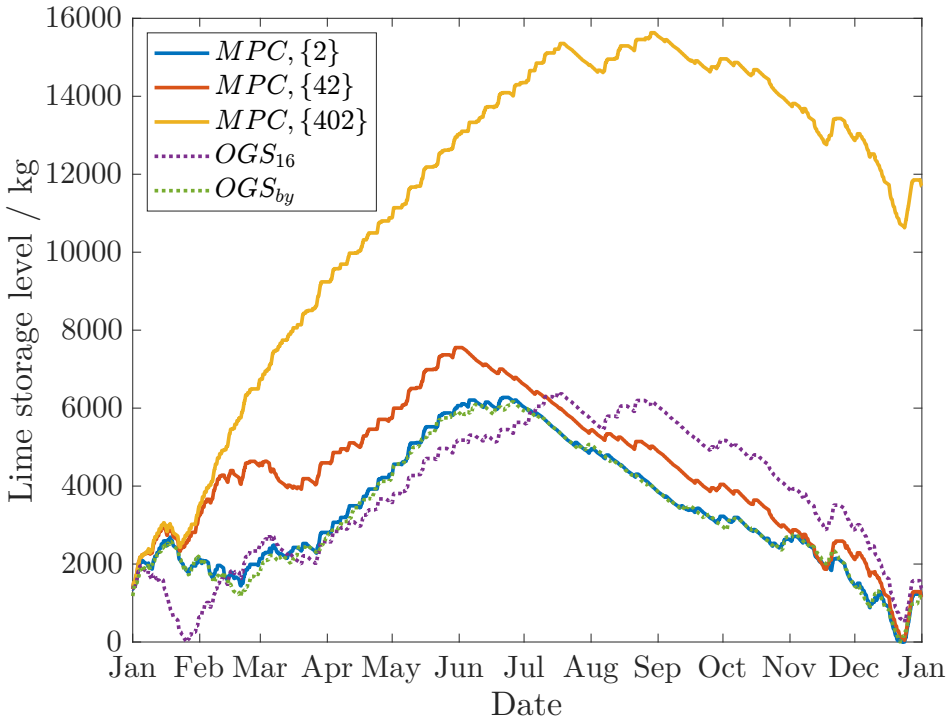

Figure 3.5: Lime storage trajectory of the flexible reference tracking control approach 2 with system configuration *LS*. The courses by the MPC control are distinguished by $\{t_{trans}$ / days$\}$.

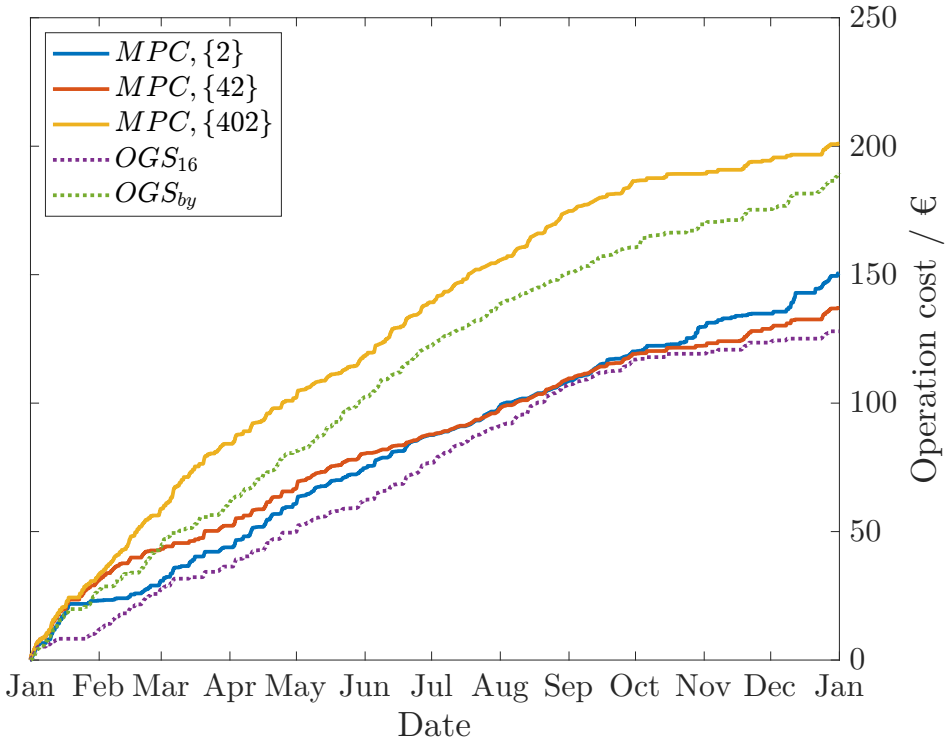

Figure 3.6: Operation cost of the flexible reference tracking control approach 2 with system configuration *LS*. The courses by the MPC control are distinguished by $\{t_{trans}$ / days$\}$.

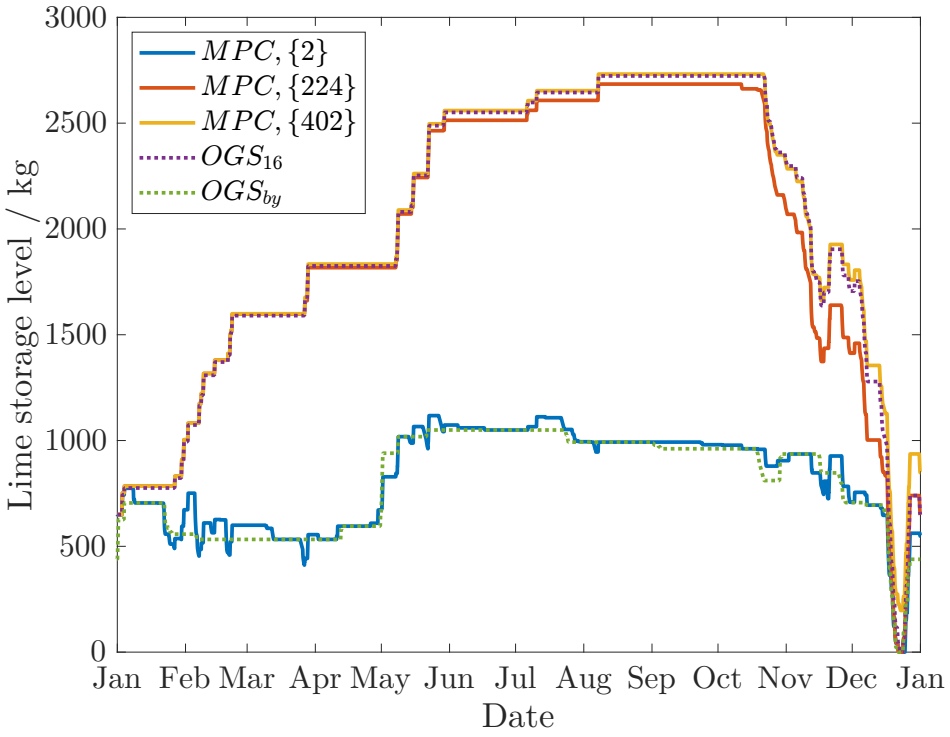

Figure 3.7: Lime storage trajectory of the flexible reference tracking control approach 2 with system configuration *LSHP*. The courses by the MPC control are distinguished by $\{t_{trans}$ / days$\}$.

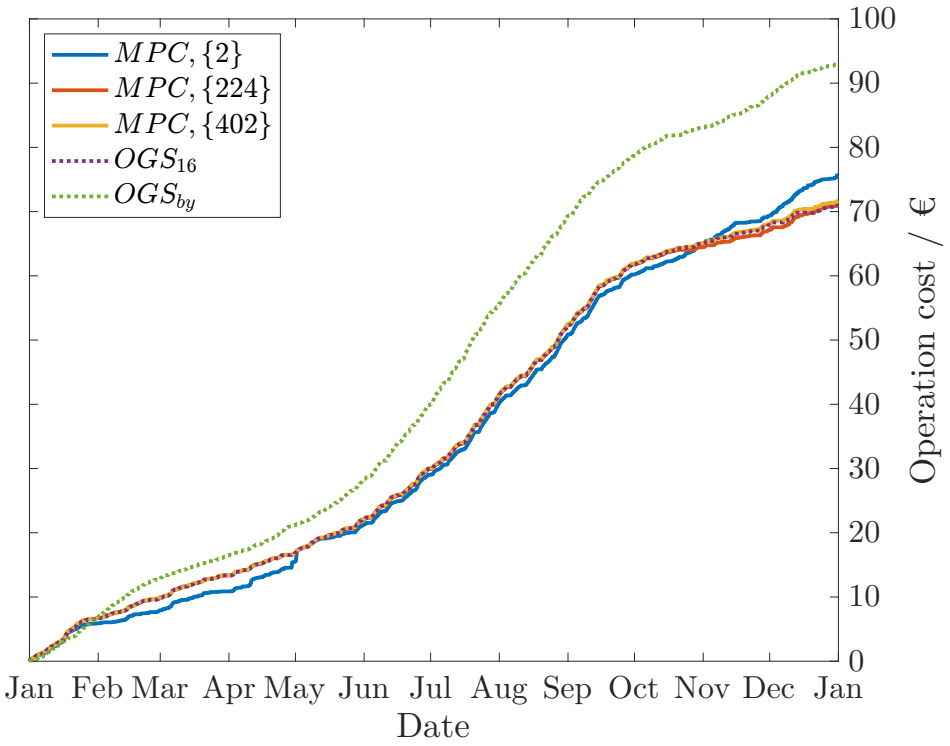

Figure 3.8: Operation cost of the flexible reference tracking control approach 2 with system configuration *LSHP*. The courses by the MPC control are distinguished by $\{t_{trans}$ / days$\}$.

In December, however, this is reversed. Now the regulator with a transition time of 224 days meets the optimal line better than the one with 402 days. While there is still a difference in the operating cost curve for a transition period of 2 days, the operating cost curves $MPC, \{224\}$, $MPC, \{402\}$ and OGS_{16} are almost indistinguishable throughout the year.

3.4 Comparison of the MPC Settings for the Mixed Approach

The investigation of the mixed approach is carried out with the variation of the prediction period t_{by} of the base year disturbance as well as the time step size dT_{by} for the discretisation of the second integral part, cmp. Equation 2.152. The discretisation of the first part is $dT_{cy} = 3600\,\mathrm{s}$ or one hour. For reasons of time, the investigation of the parameter t_{skip} is omitted here.

Table 3.7: Results of the relative deviation rdev and computation time t_{cmp} of system configurations *LS* and *LSHP* varying optimal setting parameter t_{by} and the discretisation step dT_{by}.

dT_{by} / h	1						24					
t_{trans} / days	2	44	93	163	360	402	2	44	93	163	360	402
$rdev_{LS}$ / %	26	11	3	12	44	48	25	34	40	54	96	106
$rdev_{LSHP}$ / %	6.23	2.18	0.46	0.18	0.32	0.60	5	8	11	11	17	17
$t_{cmp,LS}$ / min	3	30	54	125	361	405	2	3	5	7	16	18
$t_{cmp,LSHP}$ / min	3	33	67	146	478	557	3	4	6	9	23	24

Table 3.7 summarises the results of the mixed approach. For the configuration *LS*, the relative deviation is optimal at $rdev^* = 3\,\%$ with a prediction horizon, $t_{by} = 93\,\mathrm{days}$ of 3.5 months and a discretisation of one hour. A smaller or larger prediction horizon leads both to an increase in relative deviation. For the configuration *LSHP* with the same discretisation step, the behaviour is different. The deviation starts below that of the configuration *LS* and decreases to an optimal value of $rdev^* = 0.18\,\%$ at a base year prediction horizon, $t_{by} = 163\,\mathrm{days}$ of 6 months. This deviation is the smallest in comparison of all control approaches. A further increasing prediction horizon leads to a very small increase of the deviation but to a significantly higher computing time t_{cmp}. This increases almost linearly with the prediction horizon. In the heat supply configuration *LSHP* the calculation time is consistently higher than in the system without a heat pump. The situation is different, if the discretisation is performed over a time step of one day, 24 hours. The results of both configurations show no minimum of relative deviation for this discretisation with respect to the transition period. The deviations are smallest for a transition period of 2 days. As the transition period increases, the deviations are significantly higher than for a discretisation of one hour. However, the computing times are up to 20 times less than those with a discretisation of one hour.

The following figures visualise the results of the mixed approach at different transition times and discretisation time steps. As in the previous sections, a uniform visualisation was introduced for this purpose. The lime storage graphs which are created by the MPC control with a discretisation of one hour are marked with continuous lines. Those results with a discretisation of 24 hours are shown in dashed lines. The comparison curves of the scheduling algorithms of the base year and the current year 2016 are shown in dotted green and purple lines, respectively.

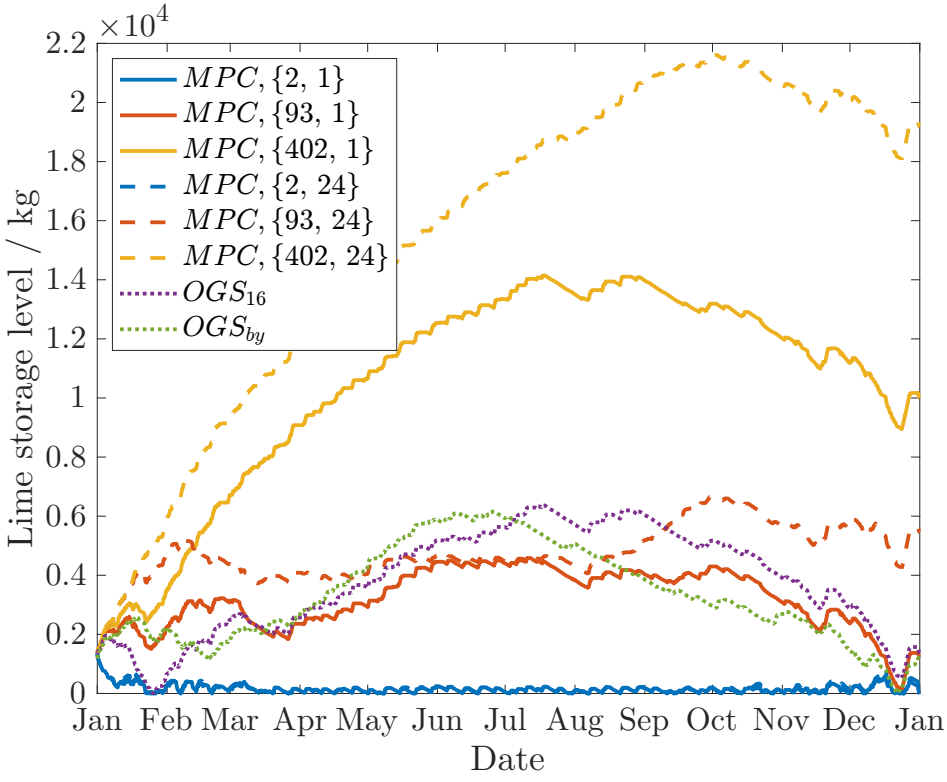

Figure 3.9: Lime storage trajectory of different mixed approaches with system configuration *LS*. The courses by the MPC control are distinguished by the tuple $\{t_{by}$ / days, dT_{by} / hour$\}$.

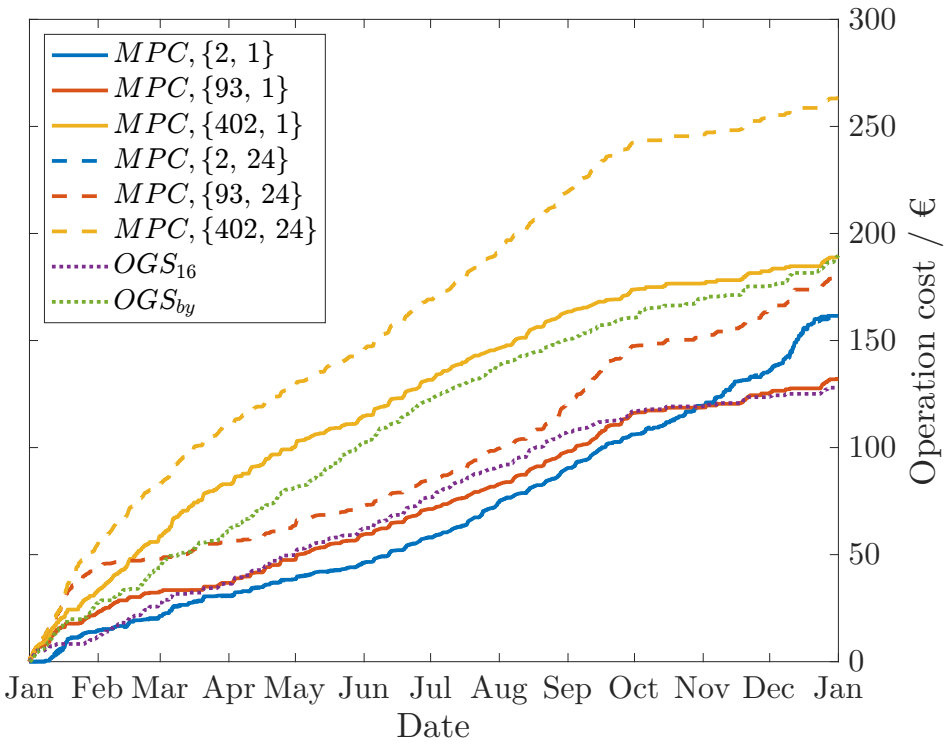

Figure 3.10: Operation cost of different mixed approaches with system configuration *LS*. The courses by the MPC control are distinguished by the tuple $\{t_{by}$ / days, dT_{by} / hour$\}$.

In Figure 3.9 the lime storage characteristics of the system *LS* are shown. With a low prediction horizon of $t_{by} = 2$ days the lime storage level drops to a zero level. This result is comparable to that of the first reference tracking approach with a pre-factor of zero. It is no difference recognisable in the graphs with regard to the discretisation time step. With a prediction horizon of $t_{by} = 402$ days and a discretisation of one hour, the lime storage level rises sharply to a level almost twice as high and decreases only slightly by the end of the year. With a discretisation dT_{by} of one day the lime storage level rises even higher. The curve with an optimal prediction horizon, $t_{by} = 93$ days of 3.5 months follows the OGS_{16} line in the contour but differs significantly in the amount of lime. The trajectory of the lime storage mass with a discretisation of 24 hours is above that with a discretisation of one hour. The operation cost in Figure 3.10 show that the lines of the optimal prediction horizon as well as the horizon $t_{by} = 360$ days lie over each other. They are very similar to the best possible operating cost line throughout. The lines with a discretisation step of 24 hours have a higher cost than their comparable line with a discretisation step of one hour. This trend is not valid for the prediction horizon of 2 days. Accordingly, the differences in operating costs or lime reservoir levels between the comparable curves with a discretisation of 24 hours and 1 hour are larger with increasing prediction horizon.

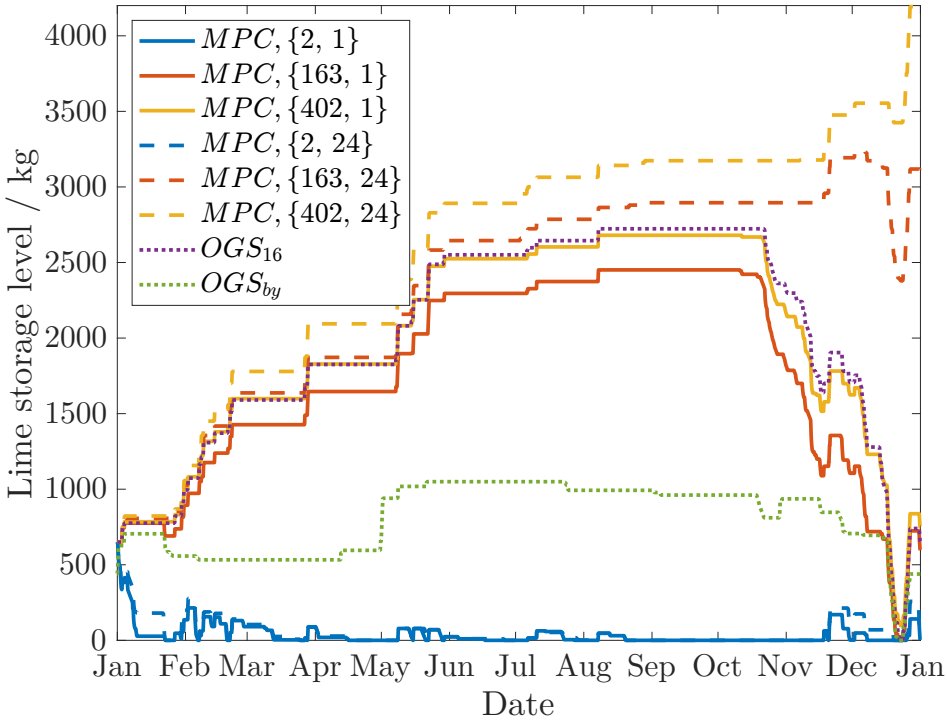

Figure 3.11: Lime storage trajectory of different mixed approaches with system configuration *LSHP*. The courses by the MPC control are distinguished by the tuple {t_{by} / days, dT_{by} / hour}.

Figure 3.11 shows the lime storage curve of the heat supply configuration *LSHP* using the mixed approach. With a prediction horizon, t_{by} of two days the graph drops to zero from the beginning. It is no difference recognisable in the graphs with regard to the discretisation time step. The lime storage curve with a prediction horizon of 402 days is more similar to the OGS_{16} than those with the optimal prediction horizon, $t_{by} = 163$ days of 6 months. A discretisation of 24 hours leads again to a higher lime storage level compared to the curves with a discretisation of one hour. And additionally shows unstable behaviour at the end of

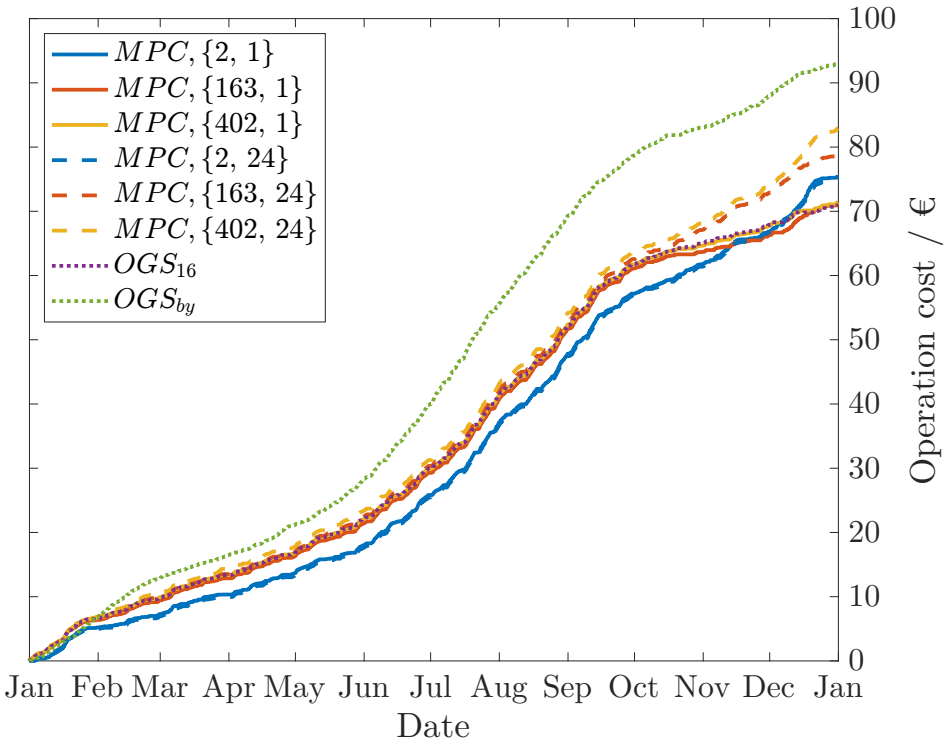

Figure 3.12: Operation cost of different mixed approaches with system configuration *LSHP*. The courses by the MPC control are distinguished by the tuple $\{t_{by}$ / days, dT_{by} / hour$\}$.

the year. The operating costs, cmp. Figure 3.12 for the prediction horizons $t_{by} = 163$ days and $t_{by} = 360$ days run on top of each other throughout the year and fit almost continuously the OGS_{16} line. This is also the case for the curves with the same prediction horizons but a discretisation of 24 h until the time in October when the lime reservoir is depleted, then their operating costs increase strongly.

3.5 Summary Comparison of all MPC Approaches

The following diagrams compare the lime storage and operating cost curves of all control concepts. According to the approach, its optimal control parameters are used.

Figure 3.13 and 3.14 refer to the configuration *LS*. The lime storage level $MPC, flex1$ is almost continuously below all other curves. As described above, its lime storage level reaches the empty level at the beginning of December and the cost curve is simultaneously rising strongly above the level of the other two control concepts. The lime storage curves of the $MPC, flex2$ and $MPC, mixed$ concepts differ considerably until the beginning of October. In the meantime, the $MPC, flex2$ concept has almost twice the level of the $MPC, flex1$ and $MPC, mixed$ concepts. At the beginning of October, the $MPC, mixed$ lime storage curve then increases above that of $MPC, flex2$. During the same period, the operating cost curves $MPC, flex2$ and $MPC, mixed$ stop converging and remain at the same difference until the end of the year.

Figure 3.15 and 3.16 refer to the configuration *LSHP*. In terms of the lime storage graph, the second reference tracking approach is much closer to the optimal curve OGS_{16} than the mixed approach although the relative deviation is even a little smaller. The course of the first reference tracking approach is oriented to the optimal course of the base year and thus differs significantly from the other approaches. This trend is also shown in the operation cost curves. The $MPC, flex1$ approach shows clear differences to the optimal line OGS_{16} than the other approaches.

The comparison between the two heat supply configurations shows that the optimal operating costs and the lime storage level OGS_{16} are consistently better met by the control concepts $MPC, flex2$ and $MPC, mixed$ if the hybrid configuration *LSHP* is applied. Furthermore, the lime storage levels of the configuration *LSHP* change much less often than those of the configuration *LS*. The computing time of the approaches with their optimal parameters, however, differ enormously. The computing time for the $MPC, flex1$ approach is 2 min / 2 min ($LS/LSHP$), for the $MPC, flex2$ approach 24 min / 103 min ($LS/LSHP$) and for the $MPC, mixed$ approach 54 min / 146 min ($LS/LSHP$). The calculation time for the configuration *LSHP* is on average 3 times as much as for the configuration without the additional heat pump input.

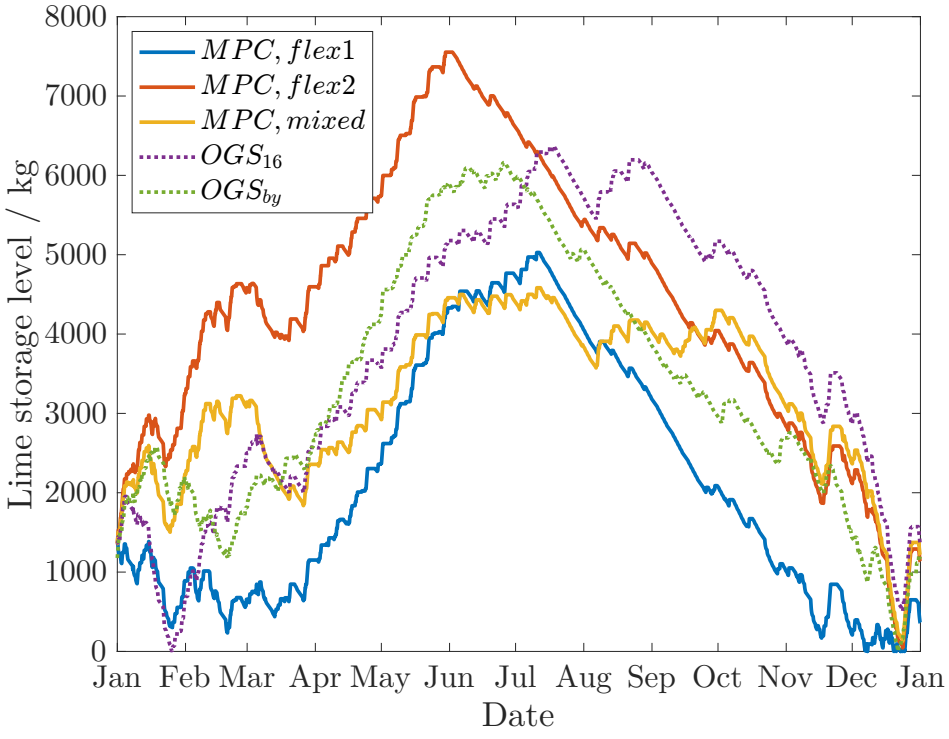

Figure 3.13: Lime storage trajectory comparing all presented control approaches with system configuration *LS*.

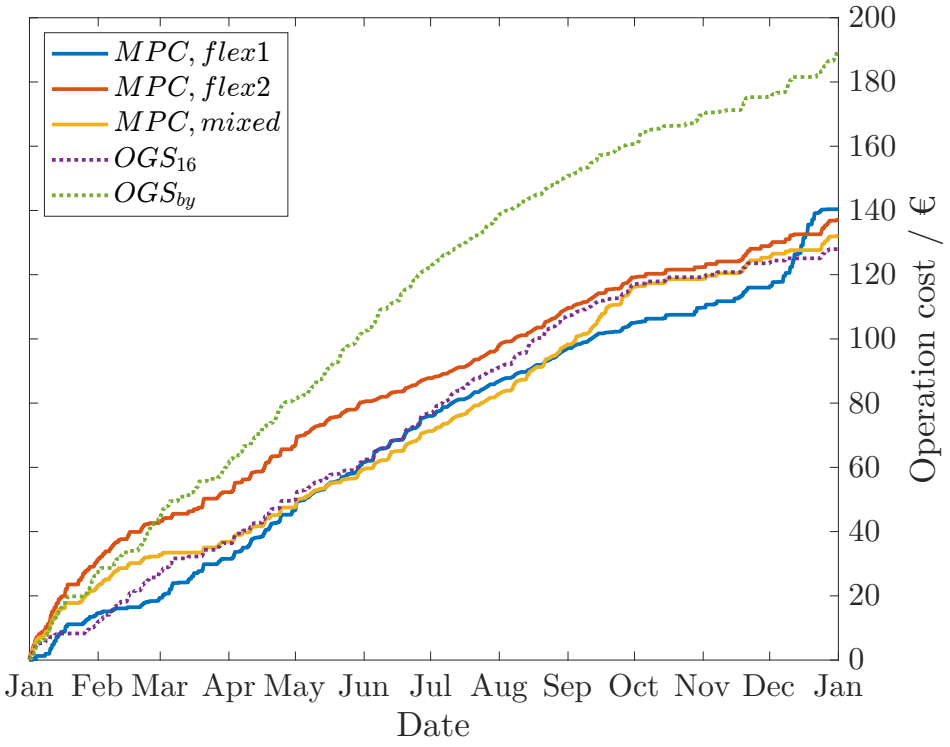

Figure 3.14: Operation cost comparing all presented control approaches with system configuration *LS*.

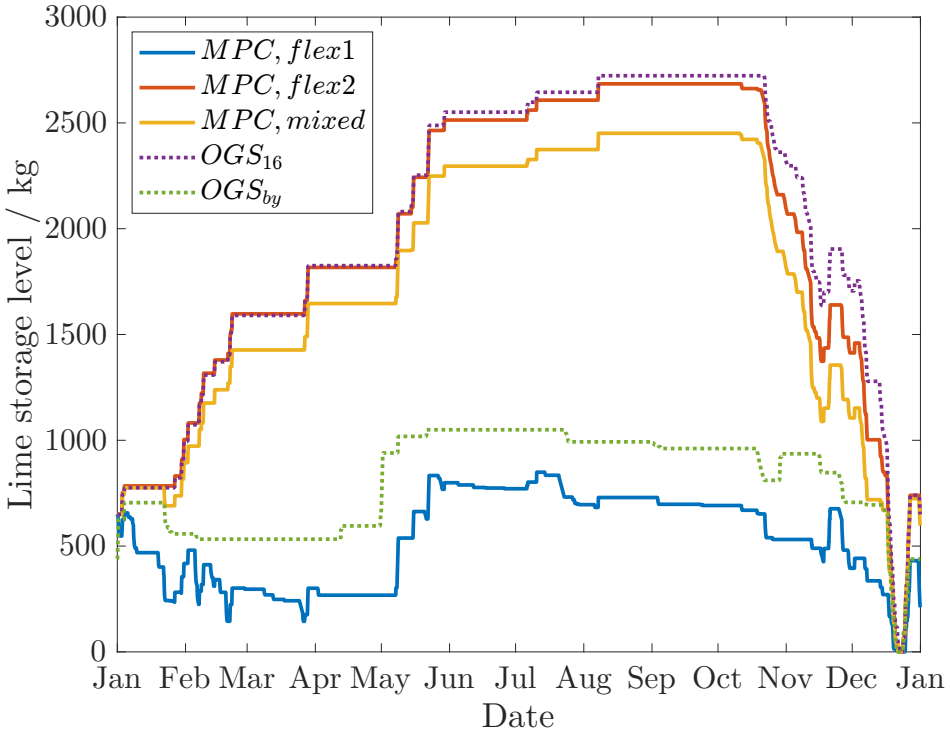

Figure 3.15: Lime storage trajectory comparing all presented control approaches with system configuration *LSHP*.

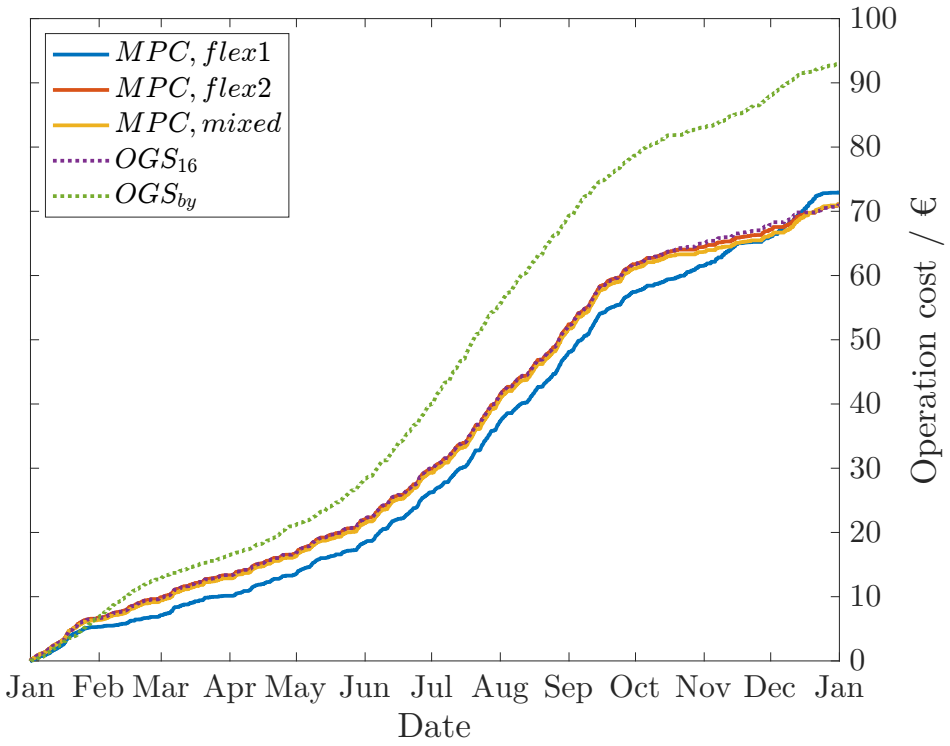

Figure 3.16: Operation cost comparing all presented control approaches with system configuration *LSHP*.

3.6 Comparison of the Base Year Disturbance Input

Finally, results are presented which classify the suitability of the averaged weather data as base year disturbance input. While the disturbance inputs of the current year enable the weather forecast of the first 5 days, the disturbance inputs of the base year serve the superordinate planning and weather forecast in the transition period or the prediction horizon of the base year. For this investigation, weather data from 2015 are used for the base year and applied to the control of the current year 2016. In addition, data from the typical meteorological year and the year 2016 are both applied as base year for the control of the current year 2015. For this purpose, the previously presented optimal parameters of the control concepts are applied. A further optimisation of the control parameters to the respective situation is not carried out, as it exceeds the scope of this work. Table 3.8 therefore compares the relative deviations $rdev$ of the current year annual operation cost $AOC_{MPC,cy}$ with the optimal annual operation cost $AOC_{OGS,cy}$. The base year from the previous results consisted of the averaged data. In Table 3.8 this base year is marked as typical meteorological year tmy. The factor $\Delta base$ describes the relative change of the AOC with the same current year and control concept but different base year. If the value of $\Delta base$ is less than zero, the typical meteorological year data are more suitable as a base year than the respective year 2015 or 2016.

Table 3.8 shows that the value $\Delta base$ is almost always less than zero. Only for the current year 2015 with the flexible reference tracking approach 2 and the mixed approach this is not the case. Here, the disturbance input 2016 as base year leads to a smaller relative deviation $rdev$ than the typical meteorological year data.

Table 3.8: Results of the relative deviation rdev varying current and base year disturbance input, the system configuration and the applied control approach.

config.	control approach	current year	base year	rdev / %	Δ base / %
LS	flex 1	16	15	19.8	
			tmy	9.7	-8.5
	flex 2		15	9.9	
			tmy	7.1	-2.5
	mixed		15	12.2	
			tmy	3.2	-8.0
LSHP	flex 1		15	4.7	
			tmy	2.8	-1.8
	flex 2		15	1.2	
			tmy	0.2	-0.9
	mixed		15	1.5	
			tmy	0.2	-1.3
LS	flex 1	15	16	12.9	
			tmy	4.5	-7.4
	flex 2		16	9.5	
			tmy	16.8	6.7
	mixed		16	10.6	
			tmy	11.9	1.1
LSHP	flex 1		16	5.5	
			tmy	1.2	-4.1
	flex 2		16	6.4	
			tmy	5.9	-0.5
	mixed		16	4.0	
			tmy	3.3	-0.7

Chapter 4

Discussion

4.1 Comparison of the Energy System Settings

As in the results section, the discussion of the comparison of energy system settings is divided into two areas. In the first area those simulations are discussed whose system inputs and states have upper bounds at infinity. In the second section the results are discussed which have been simulated with real input and state constraints.

The comparison of the operating costs of configurations with light and heavy concrete shows that the goal of the Collaborative Research Centre CRC 1244 to reduce material costs is even accompanied by an small improvement of the AEC and AOC by 2 % each. It is therefore worth using light concrete not only from the aspect of material costs and emission reduction in buildings, but also from the aspect of operating costs and energy consumption. However, these savings should not be overestimated. It presumes that there is a material that has the same thermal conductivity, capacity and stability properties as concrete and has a 25 % lower density. It is most important to emphasise that the building mass has no decisive influence on the annual operation cost or energy consumption.
It becomes unambiguous when comparing the configurations with different optimisation targets. The target value operating costs *oc* has a significantly higher cost saving of 190 % for configurations with a heat pump in relation to the higher energy consumption of 34 %. According to this, a minimisation of the operating costs simultaneously results in a limited minimisation of the energy consumption, but not the other way round. For the configuration *LS*, the performance measure *oc* is even more ecologically and economically optimal. This is because the electricity price used reflects the current electricity market. This market is demand-based. However, future electricity markets will be supply driven due to the increasing share of renewable energy generation. As a result, the electricity price will change towards the supply side. Therefore, by using an electricity price curve as presented by the authors [FLZ15], which is more expensive in winter than in summer due to the higher demand, the controversy between the objectives could be released. The optimisation with respect to the operation costs could thus more clearly include the energy consumption optimum. It would also be conceivable to replace the price of electricity with the current certificate price for the emission of carbon dioxide and thus minimise emissions instead of minimising operating costs. In addition, the unlimited power of the heat pump, the reactor input power and the capacity of the buffer storage tank enable the system to store the entire annual energy quantity at few times of the year when electricity is cheap. A closer examination of Table 3.2 qualifies this assumption, since configurations with *oc* as a target value only operate on the hours of the year when the electricity price was set to the minimum value of 0.1 €/MWh. This setting of

the minimum electricity price thus directly affects the annual operation costs of the system. Therefore, the heat supply systems must have high design specifications for rare operation during the year. A dimensioning of the plants with unlimited performance specifications is not only unrealistic but also leads to high investment costs.
Considering the differences within an optimisation target and concrete density, the configurations with heat pump are significantly more energy efficient. A look at Table 3.2 shows that the lime storage module is not used in as far as the heat pump is in the system, because the maximum lime storage volume is zero. From the energy point of view *ec*, it is also not reasonable to install a water buffer storage tank, because the water buffer storage is always zero during the year. The heat is therefore supplied directly to the building, since this means that no losses occur in the lime storage tank and the water buffer tank. From a monetary point of view, the heat pump is also used because it can produce heat more cheaply due to its COP.
A further insight is provided by the results concerning the conversion efficiency η. A reduction from $\eta = 1$ to $\eta = 0.7$ increases the energy consumption but not the operation costs as long as the operating costs are the objective. A η deviating from the ideal value, due to possible heat transfer inefficiencies, would therefore not directly lead to an increase in operation costs. This assumes that the reactor input power is unlimited and that the electricity costs are low for a certain period of time in order to realise the required heat input into the reactor.
The main statement of the first part of the system results is that the lime storage module is ecologically as well as economically unattractive with unlimited inputs.

After the introduction of the upper limits $\dot{Q}_{CHI,ub} = 5.3\,\text{kW}$, $\dot{Q}_{HP,ub} = \dot{Q}_{RAD} = 5.6\,\text{kW}$ and $P_{R,dc,ub} = 10\,\text{kW}$ a different situation occurs as the operating costs *oc* are optimised. The energy consumption of the heat supply decreases. Especially if there is a heat pump in the system. This reduction in consumption is caused by the smaller water tank volume, since the heat loss is directly proportional to the water tank volume. Therefore, an increase in water tank capacity should result in an increase in energy consumption. The heat losses are also lower, since the power is no longer injected punctually into the system but distributed over the year. This is shown by the increased electricity prices at which the output is brought in. The reduction of flexibility in heat supply, by reducing water tank capacity and power limits, leads to a significant increase in energy costs. Therefore, a compromise should be found between maximum flexibility and feasibility in an everyday application such as building conditioning. Since a higher upper limit of a water buffer tank or the reactor input power leads to higher investment costs of the whole plant due to the design specifications. This could be countered by decoupling the seasonal lime storage from the short-term buffer storage. At present, the lime storage tank is coupled to the buffer storage tank and thus to its capacity and the heating and hot water loads. A decoupling of the two storage types, e.g. by means of an outlet valve for water from the buffer tank, reduces the energy efficiency of the overall system but could increase the monetary efficiency. Energy efficiency can be improved by integrating the gratis ventilation input available from the BRCM Toolbox or the energy recovery system into the building system. This would enable the building to be pre-cooled at night with cold ambient air. Up to now this has been done by the cost-intensive chiller input. In addition, the outlet air flow could be used to pre-cool or heat the volume flow regulated by the air change rate.
From a simple energy point of view, if the energy consumption *ec* is optimised, the effects of operation cost minimisation will not occur. This is because the power and water volume are permanently below the limits or maximum capacity. From a monetary point of view,

however, it is now well worth integrating the lime storage tank into the overall system. From a purely energetic point of view, the lime storage module brings no advantages, as the storage is not used at all. On-demand energy is provided more cheaply via the heat pump. From an energy point of view, however, a small water storage tank $V_{BS,max} = 62\,\mathrm{l}$ is now beneficial. The main statement of the second part of the system results is that by introducing the upper limits the monetary advantage of the lime storage module in the configuration *LSHP* becomes visible, albeit they are very small at 5 %. Future work may find settings where the *LSHP* configuration will have operation costs significantly less than 5 % lower than the *HP* configuration.

4.2 Comparison of the MPC Settings for the Flexible Reference Tracking Approach 1

The comparison of the annual energy costs with varying potency parameter m shows that squaring the difference between the lime storage level and the reference of the OGS algorithm leads to smaller relative deviations of the operating costs. By the parameter $m = 1$ lime storage levels above the reference can lead to a cost minimisation, cmp. Equation 2.150. The higher costs could be caused by the fact that the controller aims at a higher lime storage level to minimise the cost function and thus the energy costs increase in the first prediction interval. By squaring the difference, this evaluation is not possible. The lime storage levels are therefore always below the reference trajectory, since higher lime storage levels now no longer contribute to minimisation. A further possibility would be to set the reference tracking fraction of the target value in absolute value. Unfortunately this was not possible with the CasADi toolbox. A large pre-factor, e.g. $p_v = 1$, causes a high absolute value of the reference tracking fraction of the target value in the transition period. Therefore the focus of the minimisation is on this part of the target value and thus the lime storage trajectory follows that of the base year. On the other hand, a disappearing pre-factor $p_v = 0$ causes a pure optimisation of the operating costs of the first prediction section within t_{cy}. Possible advantages due to seasonal energy storage cannot be included in this way. A medium pre-factor releases the target function from the disturbance inputs of the base year and allows advantages through the seasonal storage in the lime storage. With the configuration *LS*, the costs are reduced by 17 % by applying the optimum reference sequence p_v^* compared to $p_v = 0$. On the other hand, the costs are only reduced by 6 % with the configuration *LS*. This leads to the conclusion that seasonal energy storage plays a greater role in the system *LS* than in the system with heat pump *LSHP*. This is also shown by the lower quantities of lime stored in the system with heat pump.

4.3 Comparison of the MPC Settings for the Flexible Reference Tracking Approach 2

The higher the transition period, the more the lime storage process is released from that of the base year and the lower the influence of the final state constraints of the lime storage level. A short transition period of two days does not allow the controller to react flexibly to higher or lower yields in the current year due to the final state constraint. With a transition period up to one year, the controller can respond flexibly to current weather forecasts. The OGS_{16}

lime storage curve in the system *LSHP* is almost ideally met by the flexible reference tracking approach two, with a sufficiently high transition time, whereas the same curve remains below the OGS_{by} curve by the first control concept. According to this, the explicit inclusion of the inputs of the transition period in the objective function of the optimisation results in a significant flexibility of the lime storage levels. Thus the OGS_{16} lime trajectory can be traced almost identically. Compared to the configuration *LSHP* the lime storage exceeds the OGS_{16} level with the configuration *LS* at transition time above one year. This could be due to the fact that the lime storage level fluctuates much less in a system with heat pump *LSHP* meaning that it remains constant for longer periods because the reactor for dehydration is less often in operation, cmp. Figure 3.7, as it is the case with the system *LS*. This rate of fluctuation, in combination with the higher transition period, could be the reason for the significant increase in the lime storage level in Figure 3.5. This hypothesis can be supported by the behaviour of the lime storage levels in the configuration *LSHP* at the beginning of December, cmp. Figure 3.7. The trajectory OGS_{16} shows a higher fluctuation which makes the trajectory $MPC, \{224\}$ more different from OGS_{16} than in the months before. It seems that it is more difficult to follow fluctuating vs. constant references at high transition times. However, this hypothesis has not yet been clearly proven. The curves in Figure 3.5 and 3.7 also suggest that the accuracy with which control concept 2 follows the optimal lime storage curve is higher for increasing lime storage levels than for decreasing curves. A further attempt at explanation of the exaggerated lime storage increase at the beginning of the year is given in the comparison discussion of all control approaches.

4.4 Comparison of the MPC Settings for the Mixed Approach

A short prediction horizon of the base year t_{by} cannot be used for the long-term planning of the lime storage level. The result corresponds to that of the flexible reference tracking approach one with absence of a pre-factor. Furthermore, the question arises why the lime storage curve OGS_{16} is better met with a mid-range prediction horizon $t_{by} = 163\,\text{days}$. Accordingly, integrative effects of the formation and decay of the lime storage take place within 3.5 months. An increase of the prediction horizon to one year leads to more lime being accumulated even with the mixed approach. In the discussion of the flexible reference tracking approach two, the differences of the deviations of the lime reservoir levels from the ideal curve OGS_{16} between the configurations *LS* and *LSHP* were explained by the fact that the curves differ in their fluctuation and frequency of storage. These explanations also apply to the mixed approach. A further attempt at explanation of the exaggerated lime storage increase at the beginning of the year is given in the comparison discussion of all control approaches.
The choice of a higher time step for discretisation leads to a reduction of the computational time as well as to a higher lime storage with increasing prediction horizon. This is because the controller overestimates the energy required within the base year prediction horizon. This overestimation of the energy requirement is due to the discretisation of the occupancy probability. With high discretisation, there are more times when the average occupancy density within the time step is greater than zero, and the comfort condition thus takes action. This higher number of times in which heating or cooling is required leads to an overestimation of the lime storage. This overestimation also results from the discretisation method used, the explicit Euler method. This method has only a convergence order of one, which is why the discretisation error increases significantly with the step size which leads to a lower energy

conservation. Therefore, a better discretisation method should be used, such as the trapezoidal or Runge-Kutta method. But that was not the subject of this work. Perhaps such a control concept could be developed which combines the advantage of time savings, which can be up to 20 times less than with a step size of one hour, with a higher accuracy.

4.5 Summary Comparison of all MPC Approaches

With the second and third control concept, excessive lime accumulation occurs at the beginning of the year during high transition periods or prediction horizons. For the mixed approach, the quantity of lime at the end of the prediction horizon t_{by} is always zero within each MPC prediction, as it is optimal to leave no lime left, both in terms of costs and energy. This circumstance is detected as an invisible zero terminal constraint. This pushes the lime storage level at the end of the prediction horizon to zero and thus unstable the annual development of the lime storage. In times of lime storage build-up, at the beginning of the first half of the year, this invisible constraint leads to the production of significantly more, approximately twice as much lime. There is an forward shift of the cheap lime storage build-up from the time at the beginning of 2016 after the prediction horizon t_{by} to the same time of the prediction horizon of the current year t_{cy}. The increase of the horizons from $t_{trans} = 360\,\text{days}$ or $t_{by} = 360\,\text{days}$ to $t_{trans} = 402\,\text{days}$ or $t_{by} = 402\,\text{days}$ should actually prove the hypothesis of forward shifting. Since that increase should give the flex 2 approach, which has a final state constraint at an elevated lime level, the possibility to let the favourable lime storage build up take place at the beginning of the following year without shifting it forward. For the mixed approach, a larger amount of lime should be brought forward due to the invisible zero terminal constraint. Unfortunately, the results presented do not support this hypothesis.
The influence of the additional prediction horizon t_{trans} or t_{by} on the relative deviation is not as strong with the flexible reference tracking approach 1 as with the other two concepts, since its objective doesn't inclued inputs of that period. Between the last two approaches the question arises why the transition period / prediction period with $t^*_{trans} = 42$ and $t_{by} = 93$ are different for the heat supply configuration *LS*. This could be because the controller with the mixed approach has to predict longer periods of time, as it does not know the superordinate scheduling information. However, this behaviour is reversed for the configurations *LSHP*. The transition period of the second concept is longer than the prediction horizon of the mixed approach. This could again be due to the fact that the curve hardly fluctuate.
The differences in computing time between the configurations *LS* and *LSHP* are due to the fact that the configuration *LSHP* with the heat pump has one more input in the system. This shows that for general problems, which require a much more detailed description of the energy system, a much longer calculation time is to be expected. This effort could not be done with a sampling rate of one hour. One could either use a model reduction procedure or add another control hierarchy. A further hierarchical level with a prediction horizon of 2.5 days is suitable for this purpose since the sampling rate of the dynamic MPC controls is $t_{skip} = 60\,\text{days}$. It should therefore use the flexible reference tracking approach one or two as optimisation setting.
In summary it can be said that the first reference tracking approach requires the least computing time, but causes the highest annual deviation of the operating costs compared to the respective optimal lime storage trajectory OGS_{16}. The mixed approach is the most promising control approach for the energy system with seasonal lime storage but with the most inten-

sive computing capacity. It provides the lowest possible annual operating costs for both heat supply configurations.

4.6 Comparison of the Base Year Disturbance Input

The comparison of the base year input shows both the suitability of the typical meteorological year as the approximation of future weather data and the transferability of the control parameters to other combinations of base and current year. In the previous results, the typical meteorological year always served as weather data for the base year disturbance input and the weather data of 2016 as current year disturbance input. The results for the year 2016 as current year, cmp. Table 3.8 are therefore obligatory, because the parameters of the control approaches have been adapted to exactly this combination of current and base year disturbance input. It is therefore more important to look at the results when 2015 is the current year. For the heat supply configuration *LSHP* the typical meteorological data as base year across all control approaches are more suitable than a single year like the weather data of 2016. For the configuration *LS* this is only valid for the flexible reference tracking approach one. Its control parameters can therefore be transferred more reliably with the typical meteorological data as base year input than the control parameters of the other two approaches. It is possible that this approach, in conjunction with the typical meteorological year input, can react more robust to changes in weather data than all other approaches. With these two approaches it is to be assumed that the control parameters would have to be adjusted again. Due to the low data depth only tendencies and no reliable unambiguous generally valid statements can be made. This scheme should therefore be applied to further current year disturbance inputs. In order to increase the transferability of the base year data as well as the control parameters and to maintain the advantages of the control approaches, a further study should be carried out. This study should find base year disturbance data and control parameters adapted to several current year disturbance data.

Chapter 5

Summary

This thesis has developed a model of an energy system consisting of a building, water buffer storage, heat pump and a lime storage module. In addition, control concepts have been developed which should operate the system optimally over a period of one year. The simulations were implemented in Matlab. The optimisation problems were solved with the algorithmic differentiation Matlab toolbox CasADi [And+19].

The building model was created with the BRCM Matlab Toolbox [Stu+14]. This provides a thermal network model, which was based on the resistance capacitance modelling of electrical circuits. The water buffer tank model was derived from an isothermal energy balance. The lime storage module was modelled as a cycle process of an instationary mass storage between stationary charge and discharge reactors. The whole system was exposed to disturbance inputs which are not influenceable but can be estimated or predicted. All control approaches were applied to the overall system model under the influence of the disturbance data of the upcoming 5 days of the current year. With the current year the year 2016 was meant. The disturbance inputs are the occupancy probability of the building, the ambient temperature and the solar radiation on each facade of the building. The occupancy density was taken from the publication [FLZ16] and applied to each weekday of the year. The weather data for the year 2016 were taken from the European Union database [HMG12]. In order to use the lime storage at all, the forecast of disturbance variables must be approximated beyond the puble forecast period of 5 days. The disturbance inputs of the so-called base year serve this purpose. Its occupancy data were the same as those of the current year 2016, but the weather data were those of the typical meteorological year meaning the weather data averaged over several years. The states of the building energy system were the temperature of the room, the ceiling, the floor and all walls as well as the volume of the water buffer tank and the mass of stored lime. The manipulated variables on the overall system were the blinds positions, the heating and cooling power into the building, the heat power of the heat pump as well as two lime storage specific inputs, which enable its charging and discharging.

Three model-predictive control concepts have been developed to control the overall system. They take over exclusively the tasks of the supervisory hierarchy and specify set points to field level controllers. The hierarchy of two control approaches includes a higher-level annual scheduling which was called the optimal generation scheduling (OGS) and a lower-level dynamic MPC control. These approaches pursue the goal of an optimal path following of the lime storage trajectory on the one hand and to use possible increased or decreased yields in the current year on the other hand. The third approach does not require higher-level scheduling. The annual schedule was a single optimisation and uses the disturbance variables of the base year to find optimal control variables for the entire year, so that state and input

constraints were met. The inputs were determined on the basis of the objective measures operating costs and energy consumption of the cooling system, heat pump and reactor input power of the lime storage module. In order to be able to estimate the results of the control approaches, a reference, the lime storage trajectory was established by the OGS algorithm based on the disturbance variable inputs of 2016. The represent the best possible operating costs. The relative deviation of the annual operating costs caused by the control system from these previously mentioned optimal costs was the central evaluation criterion of the control approaches.
The first approach was called flexible reference tracking approach one, briefly flex1. Its objective includes the costs based on the disturbance inputs of the coming 5 days of the current year as well as those costs caused by the deviation of the lime storage level from the optimal annual schedule. In addition, two factors were introduced, which allow a weighting of the two cost components and a potentiation of the lime storage difference. The objective of the second approach, flexible reference tracking approach two, briefly flex2, also includes the costs based on the disturbance prediction of the upcoming 5 days of the current year as well as those costs which arise during a transition period. At the end of the transition period, the lime storage level must correspond to those of the base year scheduling. The costs during the transition period were included in the optimisation by explicit inputs. Here, the controller uses disturbance input data from the base year.The third approach was called mixed approach. Its objective also includes the costs based on the disturbance inputs of the coming 5 days of the current year and further costs within a base year prediction horizon. The third approach was called mixed approach. Its objective also includes the costs based on the disturbance inputs of the coming 5 days of the current year and further the costs within a base year prediction horizon. The inputs within the base year prediction horizon were also included in the optimisation. For this purpose, the controller also accesses disturbance variable data of the base year. This approach differs from the flex2 approach, as it does not specify a final state.

The overall system was examined with varying settings by annual simulations. The settings included the building weight, the configuration of the heat supply and the system design specification. For this purpose, the upper limits of some system inputs and states were set to infinite without limitation and to the values of the specification of a commercially available device. The heat supply of the system was analysed by three different configurations. In the configuration *HP* the heat pump was exclusively responsible for the heat supply. In the configuration *LS* the lime storage module takes over the entire heat supply and in the hybrid configuration *LSHP* the heat pump and the lime storage module take over the heat supply.
The results showed that the weight of the building has no negative effect on energy consumption or operating costs. The main focus, however, was on the different configurations for heat supply. As far as no constraints were set for selected inputs and states, the lime storage module shows no economic or ecological attractiveness. In the configuration *LSHP* it was not used at any time of the year. Only the introduction of constraints results in financial benefits from the lime storage module in the configuration *LSHP*. The configuration *LS* was significantly more expensive in terms of heat supply compared to the other two configurations. Table 5.1 shows the annual operating costs and energy consumption of the different configurations for the supply of space heating and hot water.

The control concepts were validated by applying them to the overall system. At the same time, the parameters of each approach will be optimised in such a way that the aforementioned relative deviation of the annual operating costs from the optimal costs of the annual scheduling

Table 5.1: Annual energy consumption (AEC) and annual operation cost (AOC) of heat supply configurations with the financial objective and limited state and inputs.

Config.	*HP*	*LS*	*LSHP*
AEC / kWh	3673	9583	4311
AOC / €	98	190	93

was minimised. Table 5.2 shows the relative deviation of the respective control concepts and heat supply configurations. It shows that the mixed approach was the most suitable control approach for the seasonal control of a building energy system with lime storage for both configurations *LS* and *LSHP*. In addition, the suitability of the disturbance data of the typical meteorological year as a base year was investigated and it was found that it was adequate for the approximation of the disturbance data in the base year.

Table 5.2: Relative deviation *rdev* achieved by the different control approaches on the heat supply configurations *LS* and *LSHP*.

Control approach	flex1	flex2	mixed
$rdev_{LS}$ / %	9.7	7	3
$rdev_{LSHP}$ / %	2.8	0.25	0.18

In retrospect, the main questions can now be answered as follows:
How can an energy system of a building, water buffer storage and heat supply be optimally operated over one year under consideration of comfort criteria as well as weather and occupancy forecasts?
The overall system can be optimally operated over a whole year under consideration of comfort criteria as well as weather and occupancy forecasts by using the heat supply *LSHP* with the presented lime storage module and the mixed approach as model-predictive control.
Which is the optimal configuration of the heat supply consisting of a heat pump and or a thermochemical energy storage module?
The hybrid system of heat pump and lime storage module was the most cost efficient system for supplying heat to the building. From an energy point of view, the use of the lime storage module was not suitable compared to the heat pump, as the latter provides heat more efficiently.
Can cost and resource efficiency of the plant be increased by integrating a thermochemical energy storage system?
Yes, the integration of the lime storage module has been proven to reduce annual operating costs.

This paper highlights two decisive research contributions. On the one hand, a system model consisting of building, buffer storage, lime storage module and heat pump was established, and on the other hand, three control approaches were developed which integrate the lime storage module as a seasonal energy storage and thus optimally operate the entire system over an entire year.

5.1 Future Work

5.1.1 On the Energy System Settings

Future work could further exploit the possibilities of the BRCM Toolbox. On the one hand, it offers the possibility of implementing a ventilation system that pre-cools the building at night for the day. In this work, the cost-intensive cooling performed this function. Furthermore it offers the possibility to implement a heat recovery system. This unit transfers the heat or cold of the outgoing air flow to the fresh air flow, which was prescribed by the air change rate.
With regard to the energy storage system, the short-term water buffer storage tank could be decoupled from the lime storage module. This decoupling could be realised by an additional input, which channels excess hot water into the canalisation. This could result in further financial benefits due to the lime storage module.
In addition, the energy storage system could be applied to a apartment building or a building district and more detailed building models could be used. Generally speaking, a system specification should be found in which the heat supply by the hybrid system can be operated even more cost-efficiently than the individual configurations. The extension of the energy system, which so far only considered the heat supply, to a decentralised energy system, which also considers the supply of electric power, could be the subject of further work. For this purpose, the integration of photovoltaic, solar thermal collectors and/or battery storage could be investigated.
In addition, the entire system should be considered under future disturbance inputs. The effects of climate change could be included in the weather forecasts. Furthermore, it should be investigated how a future electricity price trend, which was more expensive in winter than in summer, will affect the suitability of the lime storage module.

5.1.2 On the MPC Approaches

Within the derivation of the flex1 approach, a linear decay of the lime storage level difference within the transition period was assumed, cmp. Equation 2.137. With the help of the flex2 approach this assumption could be validated and possibly lead to other models. Furthermore, another optimisation solver could be used to integrate the difference of the water buffer storage level into the objective function. This also applies to the flex2 approach. So far, the flex2 as well as the mixed approach worked without a weighting of the short and long-term cost components. Future work could also introduce weights for these two approaches and investigate their influence. As suggested in the discussion, the mixed approach could combine the advantages of lower computational time with higher accuracy by applying a more precise discretisation procedure for the second objective component.
In the results presented, the sampling rate was due to the lower computational effort at 2.5 days, $t_{skip} = 60\,\mathrm{h}$. However, a reduction of the sampling rate leads to a significant increase in computing time. This was especially the case for large real systems. Therefore the introduction of a further hierarchy level was proposed, which works with a prediction horizon of 2.5 days. The overall hierarchy could then consist of a higher-level control, according to the mixed approach, and a short-term control, according to the flex1 or flex2 approach.
Finally, it should be emphasised that this thesis only presents control concepts whose predictions do not change over time. In reality, however, predictions are always subject to errors.

Future work should focus on verifying the control concepts to all system variable prediction errors. Nevertheless, the control concepts could prove a certain robustness, the topic of robust or stochastic control must be treated in future work.

Appendix A

Appendix

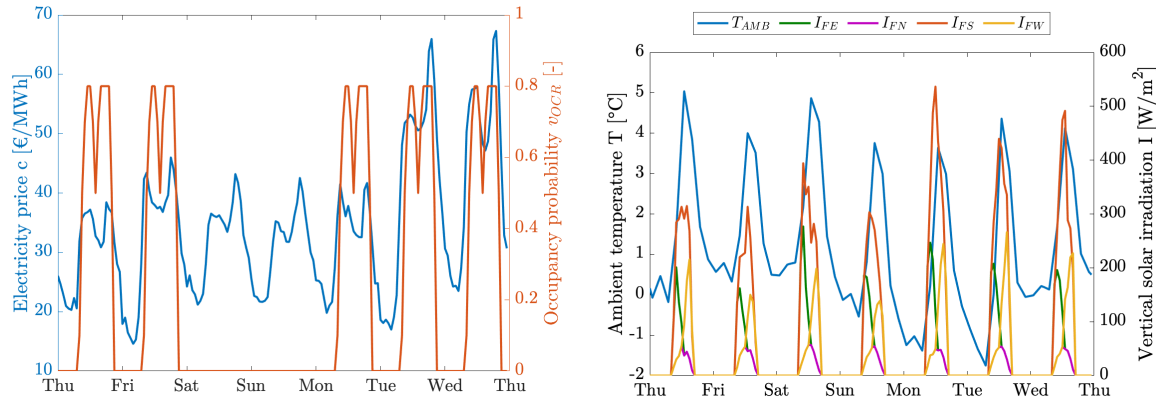

Figure A.1: Base year disturbance data of a week in January. Data starts on Thursday at zero o'clock. The weekend days are in between.

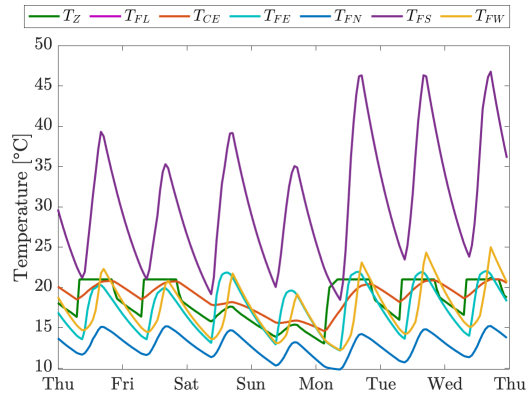

Figure A.2: OGS_{by} results of temperatures of the building element based on the specified disturbance data, cmp. Figure A.1. Therefore, variations in the heat supply configuration and the optimisation do not influence the temperature curves.

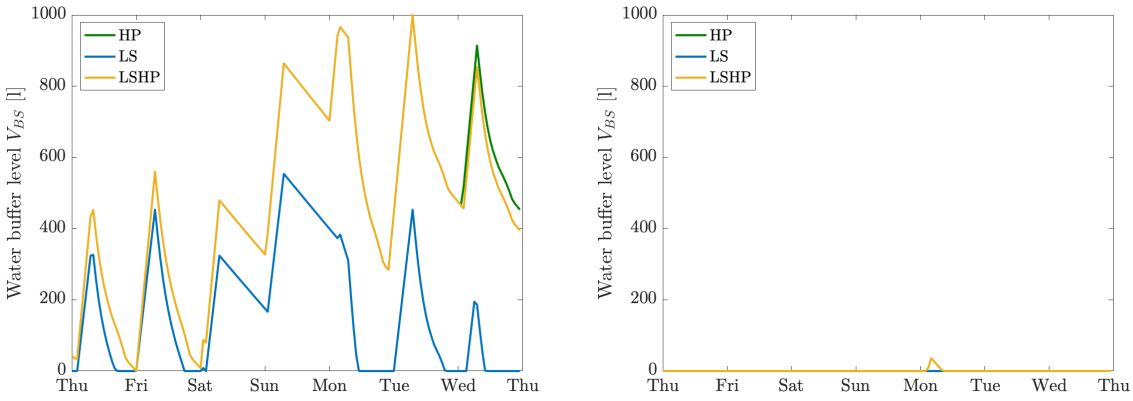

Figure A.3: OGS_{by} results of the water buffer storage volume based on the specified disturbance data, cmp. Figure A.1, varying the heat supply configuration and optimisation target. The volume of the configuration HP and LSHP do not vary. Left: Optimisation target *oc*. Right: Optimisation target *ec*.

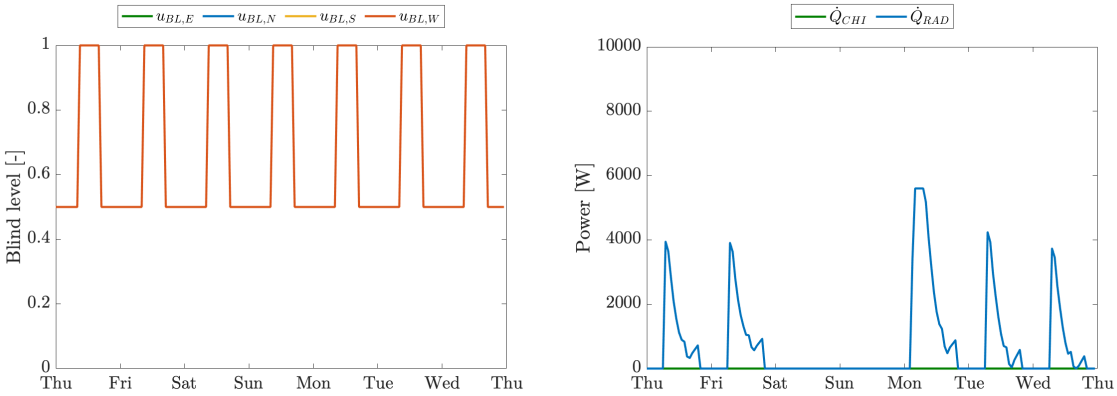

Figure A.4: OGS_{by} results of the blind positions and heating or cooling power based on the specified disturbance data, cmp. Figure A.1. Left: Blind positions within each window. Blind positions do not vary with the window, the heat supply configuration and the optimisation target . The initial value for the blind positions is 0.5. Right: Heating and cooling power. Building heat and cooling power do not vary with the window, the heat supply configuration and the optimisation target.

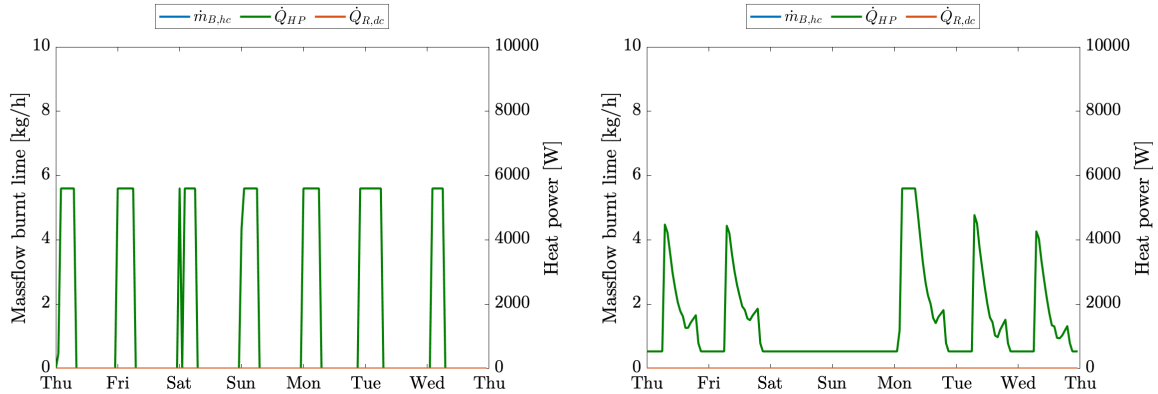

Figure A.5: OGS_{by} results of the heat supply inputs based on the specified disturbance data, cmp. Figure A.1. Heat supply inputs based on the configuration HP varying the objective. The heat supply inputs of the configuration HP and LSHP do not vary. Left: Optimisation target *oc*. Right: Optimisation target *ec*.

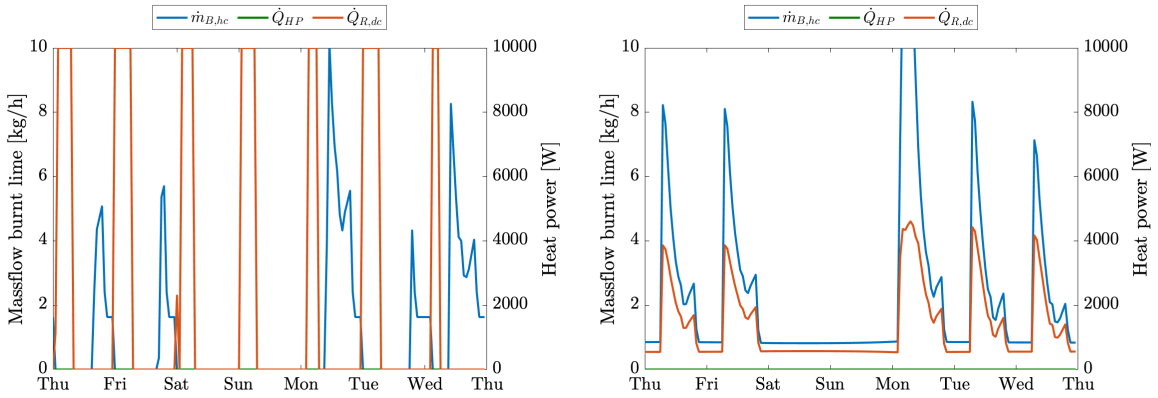

Figure A.6: OGS_{by} results of the heat supply inputs based on the specified disturbance data, cmp. Figure A.1. Heat supply inputs based on the configuration LS varying the objective. Left: Optimisation target *oc*. Right: Optimisation target *ec*.

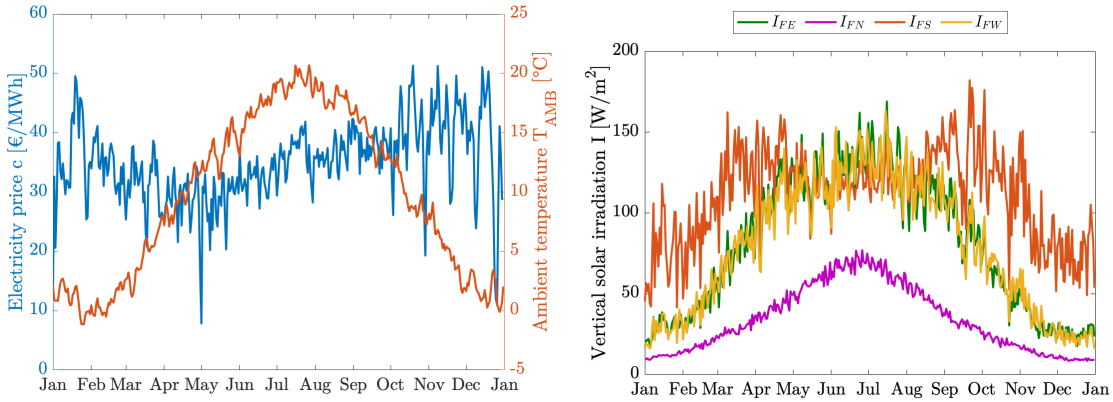

Figure A.7: Daily averaged disturbance data of the total base year. .

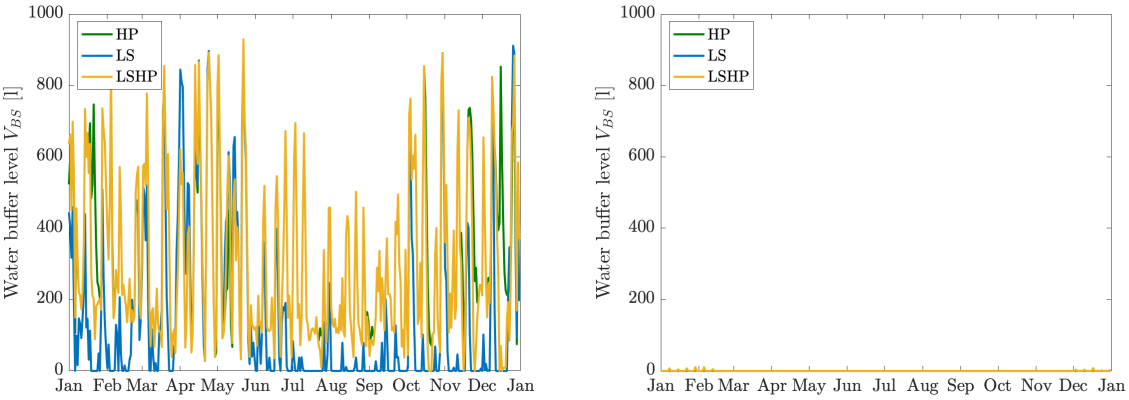

Figure A.8: OGS_{by} results of the water buffer storage volume based on the specified disturbance data, cmp. Figure A.7. Daily averaged volume of the water buffer storage varying the heat supply configuration and optimisation target. Left: Optimisation target *oc*. Right: Optimisation target *ec*.

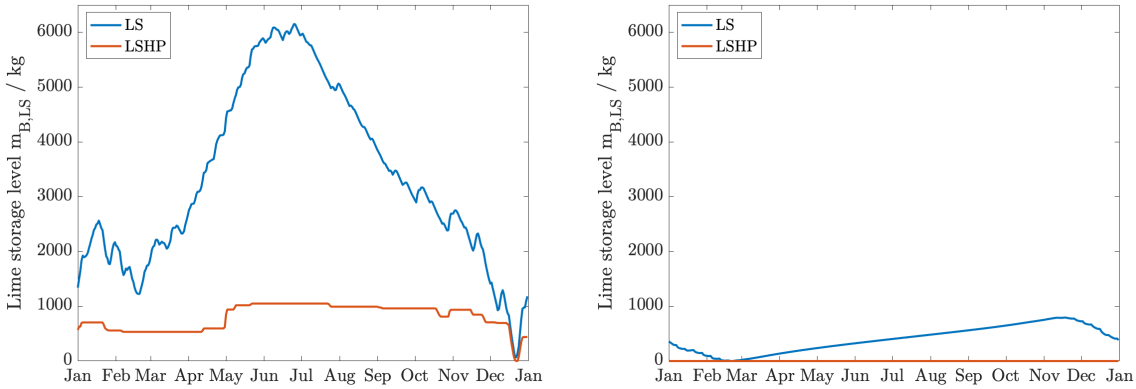

Figure A.9: OGS_{by} results of the annual lime storage level based the specified disturbance data, cmp. Figure A.7. Daily averaged mass in the lime storage tank varying the heat supply configuration and optimisation target. Left: Optimisation target *oc*. Right: Optimisation target *ec*.

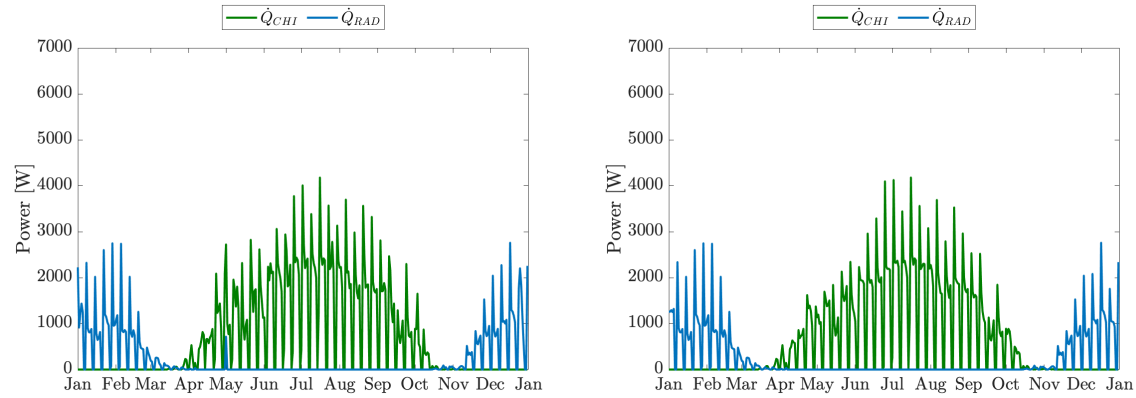

Figure A.10: OGS_{by} results of the annual heating and cooling power based on the specified disturbance data, cmp. Figure A.7. Daily averaged heating and cooling power varying the optimisation target. Left: Optimisation target *oc*. Right: Optimisation target *ec*.

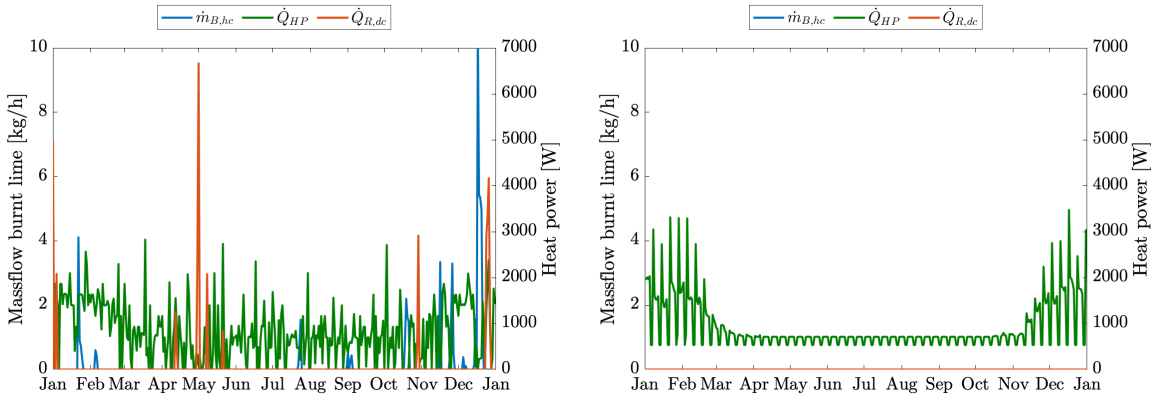

Figure A.11: OGS_{by} results of the annual heat supply inputs for config HP based on the specified disturbance data, cmp. Figure A.7. Daily averaged heat supply inputs based on the configuration HP varying the objective. The heat supply inputs of the configuration HP and LSHP do not vary. Left: Optimisation target *oc*. Right: Optimisation target *ec*.

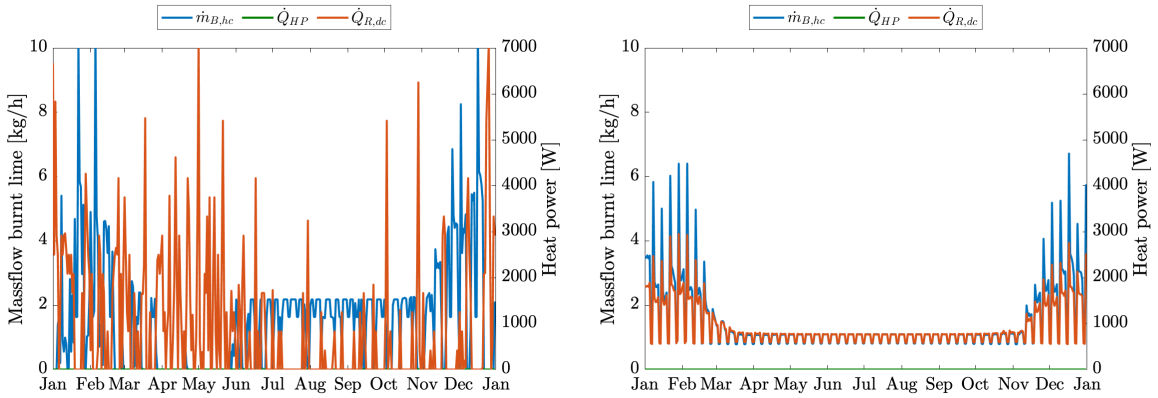

Figure A.12: OGS_{by} results of the annual heat supply inputs for config LS based on the specified disturbance data, cmp. Figure A.7. Daily averaged heat supply inputs based on the configuration LS varying the objective. Left: Optimisation target *oc*. Right: Optimisation target *ec*.

List of Figures

List of Tables

Bibliography

[201] *Paris Agreement*. URL: https://treaties.un.org/pages/ViewDetails.aspx?src=TREATY&mtdsg_no=XXVII-7-d&chapter=27&clang=_en.

[202] *Project description: Adaptive Shells and Structures for the Built Environment of the Future*. URL: https://www.isys.uni-stuttgart.de/en/research/civilSystemsEngineering/sfb/ (visited on 04/20/2020).

[And+19] J. A E Andersson, J. Gillis, G. Horn, J B Rawlings, and M Diehl. „CasADi – A software framework for nonlinear optimization and optimal control". In: *Mathematical Programming Computation* (2019). DOI: 10.1007/s12532-018-0139-4.

[Ang+18] M. Angerer, M. Becker, S. Härzschel, K. Kröper, S. Gleis, A. Vandersickel, and H. Spliethoff. „Design of a MW-scale thermo-chemical energy storage reactor". In: *Energy Reports* (2018). DOI: https://doi.org/10.1016/j.egyr.2018.07.005.

[Bun] Bundesnetzagentur. *Strommarktdaten*. URL: https://www.smard.de.

[Bun20] Deutsche Bundesregierung. „Was tut die Bundesregierung für den Klimaschutz?" In: (2020). URL: https://www.bundesregierung.de/breg-de/themen/klimaschutz/bundesregierung-klimapolitik-1637146 (visited on 03/2020).

[Cri+17] Y. Criado, A. Huille, S. Rougé, and J. C. Abanades. „Experimental investigation and model validation of a CaO/Ca(OH)2 fluidized bed reactor for thermochemical energy storage applications". In: *Chemical Engineering Journal* (2017). DOI: https://doi.org/10.1016/j.cej.2016.11.010.

[Ene+20] D. Enescu, G. Chicco, R. Porumb, and G. Seritan. „Thermal Energy Storage for Grid Applications: Current Status and Emerging Trends". In: *Energies* (2020). DOI: 10.3390/en13020340.

[FLZ15] C. Finck, R. Li, and W. Zeiler. „An Optimization Strategy for Scheduling Various Thermal Energy Storage Technologies in Office Buildings Connected to Smart Grid". In: *Energy Procedia* (2015). 6th International Building Physics Conference, IBPC 2015. DOI: https://doi.org/10.1016/j.egypro.2015.11.105.

[FLZ16] C. Finck, R. Li, and W. Zeiler. „Operational load shaping of office buildings connected to thermal energy storage using dynamic programming". In: 12th REHVA World Congress (CLIMA 2016), May 22-25, 2016, Aalborg, Denmark, CLIMA 2016 ; Conference date: 22-05-2016 Through 25-05-2016. 2016.

[Fin+18] C. Finck, R. Li, R. Kramer, and W. Zeiler. „Quantifying demand flexibility of power-to-heat and thermal energy storage in the control of building heating systems". In: *Applied Energy* (2018). DOI: https://doi.org/10.1016/j.apenergy.2017.11.036.

[Fio+17] M. Fiorentini, J. Wall, Z. Ma, J. H. Braslavsky, and P. Cooper. „Hybrid model predictive control of a residential HVAC system with on-site thermal energy generation and storage“. In: *Applied Energy* (2017). DOI: https://doi.org/10.1016/j.apenergy.2016.11.041.

[HMG12] T. Huld, R. Müller, and A. Gambardella. „A new solar radiation database for estimating PV performance in Europe and Africa“. In: *Solar Energy* (2012). DOI: https://doi.org/10.1016/j.solener.2012.03.006.

[Jon+19] M. Jonin, M. Khosravi, A. Eichler, W. Villasmil, P. Schuetz, C. N. Jones, and R. S. Smith. „Exergy-based model predictive control for design and control of a seasonal thermal energy storage system“. In: *Journal of Physics: Conference Series* (2019). DOI: 10.1088/1742-6596/1343/1/012066.

[LM] P.J. Linstrom and W.G. Mallard. *NIST Chemistry WebBook, NIST Standard Reference Database Number 69*. Ed. by National Institute of Standards and Technology. URL: https://doi.org/10.18434/T4D303 (visited on 02/08/2020).

[Lef+13] A. Lefort, R. Bourdais, G. Ansanay-Alex, and H. Guéguen. „Hierarchical control method applied to energy management of a residential house“. In: *Energy and Buildings* (2013). DOI: https://doi.org/10.1016/j.enbuild.2013.04.010.

[MRAR18] M-Royapoor, A. Antony, and T. Roskilly. „A review of building climate and plant controls, and a survey of industry perspectives“. In: *Energy and Buildings* (2018). DOI: https://doi.org/10.1016/j.enbuild.2017.10.022.

[Old+10] F. Oldewurtel, A. Parisio, C. Jones, M. Morari, D. Gyalistras, M. Gwerder, V. Stauch, B. Lehmann, and K. Wirth. „Energy efficient building climate control using Stochastic Model Predictive Control and weather predictions“. In: *Proceedings of the 2010 American Control Conference, ACC 2010* (2010). DOI: 10.1109/ACC.2010.5530680.

[PZ17] Z.H. Pan and C.Y. Zhao. „Gas–solid thermochemical heat storage reactors for high-temperature applications“. In: *Energy* (2017). DOI: https://doi.org/10.1016/j.energy.2017.04.102.

[Pet+16] M. Petrollese, L. Valverde, D. Cocco, G. Cau, and J. Guerra. „Real-time integration of optimal generation scheduling with MPC for the energy management of a renewable hydrogen-based microgrid“. In: *Applied Energy* (2016). DOI: https://doi.org/10.1016/j.apenergy.2016.01.014.

[RL19] S.. Raković and W. Levine, eds. *Handbook of Model Predictive Control*. Birkhäuser Basel, 2019. DOI: 10.1007/978-3-319-77489-3.

[Sca09] R. Scattolini. „Architecture of Distributed and Hierarchical Model Predictive Control—A Review“. In: *Journal of Process Control* (2009). DOI: 10.1016/j.jprocont.2009.02.003.

[Sch+12] F. Schaube, L. Koch, A. Wörner, and H. Müller-Steinhagen. „A thermodynamic and kinetic study of the de- and rehydration of Ca(OH)2 at high H2O partial pressures for thermo-chemical heat storage“. In: *Thermochimica Acta* (2012). DOI: https://doi.org/10.1016/j.tca.2012.03.003.

[Sch+13] F. Schaube, I. Utz, A. Wörner, and H. Müller-Steinhagen. „De- and rehydration of Ca(OH)2 in a reactor with direct heat transfer for thermo-chemical heat storage. Part B: Validation of model“. In: *Chemical Engineering Research and Design* (2013). DOI: https://doi.org/10.1016/j.cherd.2013.02.019.

[Sch+14] M. Schmidt, C. Szczukowski, C. Roßkopf, M. Linder, and A. Wörner. „Experimental results of a 10 kW high temperature thermochemical storage reactor based on calcium hydroxide“. In: *Applied Thermal Engineering* (2014). DOI: https://doi.org/10.1016/j.applthermaleng.2013.09.020.

[Stu14] D. Sturzenegger. „Model predictive building climate control - Steps towards practice“. PhD thesis. Automatic Control Laboratory, ETH Zürich, 2014. DOI: https://doi.org/10.3929/ethz-a-010379191.

[Stu+14] D. Sturzenegger, D. Gyalistras, V. Semeraro, M. Morari, and R. S. Smith. „BRCM Matlab Toolbox: Model generation for model predictive building control“. In: *2014 American Control Conference*. 2014. DOI: 10.1109/ACC.2014.6858967.

[TB16] C. R. Touretzky and M. Baldea. „A hierarchical scheduling and control strategy for thermal energy storage systems“. In: *Energy and Buildings* (2016). DOI: https://doi.org/10.1016/j.enbuild.2015.09.049.

[TPL13] P. Tatsidjodoung, N. Le Pierrès, and L. Luo. „A review of potential materials for thermal energy storage in building applications“. In: *Renewable and Sustainable Energy Reviews* (2013). DOI: https://doi.org/10.1016/j.rser.2012.10.025.

[Tan+17] M. Tanaskovic, D. Sturzenegger, R. Smith, and M. Morari. „Robust Adaptive Model Predictive Building Climate Control“. In: *IFAC-PapersOnLine* (2017). DOI: https://doi.org/10.1016/j.ifacol.2017.08.257.

[Umw] Umweltbundesamt. *Datenbasis zur Bewertung von Energieeffizienzmaßnahmen in der Zeitreihe, FKZ 3712 12 102, Endbericht 2017.* URL: https://www.umweltbundesamt.de/publikationen/datenbasis-zur-bewertung-von-1.

[V.a] DIN Deutsches Institut für Normung e. V. *DIN EN ISO 6946 : 2018-03, Bauteile - Wärmedurchlasswiderstand und Wärmedurchgangskoeffizient - Berechnungsverfahren*. Beuth Verlag, Berlin. DOI: https://dx.doi.org/10.31030/2518301.

[V.b] DIN Deutsches Institut für Normung e. V. *DIN V 18599-8: Energetische Bewertung von Gebäuden – Berechnung des Nutz-, End- und Primärenergiebedarfs für Heizung, Kühlung, Lüftung, Trinkwarmwasser und Beleuchtung – Teil 8: Nutz- und Endenergiebedarf von Warmwasserbereitungssystemen*. Beuth Verlag, Berlin. DOI: https://dx.doi.org/10.31030/2878217.

[V.c] DIN Deutsches Institut für Normung e. V. *Energetische Bewertung von Gebäuden – Berechnung des Nutz-, End- und Primärenergiebedarfs für Heizung, Kühlung, Lüftung, Trinkwarmwasser und Beleuchtung – Teil 10: Nutzungsrandbedingungen, Klimadaten*. Beuth Verlag, Berlin. DOI: https://dx.doi.org/10.31030/2874436.

[XD17] Q. Xu and S. Dubljevic. „Model predictive control of solar thermal system with borehole seasonal storage“. In: *Computers and Chemical Engineering* (2017). DOI: https://doi.org/10.1016/j.compchemeng.2017.02.023.

[e.V13] VDI e.V., ed. *VDI-Wärmeatlas*. 11.Auflage. Springer Vieweg, 2013. DOI: https://doi.org/10.1007/978-3-642-19981-3.

[e.V20] AG Energiebilanzen e.V. „Private Haushalte sparen bei Raumwärme und Beleuchtung“. In: (2020). URL: https://ag-energiebilanzen.de/22-0-Pressedienst.html (visited on 03/13/2020).

[Ši+11] J. Široký, F. Oldewurtel, J. Cigler, and S. Prívara. „Experimental analysis of model predictive control for an energy efficient building heating system“. In: *Applied Energy* (2011). DOI: https://doi.org/10.1016/j.apenergy.2011.03.009.

Erklärung des Autors

der Masterarbeit mit dem Titel

Model predictive approaches for building climate and seasonal energy storage control

Hiermit versichere ich,

1. dass ich meine Arbeit bzw. bei einer Gruppenarbeit den entsprechend gekennzeichneten Anteil der Arbeit selbständig verfasst habe,
2. dass ich keine anderen als die angegebenen Quellen benutzt und alle wörtlich oder sinngemäß aus anderen Werken übernommenen Aussagen als solche gekennzeichnet habe,
3. dass die eingereichte Arbeit weder vollständig noch in wesentlichen Teilen Gegenstand eines anderen Prüfungsverfahrens gewesen ist,
4. dass ich die Arbeit weder vollständig noch in Teilen bereits veröffentlicht habe und
5. dass das elektronische Exemplar mit den anderen Exemplaren übereinstimmt.

Stuttgart, den 04.05.2020

Simon Oskar Weber

Inofficial translation of the Declaration of Authorship („Erklärung des Autors“). Only the original German wording is legally recognized.

I hereby certify

1. that this thesis, resp. in a group project the appropriately labeled parts of this thesis, has/have been created by myself,
2. that no other sources than those referenced have been used, and that all ideas adopted from other work, literally or paraphrased, are appropriately labeled as such,
3. that this submitted thesis neither in full nor to a significant part has been part of any other examination process,
4. that I have neither published this thesis in full nor in parts, and
5. that the electronic version is identical to the hardcopy.